

Preparation, Characterisation and Modelling of Elongated Lipid Particles

Haoda Zhao

A thesis submitted in fulfilment
of the requirements for the degree of
Doctor of Philosophy



UNSW
SYDNEY

School of Chemical Engineering
Faculty of Engineering
University of New South Wales

December 2020

Thesis Title and Abstract sheet

Thesis Title

Preparation, Characterisation and Modelling of Elongated Lipid Particle

Thesis Abstract

Lipid particles have been widely utilized as drug delivery carriers as a result of their biocompatibility, bioavailability and biodegradability. Lipid particulate drug carriers are often spherical, but more complex shapes have attracted more attention due to novel delivery benefits. Elongated particles are of increasing interest, for example, to improve deposition of active ingredients to the human lung. Manufacture of elongated particles normally involves shaping technologies such as microfluidic flows, film stretching processes, and particle-scale moulding or sculpting. Such methods can be expensive and be limited in scale. Here, we use two methods to produce elongated lipid particles with size scales able to improve the delivery efficiency from a flow. We study behaviour of the shapes in simple shear flow and compare with more common shapes.

A hot emulsion method is used to crystallize a lipid emulsion, with careful choice of surfactant and co-surfactant to cause a unique dewetting phenomenon and generate elongated particles. The method can easily control the shape of the elongated particles, and allow tuning of shape, size and aspect ratio. Because of its simplicity, this method can be easily adapted to larger scales. The size and shape distribution of the particles are characterised and their behaviour in simple shear flow has been studied to understand their likely delivery traits.

Building on the high-temperature process, a low-temperature emulsification method is also developed, allowing direct production of elongated particles via the same dewetting mechanism but without the need for extensive heating and cooling. The solvent emulsification method produces elongated particles similar to the hot emulsion process, but also produces novel shape gradient particles with oscillatory radial dimensions. The novel shape occurs due to instabilities during coupled evaporation and solidification and exhibits a more complex curvature than most elongated particles available.

Originality statement, Copyright and Authenticity statements

ORIGINALITY STATEMENT

I hereby declare that this submission is my own work and to the best of my knowledge it contains no materials previously published or written by another person, or substantial proportions of material which have been accepted for the award of any other degree or diploma at UNSW or any other educational institution, except where due acknowledgement is made in the thesis. Any contribution made to the research by others, with whom I have worked at UNSW or elsewhere, is explicitly acknowledged in the thesis. I also declare that the intellectual content of this thesis is the product of my own work, except to the extent that assistance from others in the project's design and conception or in style, presentation and linguistic expression is acknowledged.

COPYRIGHT STATEMENT

I hereby grant the University of New South Wales or its agents a non-exclusive licence to archive and to make available (including to members of the public) my thesis or dissertation in whole or part in the University libraries in all forms of media, now or here after known. I acknowledge that I retain all intellectual property rights which subsist in my thesis or dissertation, such as copyright and patent rights, subject to applicable law. I also retain the right to use all or part of my thesis or dissertation in future works (such as articles or books).

For any substantial portions of copyright material used in this thesis, written permission for use has been obtained, or the copyright material is removed from the final public version of the thesis.

AUTHENTICITY STATEMENT

I certify that the Library deposit digital copy is a direct equivalent of the final officially approved version of my thesis.

Inclusion of Publications Statement

UNSW is supportive of candidates publishing their research results during their candidature as detailed in the UNSW Thesis Examination Procedure.

Publications can be used in the candidate's thesis in lieu of a Chapter provided:

- The candidate contributed **greater than 50%** of the content in the publication and are the "primary author", i.e. they were responsible primarily for the planning, execution and preparation of the work for publication.
- The candidate has obtained approval to include the publication in their thesis in lieu of a Chapter from their Supervisor and Postgraduate Coordinator.
- The publication is not subject to any obligations or contractual agreements with a third party that would constrain its inclusion in the thesis.

The candidate has declared that **some of the work described in their thesis has been published and has been documented in the relevant Chapters with acknowledgement.**

A short statement on where this work appears in the thesis and how this work is acknowledged within chapter/s:

Modelling part of Chapter 3 in my thesis is published. This is acknowledged as a footnote at the beginning of Chapter3.

Candidate's Declaration



I declare that I have complied with the Thesis Examination Procedure.

Abstract

Lipid particles have been widely utilized as drug delivery carriers as a result of their biocompatibility, bioavailability and biodegradability. Lipid particulate drug carriers are often spherical, but more complex shapes have attracted more attention due to novel delivery benefits. Elongated particles are of increasing interest, for example, to improve deposition of active ingredients to the human lung. Manufacture of elongated particles normally involves shaping technologies such as microfluidic flows, film stretching processes, and particle-scale moulding or sculpting. Such methods can be expensive and be limited in scale. Here, we use two methods to produce elongated lipid particles with size scales able to improve the delivery efficiency from a flow. We study behaviour of the shapes in simple shear flow and compare with more common shapes.

A hot emulsion method is used to crystallize a lipid emulsion, with careful choice of surfactant and co-surfactant to cause a unique dewetting phenomenon and generate elongated particles. The method can easily control the shape of the elongated particles, and allow tuning of shape, size and aspect ratio. Because of its simplicity, this method can be easily adapted to larger scales. The size and shape distribution of the particles are characterised and their behaviour in simple shear flow has been studied to understand their likely delivery traits.

Building on the high-temperature process, a low-temperature emulsification method is also developed, allowing direct production of elongated particles via the same dewetting mechanism but without the need for extensive heating and cooling. The solvent emulsification method produces elongated particles similar to the hot emulsion process, but also produces novel shape gradient particles with oscillatory radial dimensions. The novel shape occurs due to instabilities during coupled evaporation and solidification and exhibits a more complex curvature than most elongated particles available.

Acknowledgments

First of all, I would like to thank my supervisor, Associate Professor Patrick T. Spicer, who offered me to join his research group to persuade my research journey. He is an excellent supervisor with very creative thoughts about my research. This thesis could not be finished without his guidance and support. Many thanks for bringing me into the colloid chemistry world and provide me the opportunity to continue his work on elongated lipid particle. People say a good teacher will not tell you what to do, they will tell you where to look at. Patrick is no doubt a good teacher, because he can point out the direction of a problem with a perspective you would never thought about, but will help me to open another window to solve the problem independently. He is also very patient to explain and teach me how to apply the knowledge from textbook to practical experiment, and to have critical thinking like an engineer. Patrick is also very generous of sharing his industrial experience, which is deeply influenced me in my future career life.

Secondly, many thanks to my co-supervisor Associate Professor Stuart Prescott. Thank you for sharing your every professional advice to my project and provide many ideas about how to analysis my optical micrographies.

Moreover, I would like to thank Associate Professor Timothy J. Atherton and Mathew Q. Giso from Tufts University, USA. Their simulations of my comet crystals help me to understand my particles in geometric and dynamic perspectives.

I cannot forget to say thank you to my supervisor from the University of Queensland, Professor Lisbeth Grøndahl, who was my Master's Degree's supervisor. She refined my laboratory skills and taught me how to be responsible to my own research project. Also my Bachelor's Degree's supervisor, Professor Xiaozhong Gong from Shenzhen University, China. She brought me to the academia world and allowed me to do the researches under my interests.

Many thanks to the lab managers Eh Hau Pan and Camillo Taraborrelli from the School of Chemical Engineering, they taught me how to operate many instrumentation including DSC, FTIR and freeze drier. Also Dr Yin Yao from EMU, who was very patient and taught me how to use Pt/Cr coater and SEM. And Dr Alexander Macmillan and Dr Michael Carnell from BMIF, who helped me with my confocal

images. Also many thanks to all the staff from the School of Chemical Engineering to provide a safe and convenient campus life.

I acknowledge all the group members from Complex Fluids group at UNSW I have met : Dr Jie Song, Dr Haiqiao Wang, Dr Goldina Kwandou, Dr Zengyi Wei, Dr Firoozeh Babayekhorasani, Zhiwei Li, Maryam Hosseini, Isaac Gresham and Arslan Siddique. Thank you Jie, and Haiqiao helped me a lot on data analysis, and Firoozeh on the Matlab coding for the particle's trajectory study and Maryam helped me with SEM imaging.

Last but not the least, to my parents. Their supports and believes is the biggest motivation for me to finish my PhD journey. Thank you for understanding me and provide me the unconditional supports.

Contents

Abstract	i
1 Introduction and Research Aims	1
1.1 Introduction	1
1.2 Thesis structure and Research Aims	3
References	4
2 Literature Review	7
2.1 Shaped particles and their applications	7
2.2 Characterisation of Shaped Particles	9
2.3 Shaped Particle Raw Materials	9
2.3.1 Polymer particles	10
2.3.2 Lipid Particles	10
2.4 Shaped Particles for Controlled Delivery	14
2.4.1 How Shaped Particles Affect Delivery	14
2.4.2 Stimulus-response by Particles for Controlled Delivery	15
2.4.3 Anisotropic Particles in Flow	17
2.5 Interfacial Shaping and Surfactant-induced Flows	19
2.5.1 Surfactant Adsorption	19
2.5.2 Anisotropic Droplet Shapes via Arrested Coalescence	21
2.5.3 Rotator Phase Droplet Shapes	22
2.5.4 Marangoni Flow	24
2.5.5 Sculpting particle shape by interfacial hydrodynamics	25
2.5.6 Formation of Shape Gradients by Crystallization Instabilities	28
2.6 Drug Incorporation in Lipid-based Delivery Vehicles	29
2.7 Scale-up of Shaped Particle Production	31
2.8 Simulating the Crystallisation of an Elongated Particle	34
2.9 Conclusion	36
References	37

3	Production of Elongated Lipid Particles via Solidification of Molten Emulsion Droplets	47
3.1	Introduction	47
3.2	Materials and Methods	49
3.2.1	Preparation of Lipid Particles	49
3.2.2	Optical microscopy and Size distribution	50
3.2.3	Scanning Electron Microscopy	51
3.2.4	Confocal Microscopy	51
3.3	Results and Discussion	51
3.3.1	Dewetting and Crystallisation Rate	52
3.3.2	Initial Emulsion Droplet Size	55
3.3.3	Elongated Particle Shape and Size Distribution	56
3.3.4	Continuous Injection Production of Elongated Particles	61
3.3.5	A Dynamic Process of the Interfacial Crystallization Approach	62
3.3.6	Density of Elongated Particles	66
3.4	Conclusion	70
	References	70
4	Elongated Shape Gradient Lipid Particles via Evaporation of Lipid-Solvent Emulsions	73
4.1	Introduction	73
4.2	Materials and Methods	74
4.2.1	Solubility of Lipids in Chloroform	74
4.2.2	Preparation of Lipid-chloroform Emulsion in Surfactant Solution	75
4.2.3	Optical Microscopy and Image Analysis	76
4.2.4	Measurement of Chloroform Emulsion Evaporation Rate	76
4.2.5	Preparation of Elongated Lipid Particles	76
4.2.6	Scanning Electron Microscope	76
4.3	Results and Discussion	77
4.3.1	Solubility of Lipids in Chloroform	77
4.3.2	Evaporation Rate of Chloroform Emulsion	78
4.3.3	Characterisation of Elongated Particles	79
4.4	Conclusion	84
	References	85

5	Behaviour of Elongated Lipid Particles in Shear Flow	87
5.1	Introduction	87
5.2	Materials and Methods	88
5.2.1	Preparation of Lipid-based Elongated Particles	88
5.2.2	Observation of Particles' Behavior by Optical Microscope	89
5.2.3	Trajectory Study	89
5.3	Results and Discussion	90
5.3.1	Modes of Behaviour in Shear Flow	90
5.3.2	Comet Particle Trajectories in Shear Flow	92
5.3.3	Jeffery Orbit Comparison	95
5.4	Conclusion	97
	References	98
6	Elongated Lipid Particles: Interfacial Hydrodynamic and Drug Loading Studies	101
6.1	Observation of Marangoni Flow	101
6.1.1	Methods and Materials	101
6.1.2	Results and Discussion	102
6.2	Drug Loading for Elongated Comet Particles	104
6.2.1	Methods and Materials	105
6.2.2	Results and Discussion	106
6.3	Conclusion	107
	References	107
7	Conclusions	109
	References	111
A	Supplementary information for Chapter 3	113
B	Supplementary information for Chapter 5	119

List of Abbreviations

AR	aspect ratio
CMC	critical micelle concentration
DDS	drug delivery system
DLS	dynamic light scattering
DSC	differential scanning calorimetry
FDA	food and drug administration
HA	hyaluronic acid
PDA	polydopamine
PDMS	polydimethylsiloxane
PRINT	particle replication in non-wetting template
SA	stearic acid
SDS	sodium dodecyl sulfate
SEM	scanning electron microscope
SLN	solid lipid nanoparticles
THS	trihydroxystearin

Chapter 1

Introduction and Research Aims

1.1 Introduction

Particulate materials are widely used and valuable to industries as diverse as commodity chemicals, foods, and pharmaceuticals. The use of particles enhances the ability to handle and convey some materials, but can also increase the complexity of processes using particles. A key variable of particulate systems is the characteristic size or size distribution of particles, as this sets physical variables, such as suspension in liquids, as well as characteristics like chemical activity. Control of particle size has always been important, but became a strong focus of research during the 90s when the benefits of nanotechnology were widely realised. Since then, particle shape has become an active area of research due to experimental and theoretical insights into particle shape effects on optical, chemical, biological and physical behaviour.

Particulate dynamics are often studied using, or assuming, dense spherical particles, but shape and density can greatly affect performance. For example, when studying and designing particles for use as aerosolised drug delivery vehicles, Edwards' group realised that the ability of particles to penetrate deeply into the human lung was less a function of size than density¹. They used this insight to create very porous, relatively large porous particles that behaved like nanoparticles when moving in an inhaled gas stream. Thanks to these insights, there is great interest in

studying non-spherical particle shapes for other enhancements to drug delivery², organ targeting and medical imaging³.

Most past work has produced shaped polymeric particles by direct molding or printing, such as in microfluidic devices, but more scalable processes such as film stretching and particle replication in non-wetting template (PRINT) have also been used to control particle shape³. Lipid particles offer a different approach to biological delivery from polymers, and are advantageous for hydrophobic drug solubility, bioavailability, biodegradability, and safety⁴.

A particularly active area of shape control focuses on production and study of elongated particles like rods^{5,6}. Most rods previously studied were sub-micron colloids synthesised by polymerisation⁷ or precipitation^{8,9}. However, larger, less dense elongated particles can also be produced from biological materials, with an exotic example being viruses¹⁰. More common possibilities include interfacially crystallised lipids¹¹, and we hypothesise that combining such benefits with variations in aerodynamic diameter could expand the material space available to developers, as well as potentially enhance performance of such particles as aerosol delivery vehicles. A current limitation is the ability to produce such particles inexpensively at large scales.

Achieving scalable control of elongated particle size and shape at length scales of 0.1-10 μm is difficult for typical flow or molding processes. However, interfacial forces are most effective at those length scales and are an excellent means of molding particles. For example, interfacial dewetting can alter the shape of droplets as they crystallize by controlled dewetting^{11,12}. Emulsification is a common industrial process that is easily scaled up and could thus be harnessed to produce specialised colloids. We hypothesise that starting with micron or submicron-scale droplets allows us to produce elongated shapes via simple emulsion crystallization, an easily

scaled process. In this thesis, two methods are developed to form elongated particles via interfacial crystallisation. We use the particles and results to develop the ability to control size, shape, and density.

1.2 Thesis structure and Research Aims

The focus of this thesis is to provide an understanding of the production of elongated lipid particles by a unique emulsion crystallization process. Surfactant-induced dewetting enables control over significant elongation and variation of particle shape and density in systems that would otherwise produce only dense spherical particles.

Here in Chapter 1, the topic and motivation of the thesis are introduced to motivate the structure and research aims.

In Chapter 2, a detailed literature review is provided on particle shape control and applications, with some focus on drug delivery systems.

In Chapter 3, the preparation of elongated lipid particles by interfacial crystallization of molten emulsions is studied and the control of particle size and aspect ratio is explored in the context of aerosol delivery. Cooling rate and surfactant concentration are shown to be key variables for particle size, density, and shape control. The aerodynamic diameter of the comet particles is discussed to assess the elongated lipid particles for potential use as aerosol delivery vehicles.

In Chapter 4, a new solvent-emulsification evaporation method is developed and used to prepare elongated comet particles. The method enables low-temperature, rapid production of comets, broadening the types of materials and formulations that might be used as well as enabling possible on-demand generation in sprays. The solvent process also expands the comet shapes produced, forming in some cases tapered oscillatory particles with distinct shape gradients not typically found in colloids. In this chapter, we examine the mechanism of oscillatory comet particle

shape formation and contrast the particles with those formed by melt crystallization.

In Chapter 5, the behaviour of elongated comet particles has been investigated in simple shear flow to contrast their behaviour with more commonly-studied symmetric elongated shapes like ellipsoids and rods. The particle flow behaviour can be described by existing theoretical descriptions of rod particle Jeffery orbits.

In Chapter 6, some preliminary studies related to hydrodynamic and surface phenomena responsible for comet formation are discussed. These preliminary results are intended to suggest potential future study of comet formation to increase application and general production of particulate materials.

In Chapter 7 the thesis is concluded and summarised to position this work in the space of future synthesis and large-scale production of anisotropic particles.

References

- [1] D. A. Edwards, J. Hanes, G. Caponetti, J. Hrkach, A. Ben-Jebria, M. L. Eskew, J. Mintzes, D. Deaver, N. Lotan, R. Langer, *Science* **1997**, 276, 1868–1872.
- [2] J. A. Champion, S. Mitragotri, *Proceedings of the National Academy of Sciences* **2006**, 103, 4930–4934.
- [3] J. Chen, N. E. Clay, N.-h. Park, H. Kong, *Chemical engineering science* **2015**, 125, 20–24.
- [4] S. Kamboj, S. Bala, A. B. Nair, *Int J Pharm Sci Rev Res* **2010**, 5, 78–90.
- [5] A. P. Philipse, *Langmuir* **1996**, 12, 1127–1133.
- [6] M. Solomon, P. Spicer, *Soft Matter* **2010**, 6, 1391–1400.
- [7] G. Wilkins, P. Spicer, M. Solomon, *Langmuir* **2009**, 25, 8951–8959.
- [8] A. P. Philipse, A. M. Wierenga, *Langmuir* **1998**, 14, 49–54.

- [9] A. Mohraz, D. B. Moler, R. M. Ziff, M. J. Solomon, *Physical Review Letters* **2004**, 92, 155503.
- [10] Z. Zhang, N. Krishna, J. Vermant, E. Grelet, *Langmuir* **2009**, 25, 2437–2442.
- [11] P. T. Spicer, R. W. Hartel, *Australian journal of chemistry* **2005**, 58, 655–659.
- [12] R. C. Hayward, A. S. Utada, N. Dan, D. A. Weitz, *Langmuir* **2006**, 22, 4457–4461.

Chapter 2

Literature Review

2.1 Shaped particles and their applications

Particulate materials are a critical part of chemical, material, and biological processes and there is a long history of their study, synthesis, and characterisation. Although many of the theories describing particulate dynamics assume particle shape is spherical, particles with much more complex shapes have long been known.

Shape is a complex topic, with multiple elements beyond the single dimension of size. Figure 2.1 shows a visualisation of key aspects of particle shape developed by Glotzer and Solomon¹. Past studies of shape have been used to characterise and classify existing synthetic and natural particles², but the insight provided by Figure 2.1 is a basis for design and specification of shapes for a given application, as well as the benefits they may provide.

Only recently have the incredible advantages of particle shape for numerous applications become clear, focusing researchers on understanding such possibilities as well as trying to control particle shape more robustly. For example, anisotropic oxide particles enabled development of hybrid liquid body armour that uses shear-thickening rheology to protect against bladed weapons as well as blunt projectiles^{3,4}. Nanotechnology researchers have shown the importance of shape to plasmonic and optical response of quantum dots and other particles⁵. Despite these powerful

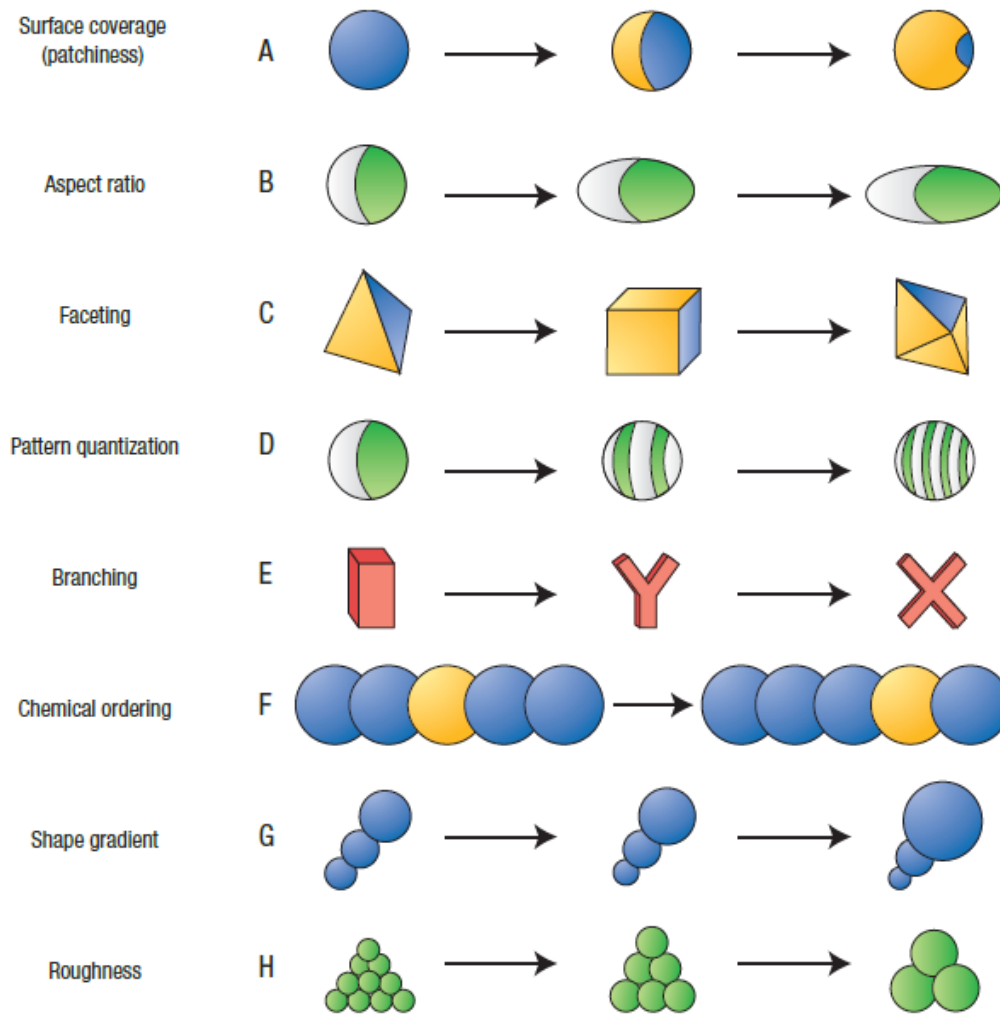


Figure 2.1: Overview of the taxonomy of shape showing the complexity and possibility of function offered by shape control. Reproduced from¹, 2007.

breakthroughs, recent work has shown even more exciting possibilities for particle shape and its control.

Particle shape is now known to be able to profoundly affect biological response, a purely physical mechanism of governing complex biochemical processes. Champion and Mitragotri⁶ showed that removal of foreign particles by phagocytosis is controllable by tuning the aspect ratio of the particle. The mechanism is exciting because it suggests the ability to create delivery systems with more persistent access

to an organism without being removed by its immune system. Delivery of such particles is usually via some flowing fluid, allowing particle shape to offer secondary benefits such as enhancing particle trajectory to aid in targeting delivery⁷.

2.2 Characterisation of Shaped Particles

Particle characterisation has historically focused on on the size and size distribution, and statistically significant measurements have been obtained using, for example, light scattering techniques⁸. While the theory of particle scattering is relatively well-understood for spherical shapes, more complex shapes can limit characterisation.

Rheo-optical and flow microscopy methods have also been used to study the effect of particle aspect ratio on the rheology of a fluid⁹. Rheo-optics extract simultaneous rheology and scattering signals from a suspension, allowing average measurements of particle aspect ratio, polydispersity, and orientation^{10–12}. Microscopy can directly represent shape as well as size, but can be less useful for collecting large numbers of measurements. Electron microscopy works well for sub-micron particles, but can be limited due to the method's sample preparation requirements, especially for lipid particles¹³. Brightfield and confocal microscopy is a useful compromise for particles above a micron in size, as they allow easier sample preparation and can reveal structural and three-dimensional details when combined with fluorescent tagging.

2.3 Shaped Particle Raw Materials

The choice of particle raw material will depend on many factors, influenced strongly by cost and application. Inorganic materials have been widely studied as a source of controlled shape particles, as their molecular crystalline symmetry is a rich source

of structure. Materials like carbon, silver, gold, and silicon¹⁴ have been applied in various medical and biological applications¹⁴. The rigidity of inorganic particles, however, limits the range of shapes that can be adopted as well as their ability to exhibit more complex behaviour like stimulus-response.

Soft particles, made of materials like polymers or lipids, offer excellent opportunities to exploit shaped particles as biocompatible carriers or delivery vehicles^{15,16}. Polymeric and lipid materials are advantageous in that many of them are safe for topical, oral, or injection delivery to tissue. Active ingredients can be encapsulated, attached, or dissolved with soft particles, and the flexibility to choose hydrophobic, hydrophilic, or amphiphilic polymers or lipids enhances formulation flexibility. Examples of compatible active ingredients include biomolecules, such as proteins and peptides^{17,18}, inert contrast agents for medical imaging^{19,20}, or surface coatings for substrates like hair or skin²¹. Past goals for active delivery have been controlled or targeted release, but more complex mechanisms are enabled by particle shape²⁰.

2.3.1 Polymer particles

Polymeric materials are versatile and can be tailored to possess multiple physical or chemical properties, including biodegradability and biocompatibility, for use as delivery vehicles²². Depending on the method of preparation, polymers can form micron-scale or nano-scale particles²³ that provide benefits in controlled release, targeted delivery, and biodegradability²⁴⁻²⁶. Polymers can be expensive raw materials, however, limiting their large-scale production capacity and focusing their use for high value-added pharmaceutical or cosmetic actives²⁷.

2.3.2 Lipid Particles

Lipid-based delivery vehicles have existed for decades, normally in the form of lipid capsules and solid lipid particles^{20,28}. A lipid capsule is a solid or semisolid shell

encapsulating a liquid oil core²⁹. Lipid particles are advantageous as they can be manufactured by emulsification of a molten lipid, or a lipid dissolved in solvent, followed by solidification²⁹. Lipid particles enable dissolution of oil-soluble active ingredients and drugs³⁰ and form a solid matrix that protects active ingredients from chemical degradation³¹. Lipid-based particles also offer enhanced bioavailability of some actives, avoiding solvent use in manufacturing. Production of quite small forms of lipid particles is now common thanks to the use of large-scale processes like high-pressure homogenization³¹⁻³⁴, high shear, and solvent emulsification and microemulsification³². Two of the most common techniques for large-scale preparation of solid lipid particles are detailed in Figure 2.2.

As the typical precursor of a lipid particle is an emulsion droplet, surfactants or emulsifiers are necessary for reduction of oil-water interfacial tension and enhancement of the colloidal stability of the resulting particle dispersion^{35,36}. Frequently used surfactants include nonionic surfactants: Tween[®] 20, 60 and 80³⁷⁻⁴⁰; anionic surfactants: sodium lauryl sulfate and sodium glycolate⁴¹⁻⁴³; and some phospholipids^{44,45}. Additives like polyvinyl alcohol, butanol, and decanol are sometimes used to enhance lipid crystallization by surface adsorption effects⁴⁶⁻⁴⁸.

Many actives to be loaded into lipid particles are temperature-sensitive, preventing the use of molten emulsification methods. Cold homogenization methods mostly avoid high temperatures during processing but can still require heat to melt lipids to combine with active ingredients⁸. In such cases an alternative is solvent emulsification, where lipid drug carriers are dissolved into solvent and then emulsified as a solution^{8,49}. Solvent emulsification and evaporation methods can also require less energy and are easily scaled up⁵⁰ but do require additional steps to deal with the solvent used⁵⁰⁻⁵². Chattopadhyay and co-workers used supercritical fluid extraction of a lipid-solvent emulsion system to produce solid lipid particles for

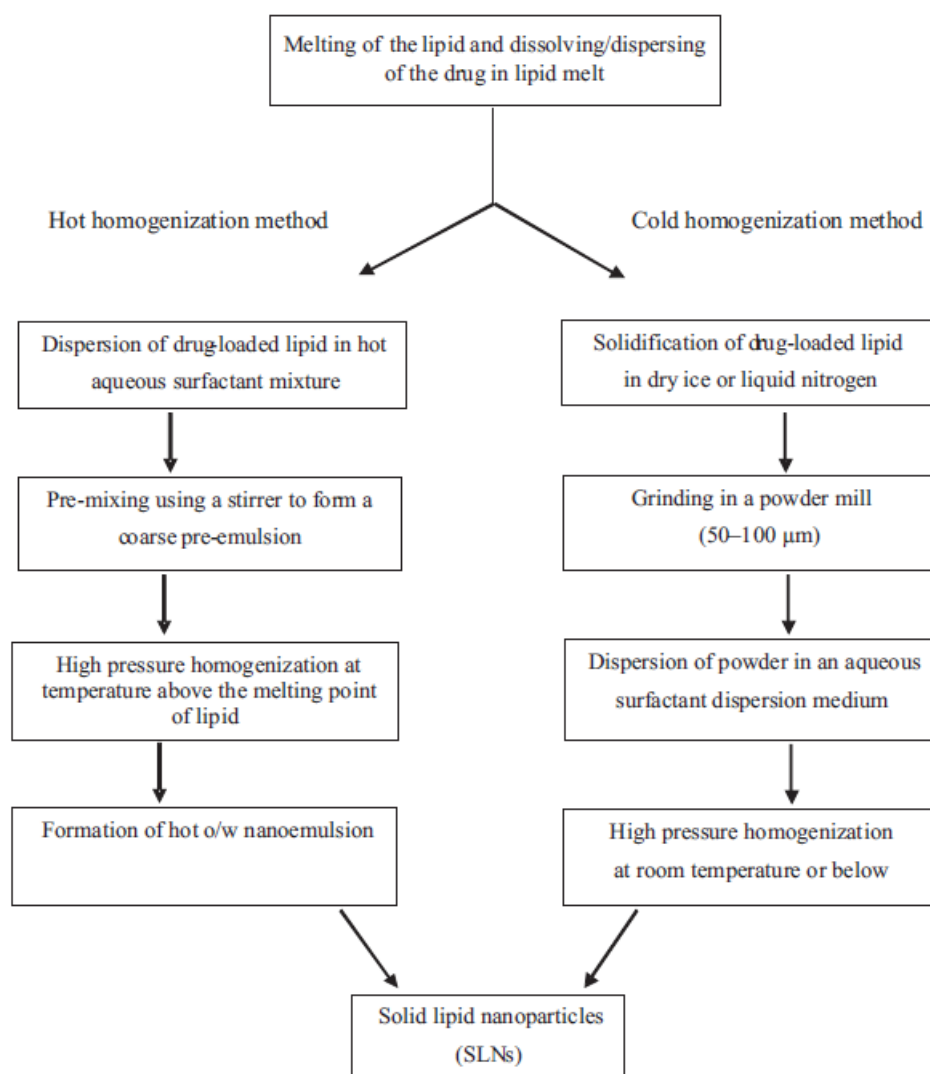


Figure 2.2: Partial listing of representative hot and cold homogenization techniques for preparing solid lipid nanoparticles. Reproduced from Pardeshi et al., 2012.

pulmonary drug delivery⁵³. Shetty and co-workers⁵⁴ also used a lipid-solvent emulsion system to produce lipid particles by aerosol methods. They simulated the relationship between solvent evaporation rate and lipid crystallinity⁵⁴. The above processes could enable large-scale production of lipid particles by solvent-evaporation method or allow the *in-situ* formation of shaped lipid particles by solvent-evaporation method during inhaler or nebuliser use.

Table 2.1: Lipid particle as drug carrier loaded with different drugs

Lipids	Lipid particle preparation technique	Application	Drug	Reference
Glycerol trilaurate and glycerol behenate	High pressure homogenization	Anesthetic	Tetracaine, etomidate and prednisolone	33
Tristearin	High pressure homogenization	Nutrition supplements	Vitamin A, β -carotene and ω -3 fish oil	55
Trimyristin, tripalmitin and tristearin	Hot homogenization	Antipsychotic	Clozapine	56
Glyceryl behenate	Cold high-pressure homogenization	Cancer and neurodegenerative diseases	Rapamycin	57
Glycerol esters	Solvent emulsification/ evaporation	Chemotherapeutic agents	Paclitaxel and Herceptin	58
Glyceryl tripalmitate	Hot homogenization	Antifungal	Clotrimazole	59
Glyceryl behenate	Hot homogenization	Anticancer	Curcumin	60
Myristyl myristate	Hot homogenization with ultrasonication	Antibiotic	Levofloxacin	61
Glycerylmonostearate, glycerol palmitostearate and stearic acid	High-shear homogenization and ultrasound, and high-pressure homogenization	Antibacterial	Rifampin	62
Glyceryl behenate	Hot self-nanoemulsification	Antiretroviral	Lopinavir	63

2.4 Shaped Particles for Controlled Delivery

2.4.1 How Shaped Particles Affect Delivery

Typically delivery application use spherical carriers, though recently the use of non-spherical or shaped particles has shown a potential beneficial influence. The shape of particles significantly affects their transportation properties in fluids, as well as the particles' adhesion in blood vessels and target cells^{6,64}. In delivery vehicle design, the capacity of drug loading, release rate, and targeting efficiency are all considered. Geng and co-workers designed worm-like micelles with bigger core volumes than spherical drug delivery carriers, increasing capacity of hydrophobic drug molecules⁶⁵. Self-assembled lipid tubules, Figure 2.3, have been investigated as sustained release vehicles of proteins and nucleic acids enabling targeted delivery⁶⁶. The hollow, open-ended microtubules can release active ingredients through their ends⁶⁷, providing sustained release over time periods of eight days⁶⁷.

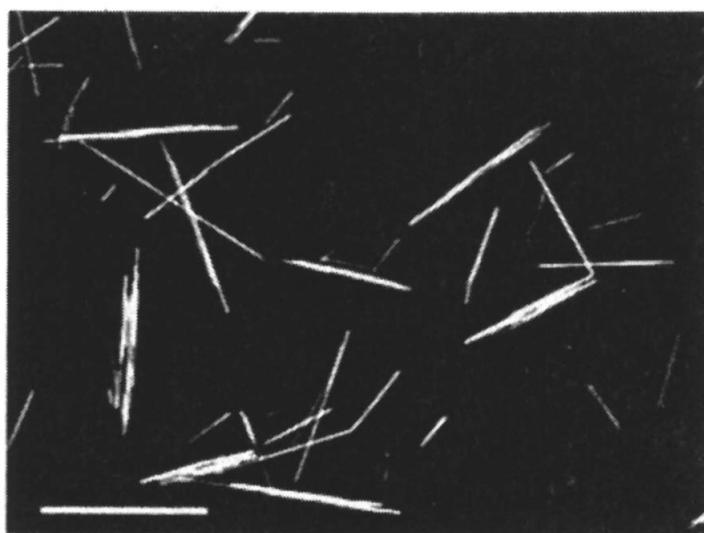


Figure 2.3: Light micrograph of lipid microtubules. Scale bar=50 μ m. Reproduced from Svenson, 2004.

Advantages of non-spherical particles for delivery can also extend to the cellular level. For example, particle shape can affect the body's ability to remove a foreign particle via phagocytosis. Depending on the process active ingredient, it might be desirable for the delivery vehicle to target a macrophage or to escape removal by a macrophage⁶⁹. Particle shape, and specifically curvature, is now known to affect phagocytosis and uptake by macrophages, allowing control over internalization of injected materials^{6,69}. Thus, when designing a shaped particle drug carrier, we need to consider how this shape will affect the phagocytosis.

2.4.2 Stimulus-response by Particles for Controlled Delivery

Two main types of stimulus are typically used in controlled release settings: chemical and biological. Examples of triggers include urea, glucose, and pH. Physical stimuli, such as temperature, magnetic fields, and light (Figure 2.4) can also trigger particle response. Normally, chemical and biochemical stimuli are endogenous, as pH change or ionic microenvironments often exist at specific targeted sites in the body, while physical stimuli are often exogenous, and can be provided through fields external to the body such as use ultrasound or light sources¹⁴.

Response has been designed in multiple drug delivery carriers, including nanoparticles, liposomes, micelles, and non-gels (Figure 2.5). The application of stimulus response is potentially quite broad. Thermoresponsive hydrogels have been used as a controlled drug release system for Docetaxel, a cancer therapy⁷¹. A second material enabled thermosensitive *in situ* gel-formation that provided ocular drug delivery⁷². Caggioni et al. developed a thermoresponsive rod-shaped droplet, made of hexadecane and petrolatum, that can collapse to nearby surfaces and remain there due to the enhanced contact areas, leading to enhanced deposition and retention

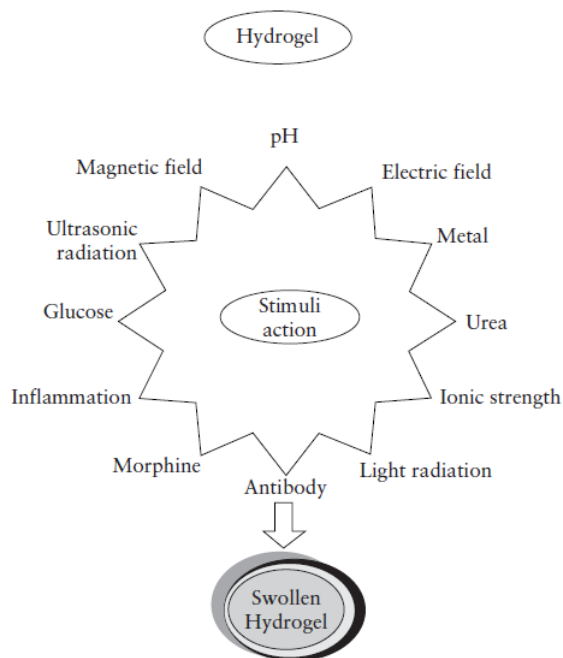


Figure 2.4: Different types of controlled release stimuli for hydrogel drug delivery systems. Reproduced from Misra, 2014.

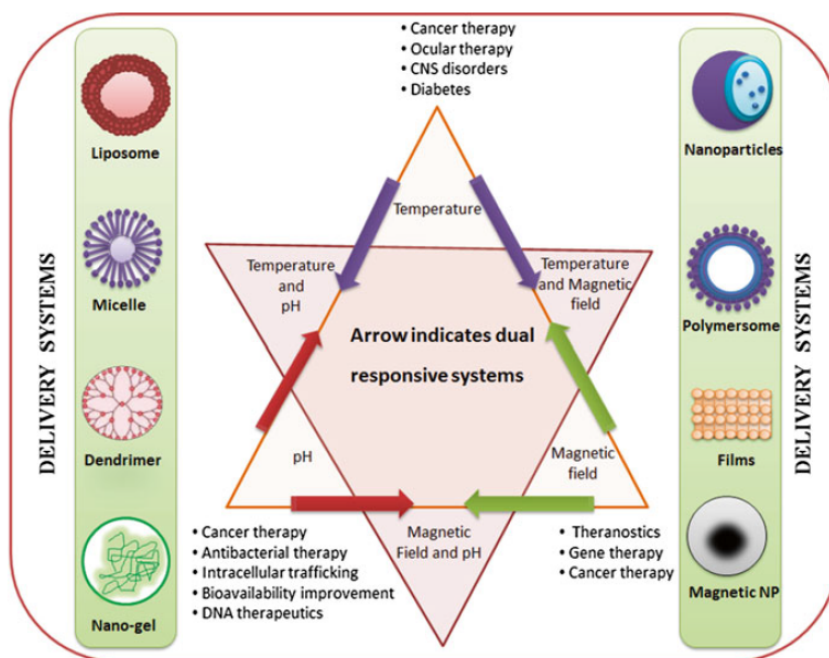


Figure 2.5: Stimulus-responsive drug delivery carriers. Reproduced from Devarajan et al., 2015.

on substrates⁷³. Other stimuli, such as changes in interfacial tension via dilution, can cause similar response when used in consumer products like shampoos⁷⁴.

2.4.3 Anisotropic Particles in Flow

Compared to spherical particles, shaped particles have unique transport properties in flows like the human circulation system¹⁹. Computational studies illustrate that higher aspect ratio particles have different trajectories in blood flow versus spheres⁷⁵ as they can more readily move toward vascular walls versus spherical particles (Figure 2.7). Black and co-workers found that gold nanorods and cubic nanocages could penetrate into a solid tumour's core, however more spherical gold nanoparticles and nanodiscs remained on the surface of the tumour⁷⁶.

Studying the flow properties of anisotropic particles can provide benefits for multiple applications: from mimicking flow in biological fluid streams to enhancing the ability to select and separate particles by shape⁷⁷⁻⁸¹.

A common approach to describing anisotropic particle motion in a flow is via Jeffery orbits⁸². Jeffery's theory describes an elongated spheroid particle's rotational period as a function of its aspect ratio⁸² and its delay relative to spheres. There are a number of applications requiring an understanding of how particles behave in the vorticity field of a shear flow. For example, the flow of red blood cells is affected by the level of shear stress present⁸³ and can be used in small-scale microfluidic channels to perform cell separation⁷⁷ (Figure 2.6). Rheology of a fluid can also affect particle Jeffery orbits, as elasticity in a fluid can cause drift in a particle's orbit⁹. Anisotropic particles can also aggregate when fluids have strong normal stress effects as they more strongly orient⁹. The rotational behaviour of more complex shapes has not been examined in great detail, though there have been exciting results showing the ability to engineer particle trajectories using shape⁷.

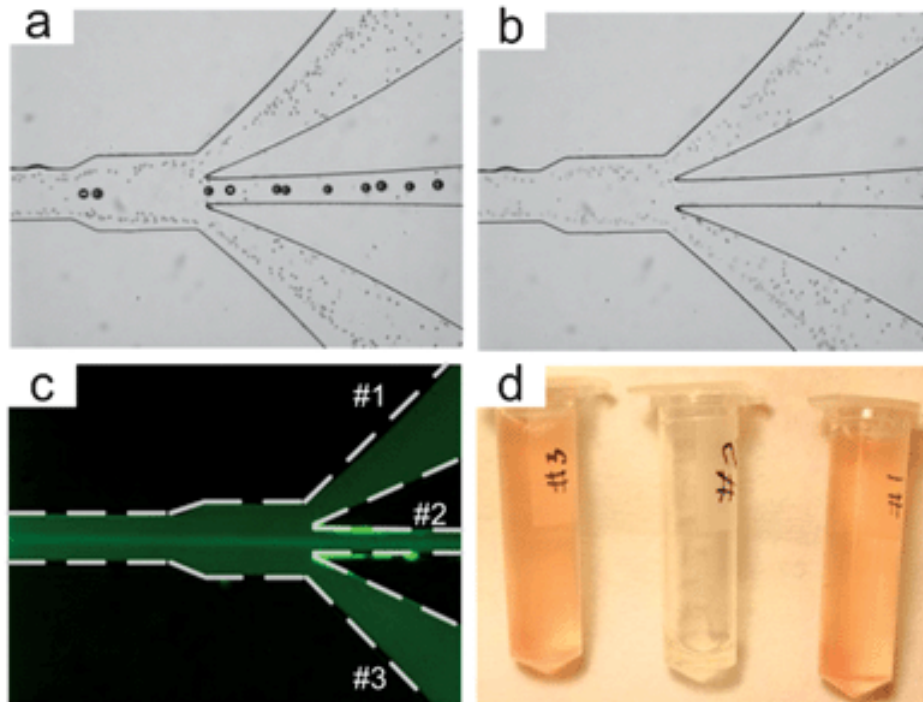


Figure 2.6: Separation by microfluidic device according to particle's size and shape. *a.* 20 μm particles separating from diluted blood. *b-d.* HPET cells separating from blood. Reproduced from Zhou et al., 2013.

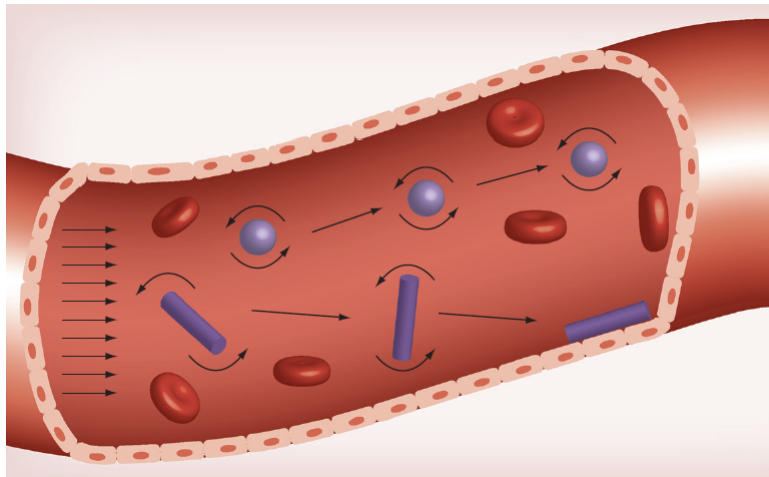


Figure 2.7: Schematic of different shapes of particles in blood flow. Reproduced from Toy et al., 2014.

2.5 Interfacial Shaping and Surfactant-induced Flows

2.5.1 Surfactant Adsorption

Surfactants are as surface active agents, as they can lower the tension at liquid-liquid, liquid-gas or liquid-oil interfaces⁸⁴. Surfactants have been widely used in cosmetics, foods, pharmaceuticals, and coatings formulations. There are many natural surfactants, such as proteins and monoglycerides that act to adsorb to and stabilise interfaces in seawater, dairy milk products, and the bile salts the human body uses for food digestion^{84,85}.

Surfactants are amphiphilic molecules, meaning they have a hydrophilic head and a hydrophobic tail⁸⁶. When surfactants are dissolved in aqueous solution, their lowest energy state is generally to be positioned at an interface so that their orientation minimises contact of its hydrophilic group with any hydrophobic phase present, for example air⁸⁷. As the surfactant concentration in the aqueous solution increases, the air-water interface will eventually fill up with surfactant molecules, leaving more in the aqueous solution. These molecules can then reduce their free energy by forming aggregates called micelles and this transition state is characterised by the critical micelle concentration (CMC), (Figure 2.8). While surfactant molecular adsorption increases, the interfacial tension is decreased due to increased packing of the interfacial molecules. Once the CMC is reached, the interfacial tension is no longer reduced because the interface has become saturated. Plots like the one in Figure 2.8 can thus be used to determine the amount of adsorption and the CMC of a given surfactant system. If surfactant concentration is increased beyond the CMC, the shape and structure of the micelle can often change. In Figure 2.9 a schematic of the most common micelle shapes and is shown structures. Increasing the concentration requires the surfactants to change their packing to accommodate

energetic considerations, and shapes can vary from spherical micelles, to cylindrical micelles to bilayered structures⁸⁶.

Surfactants are critical for many practical efforts to modify interfacial properties, and their effects can have significant impact at length scales much larger than molecular scales. Interfacial tension, its interaction with other physical forces, and its modification by changing environments, can provide numerous opportunities to engineer and optimise emulsions and other dispersions.

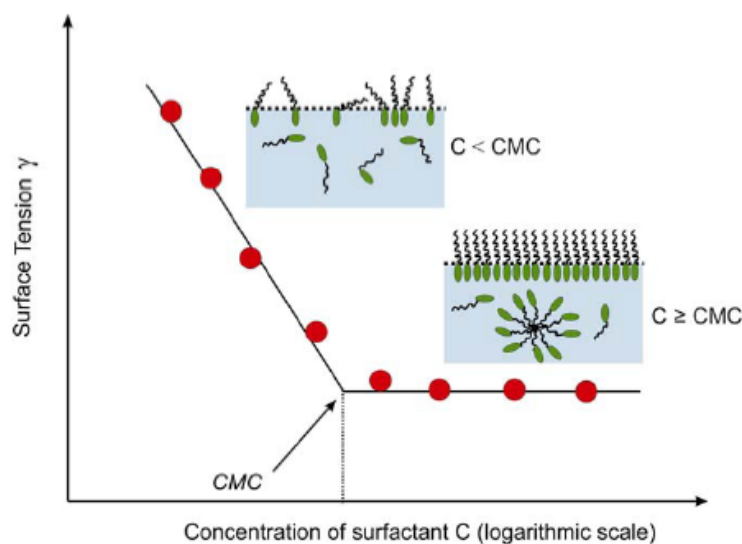


Figure 2.8: Illustration of the surface tension changes as a result of surfactant adsorption as concentration is increased. The critical micelle concentration, as well as the packing density, of a surfactant can be determined from this type of plot. Reproduced from Quijada and Marileth, 2010.

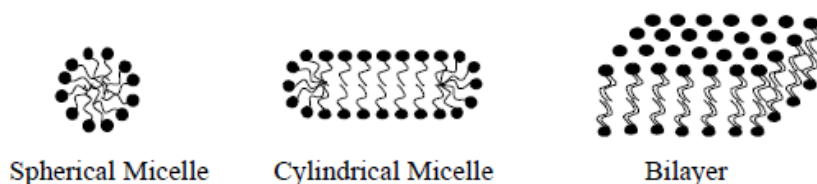


Figure 2.9: Schematic of the three most common shapes and structures of surfactant micelles in aqueous solution. Reproduced from Rangel-Yagui et al., 2004.

2.5.2 Anisotropic Droplet Shapes via Arrested Coalescence

Interfacial forces in emulsions typically drive droplets to adopt spherical shapes in order to minimise surface energy. However, droplets with sufficient rheological elasticity can offset interfacial forces and adopt stable, non-spherical shapes. The partially crystalline milkfat droplets studied by Boode and Walstra are an example of such behaviour as they exhibit what is known as arrested coalescence. Coalescence is arrested when two or more oil droplets initiate, but do not finish coalescence because droplet elasticity resists deformation, forming a stable anisotropic shape^{89–94}.

Arrested coalescence concepts were used to develop a range of elongated droplets via microfluidic moulding^{95–97}. In addition to holding moulded shapes while retaining a liquid surface, the endoskeletal droplets can change shape in response to temperature^{73,95} and interfacial tension⁷⁴ changes that upset the balance between interfacial tension and internal elasticity.

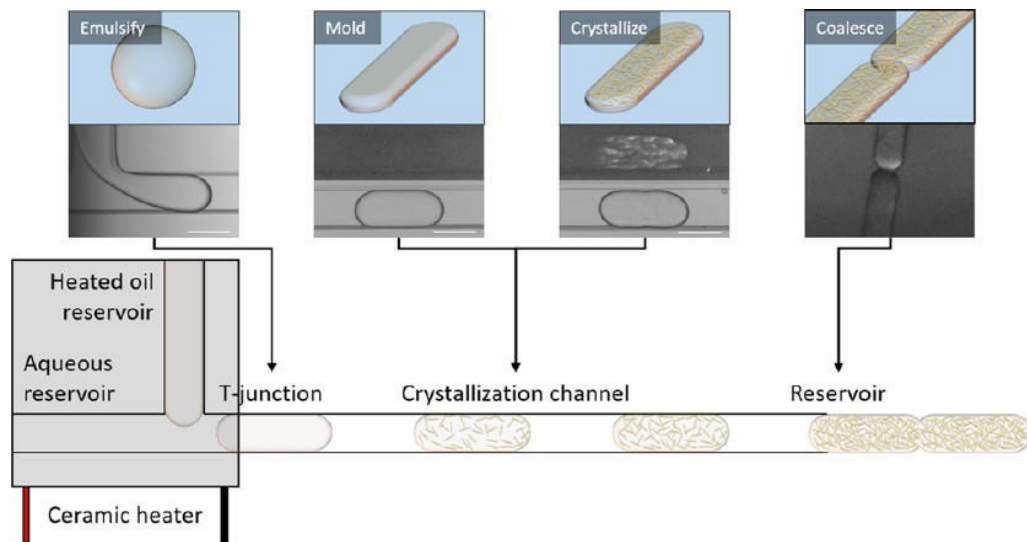


Figure 2.10: The process of making shaped endoskeletal droplets by moulding in a microfluidic device. Reproduced from Prileszky and Furst, 2016.

The above examples demonstrate the power of interfacial forces to dictate shape of complex liquid interfaces. Such effects are often not as permanent or scaleable,

however, as other techniques where interfacial forces act to sculpt particle shape during solidification.

2.5.3 Rotator Phase Droplet Shapes

The above examples showed how droplet shape can be controlled by balancing interfacial tension forces with internal viscoelastic response. A similar phenomenon can occur when the interfacial rheology of a droplet offsets interfacial tension. One example is when adsorbed colloids, forming a Pickering emulsion, arrest an interface during coalescence and arrest the structure in an anisotropic shape⁹⁸.

Some alkane droplets can perform a similar feat without added colloids by forming an elastic structure at their interface, called a rotator phase⁹⁹. As rotator phases form with crystalline symmetry, they provide both stabilisation and shape regularity. This rotator phase phenomenon occurs during the cooling process would attribute, enabling self-shaping of an oil-in-water emulsion into different shapes through a progression like sphere→polyhedron→hexagonal platelet→tetragonal or triangular platelet→rod or fibre¹⁰⁰(Figure 2.11A). The metastable shape can be frozen into a solid particle at any state¹⁰⁰. Some optical micrographs in Figure 2.11B-E show the evolution of such a transformation.

This mechanism of rotator phase shaping of an emulsion droplet can be explained by Figure 2.12. A thin layer of a hydrocarbon plastic rotator phase with thickness of h_{PL} forms due to surface freezing of the surfactant adsorption layer when the temperature is close to the melting temperature of the alkane. The plastic phase provides a large enough bending force to overcome the hydrocarbon-water interfacial tension, stabilising non-spherical shapes^{99,101,102}. Not all surfactant-alkane systems form such structures, and these systems require the length of the surfactant tail match or be slightly longer than the alkane tail¹⁰⁰.

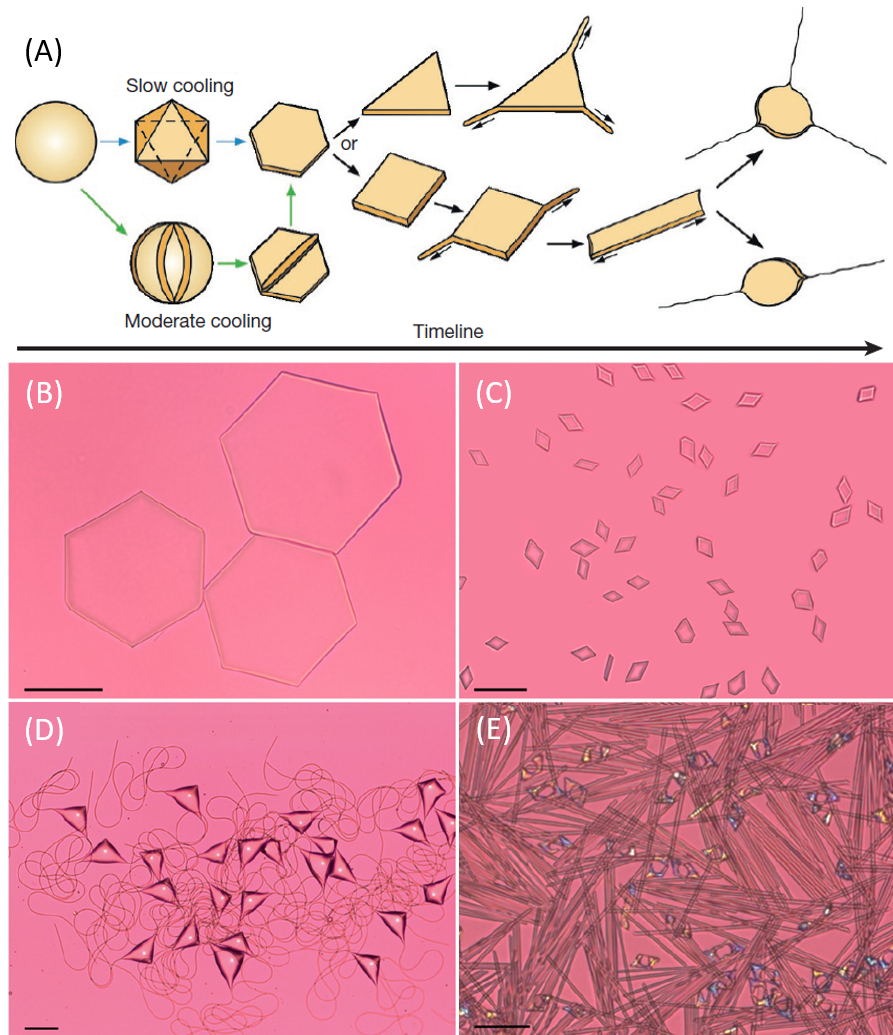


Figure 2.11: A. The schematic of a spherical emulsion in a surfactant solution transforming into different shape stages; B. hexagonal platelets; C. parallelograms; D. droplets with long tails; E. rods in coexistence with frozen parallelograms of toroidal topology. Scale bars are 50 μm . Reproduced from Denkov et al., 2015, and Cholakova et al., 2016.

From Figure 2.12C, we can see the plastic phase is forming a 'frame' at the edge of the droplet. Upon cooling, as more and more alkane molecules enter the protruding rod, the 'frame' will further stretch and form a toroidal shape¹⁰³. Further stretching will cause a breakage of the thin film, Figure 2.12C, into smaller emulsions. This phenomenon can be applied to form a large number of ultra-small emulsion droplets, ~ 300 nm in radius, without additional dispersion energy input¹⁰³.

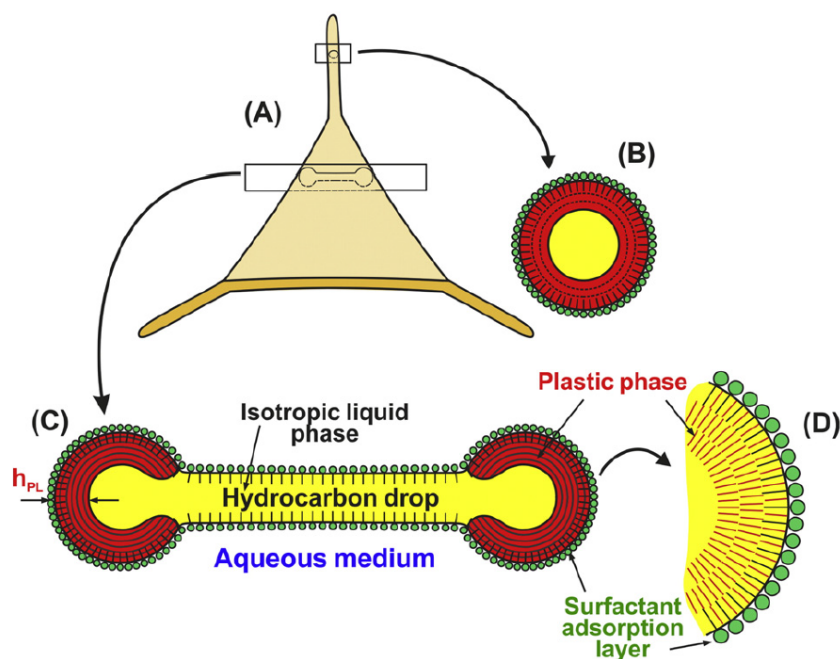


Figure 2.12: A. A triangular platelet with thin protrusions at its vertices; B. the cross-section of a rod, the red part is the plastic phase, and the yellow part is the liquid oil phase, and green part is the surfactant adsorption layer; C. the cross-section of the triangular platelet body; D. the arrangement of the surfactant tails and alkane molecules in the plastic phase, the surfactant tails are in black and the alkane molecules are in red. Reproduced from Cholakova et al., 2016.

Rotator phases can have strong influences on droplet shaping as driven by crystalline ordering patterns in the surface phase. More significant shaping often requires more dramatic stress magnitudes and additional mechanisms to expand the shapes produced.

2.5.4 Marangoni Flow

In emulsions, surfactant is often used to stabilise droplets against aggregation or coalescence, as in Figure 2.13. The surfactant molecules pack at the oil-water interface and lower the tension as they increase in concentration. Any gradients in concentration, then, will cause a tension pulling at an interface from high to low

concentrations, known as Marangoni stresses⁸⁴. The resultant Marangoni flow can strongly influence interfacial hydrodynamics⁸⁴.

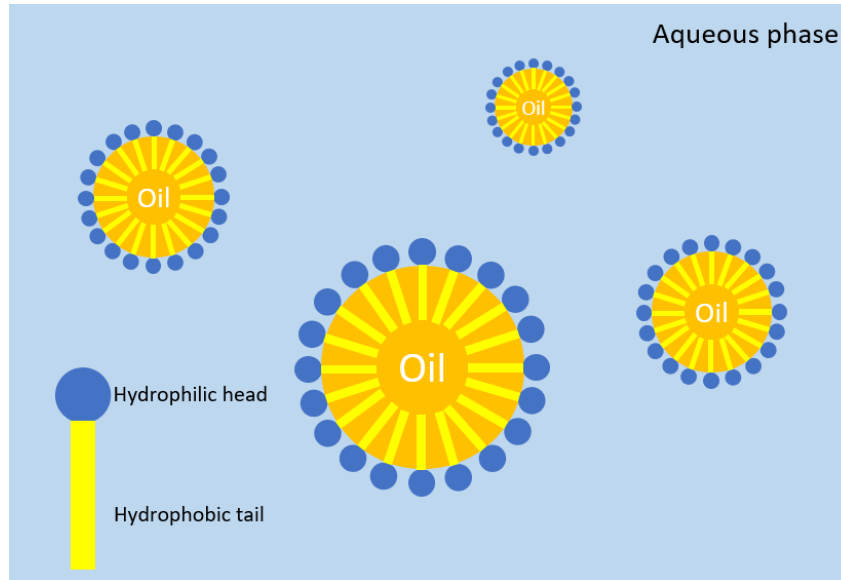


Figure 2.13: Schematic of surfactant molecules packing at an oil-water emulsion droplet interface.

An example of such a surfactant gradient is shown in Figure 2.14A, where an emulsion droplet in low Reynolds number flow has more surfactant molecules at its rear than its front, causing an interfacial Marangoni flow. In Figure 2.14B, an oil-in-water droplet can be induced to propel itself as a result of interfacial Marangoni flows. In this case the interfacial gradient is the result of solubilisation of the oil by surrounding micelles that deplete one side of the droplet more than the other^{104,105}. Once the droplet starts to move, the continuous contacting of new micelles with the leading edge of the droplet sustains its movement and leads to swimming behaviour in the aqueous solution^{104,105}.

2.5.5 Sculpting particle shape by interfacial hydrodynamics

Synthesis of shaped particles requires some driving force to mould or sculpt the particle into a desired form. However, the small length scale required for accurate

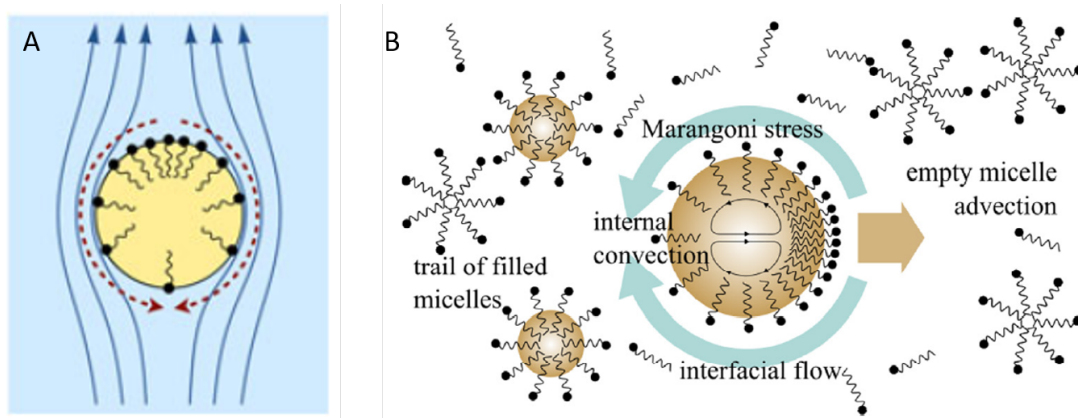


Figure 2.14: A. Schematic of the Marangoni stress caused by an interfacial concentration gradient of surfactant molecules. The solid blue arrows are the direction of the flow, and the red dashed line is the Marangoni flow direction. B. A self-swimming droplet driven by Marangoni stress caused by soubilisation. Reproduced from Manikantan and Squires, 2020 and Jin et al., 2018

moulding often restricts the ability to apply a process at large scales. For that reason, we are particularly interested in new ways to sculpt particle shape without sacrificing scaleability.

Solids are often the best at holding a shape once made, and many polymeric and metallic materials have been used. As mentioned earlier, we choose to focus on lipid particles for their advantages in cost, safety, and flexibility.

Oil-in-water emulsions are widely used in multiple material sectors, enabling processing of a dispersion rather than a bulk material. Early studies of such systems were in food contexts, as most dairy products are emulsions of milkfat, with partially crystalline fractions present that make the droplets rheologically complex^{88,106,107}.

Almost three decades ago, Boode and Walstra observed that in emulsions of triglyceride in aqueous SDS solution, oil droplets grew crystals that extended beyond the droplet boundary due to dewetting⁸⁸. Earlier work exploited the technique to purify fats by physical separation of the higher melting fractions⁸⁸. Boode and

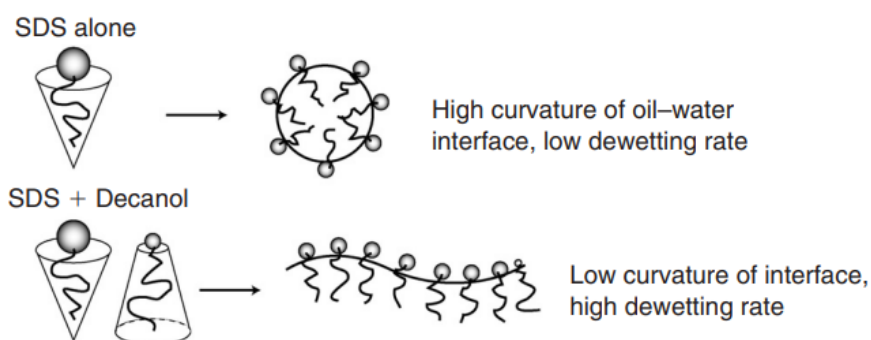


Figure 2.15: Schematic of using co-surfactant in a surfactant system to lower curvature at an oil-water interface. Reproduced from Spicer and Hartel, 2005.

Walstra noted that elongated solids were sometimes formed when dewetting effects were significant, but did not study the actual formation in detail.

Spicer and Hartel⁴⁷ investigated the production of elongated lipid particles using rapid dewetting phenomenon that occurred on the same time scale as the lipid droplet crystallization process. They modified the surfactant molecular packing geometry by adding co-surfactant (decanol) to increase surfactant (SDS) interfacial packing efficiency, increasing the dewetting rate enhance the dewetting and elongation that occurred, Figure 2.15.

Particle morphology was shown to be a function of the relative dewetting and crystallisation rates⁴⁷. Crystals could be produced that were smaller than, equal, to, or larger than the size of the starting droplet by tuning dewetting rate to be, respectively, higher, insignificant, or equal relative to the crystallisation rate⁴⁷. This thesis builds on these initial studies to explore the broader use of dewetting coupled with emulsion crystallisation to synthesise elongated lipid particles. This study not only give us a novel approach to design crystal's shape, but also important to study the stability of emulsion products, such as dairy products and drug carriers¹⁰⁸⁻¹¹⁰.

2.5.6 Formation of Shape Gradients by Crystallization Instabilities

Liquids solidified into crystals can have different morphologies, but are often constrained by their molecular crystallographic orientations. More complex shapes can, however, be produced by instabilities that occur due to interactions of thermal and interfacial forces¹¹¹. Banding or spiral structures can occur when crystal radii rotate or twist their orientation as a result of chirality or surface stresses¹¹² (Figure 2.16a-c).

Polymeric systems can also exhibit oscillatory structures due to competing volatility and solidification¹¹³. Concentric-ringed structures in organic crystals can be formed by density changes in during the liquid-solid transition phase¹¹³. When energy dissipation during crystallization becomes periodic¹¹⁴, dendrite structures can form. Examples like Figure 2.16d resemble snowflake shapes. Anisotropy of a crystallising film's surface energy can interact with a substrate¹¹⁵ and cause instabilities flow and solidification oppose one another¹¹⁶.

The mechanisms discussed above enable production of interesting shapes possessing gradients in shape. Shape gradient structures have not been sought or produced much in colloidal systems, but were part of the taxonomy discussed in Figure 2.1 and we explore their production in later chapters, having established that crystallisation instabilities can produce them.

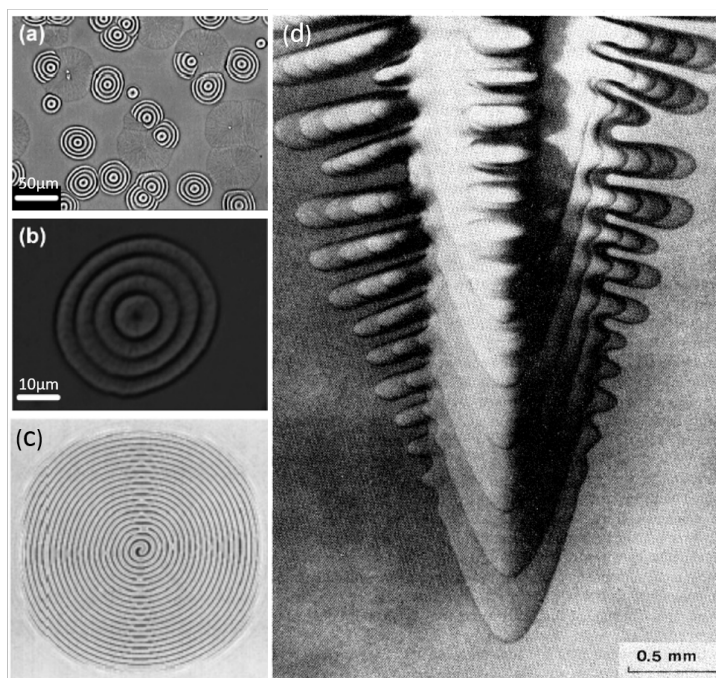


Figure 2.16: *a& b. Banded structure. c. spiral structure. d. dendrite structure. Reproduced from Wang et al., 2006, and Kyu et al., 1999, and Langer, 1980.*

2.6 Drug Incorporation in Lipid-based Delivery Vehicles

Often shaped particles are envisioned as carriers for active ingredients in commercial medical or cosmetic formulations. While shape is beneficial for desirable traits like delivery and retention, the resultant particles must also be compatible with the active ingredients.

For example, lipid-based drug carriers are quite compatible with lipophilic drugs, such as corticoids and immunosuppressants¹¹⁷, and some examples are listed in Table 2.1. The crystalline nature of solid lipid particles allows only limited space for active loading, allowing lower than 5-10 %¹¹⁷ and can often be overestimated^{117,118} or unclear due to lipid-active interactions¹¹⁹. Localisation of active in a single lipid particle has a significant impact on active release properties^{117,119,120} and can be

studied via techniques like fluorescence imaging¹²⁰. Figure 2.17 shows several schematics of possible active ingredient locations in lipid particles.

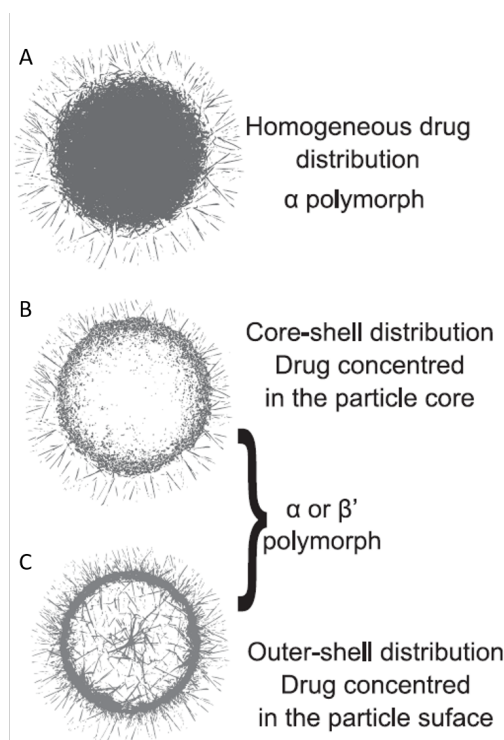


Figure 2.17: Different locations of active ingredients in lipid particles. A. Distributed uniformly; B. Core-shell structure distribution; C. Outer-shell structure distribution. Reproduced from Gordillo-Galeano and Mora-Huertas, 2018.

Temperature of preparation affects localisation of actives in lipid particles¹¹⁹ as lipids are often prepared in the molten state, and higher temperatures can alter the active ingredient's partitioning between the lipid and aqueous phases¹¹⁹. Different localisations and morphologies can result during a synthesis process, varying between homogeneous active distribution to core-shell forms in the lipid particles (Figure 2.17 A-C)^{33,119}.

Other than mixing active molecules with lipid before forming particles, surface coating is also an option. For example, hyaluronic acid (HA) can be coated onto lipid particles or liposomes by electrostatic attraction^{121,122} and can sometimes pro-

vide improved adhesion and efficacy^{121,123}. Polydopamine (PDA)-coated liposomes and lipid particles can exhibit enhanced drug loading and respond to pH and ultrasonic stimuli^{124,125}.

Although active ingredient encapsulation by lipid particles remains an active area of research, it is also the basis for a number of large-scale commercial processes in industries like foods and pharmaceuticals. Most of these processes still focus their development energy on controlling variables like size and purity, but we expect shape to increasingly become a target control variable and quality criterion. It is useful to survey the work done on scale-up of particle synthesis processes in these areas to determine the feasibility of particles like the ones we hope to develop.

2.7 Scale-up of Shaped Particle Production

Producing lipid particles via hot emulsification is quite simple at the lab scale. As such a process moves to larger systems, the transfer of mass, heat and momentum can behave differently¹²⁶ and can impact the speed at which a new lipid carrier can be applied in, for example, pharmaceutical processes¹²⁷. Lipid carrier particles have been used for decades and scale-up of their production has been studied widely^{128,129}.

Large-scale production of lipid particles from emulsion processes requires strong energy input to maintain dispersion and help set particle size. A common approach is high-pressure homogenization, and a schematic example is shown in Figure 2.18. In such a device, hot emulsion transfers to a feed container and 200 - 800 bars of pressure is used to push the hot emulsion through a piston gap to homogenize the lipid into smaller and homogeneous emulsion droplets. Scales can be as large as 60-150 L/h and the systems are often run in parallel^{130,131}.

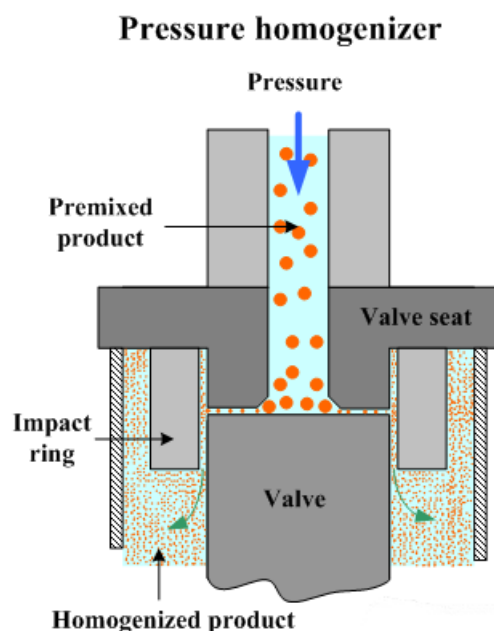


Figure 2.18: Schematic of a piston-gap high-pressure homogeniser. Reproduced from Al-Kassas et al., 2017.

Production of homogeneous lipid particle size distributions by homogenisers requires tuning of the applied pressure and orifice gap¹³⁰. Temperature also plays a role as it will set the rheology and interfacial tension that can offset the energy input for dispersion¹³¹. Despite the effectiveness of existing industrial processes for controlled particle production, most of these systems are optimised for size control and could actually be detrimental to unusually-shaped particles. Control of shape will require approaches that embrace both processing equipment and careful control of formulation variables.

Particles with more complex structures or shapes are challenging to produce in larger quantities. For example, Janus particles have dual surface chemical properties (Figure 2.1 and are often produced by microfluidic devices^{133,134}. When colloidal and chemical self-assembly are exploited, particles with Janus and other structures can be produced in ways that enable scale-up using existing processes for dis-

persion and emulsification¹³⁵⁻¹³⁸. For example, self-assembly of large quantities of silica-covered Janus wax particles was demonstrated by Pickering emulsification¹³⁹, Figure 2.19.

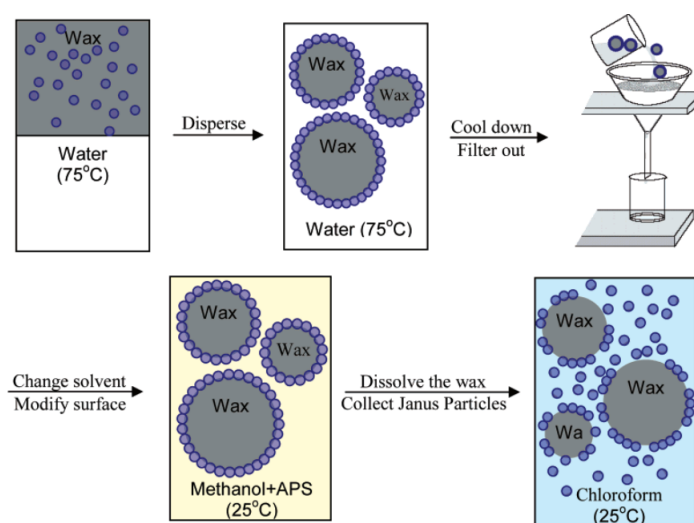


Figure 2.19: A simple method to produce large quantity of Janus particles. Reproduced from Hong et al., 2006.

We have shown several examples where shaped lipid particles could be of use for delivery applications. In our research, we can produce elongated shaped lipid particles with controlled size distribution in bulk. The process used to prepare shaped lipid particles is simple, including only mixing, heating, and controlled cooling. Heating bulk raw materials is easily achievable for large-scale production, as is emulsification by milling and bulk cooling via heat exchanger use. Proper choice of surfactant concentration and cooling rate can then be used to adjust the distribution of elongated shapes produced by the process.

2.8 Simulating the Crystallisation of an Elongated Particle

The shaped particles can be produced in a relatively simple process. However, shape can vary a lot and we need a systematic framework to use to determine optimal conditions for manufacturing shaped particles in practice. We therefore use a specific model to simulate the growth of an emulsion droplet and predict the effect of different conditions on shape.^{140,141} Anderson and coworkers used a mathematical model to simulate liquid solidification as a function of conditions at the tri-junction of the solid, the melt and the surrounding vapour.¹⁴¹ They introduced their theoretical model with different features (Figure 2.20). One of the important features is the growth angle Φ_i , the angle between the tangents to the solid-vapour and liquid-vapour interfaces at the tri-junction¹⁴¹. This theoretical model inspired our previous work on modeling the growth of an emulsion droplet solidifying in aqueous system to an elongated particle¹⁴⁰ (Figure 2.21).

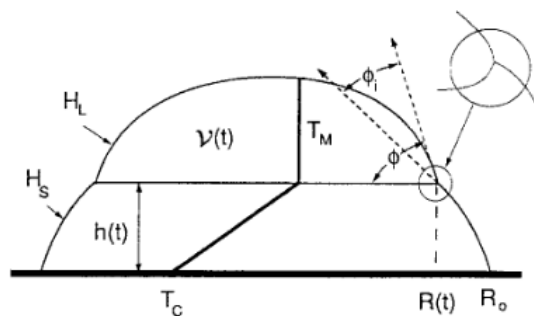


Figure 2.20: A schematic diagram showing the theoretical model used to describe how a liquid droplet solidifies. Reproduced from Anderson et al., 1996

In Figure 2.21, the growth angle Φ_g is the angle between contact angle Φ and angle Φ_{sv} , which is the angle between the solidbackground tangent at the three-phase contact line and the solidification front¹⁴⁰. This growth angle is indicating

2.8. Simulating the Crystallisation of an Elongated Particle

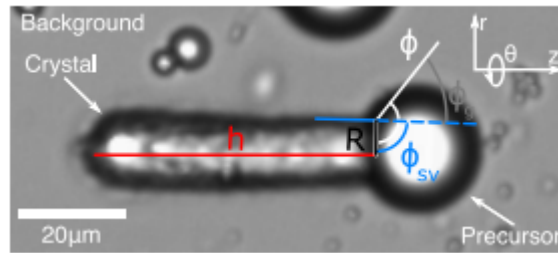


Figure 2.21: A schematic diagram showing the geometric model parameters. Reproduced from Giso et al., 2020

the growth direction of the liquid precursor¹⁴⁰. In this research, we introduced the relationship between the height (h) of the crystal, and the radius (R) of the solidification front to the growth angle Φ_g . In Figure 2.22 shows the results of the crystals formed with fixed growth angles or dynamic growth angles. The research showed good agreement between the geometric model and experimental results.¹⁴⁰

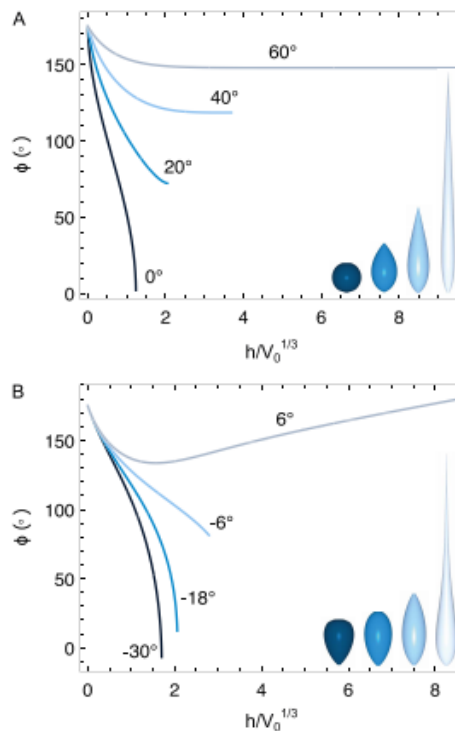


Figure 2.22: Simulation results for the crystals formed with (A) fixed growth angle and (B) dynamic growth angle. Reproduced from Giso et al., 2020

2.9 Conclusion

This review demonstrates the importance of shaped particles in different applications, and introduced different methods to produce these particles both in the laboratory scale and industrial scale. We emphasised the using the emulsification system on producing elongated lipid particles during their crystallization. Along with the interfacial crystallization method, relative phenomena such as rotator phase and Marangoni flow has been discussed. Furthermore, this review discussed the interfacial hydrodynamics theory and included information about using these shaped lipid particles as a drug carrier and their potential in the scaled-up industry.

References

- [1] S. C. Glotzer, M. J. Solomon, *Nature materials* **2007**, 6, 557–562.
- [2] F. B. Neal, J. C. Russ, *Measuring shape*, CRC Press, **2012**.
- [3] R. G. Egres Jr, M. J. Decker, C. J. Halbach, Y. S. Lee, J. E. Kirkwood, K. M. Kirwood, N. J. Wagner, E. D. Wetzel, *Composites Science and Technology* **2007**, 67, 565–578.
- [4] R. G. Egres, N. J. Wagner, *Journal of Rheology* **2006**, 50, 685.
- [5] A. Tao, P. Sinsersuksakul, P. Yang, *Nature Nanotechnology* **2007**, 2, 435–440.
- [6] J. A. Champion, S. Mitragotri, *Proceedings of the National Academy of Sciences* **2006**, 103, 4930–4934.
- [7] W. E. Uspal, H. Burak Eral, P. S. Doyle, *Nature Communications* **2013**, 4, 1–9.
- [8] C. Pardeshi, P. Rajput, V. Belgamwar, A. Tekade, G. Patil, K. Chaudhary, A. Sonje, *Acta Pharmaceutica* **2012**, 62, 433–472.
- [9] D. Gunes, R. Scirocco, J. Mewis, J. Vermant, *Journal of Non-Newtonian Fluid Mechanics* **2008**, 155, 39–50.
- [10] P. L. Frattini, G. G. Fuller, *Journal of fluid mechanics* **1986**, 168, 119–150.
- [11] J. Vermant, H. Yang, G. Fuller, *AIChE journal* **2001**, 47, 790–798.
- [12] J. A. Pathak, S. D. Hudson, *Macromolecules* **2006**, 39, 8782–8792.
- [13] A. Dubes, H. Parrot-Lopez, W. Abdelwahed, G. Degobert, H. Fessi, P. Shahgal-dian, A. W. Coleman, *European journal of pharmaceutics and biopharmaceutics* **2003**, 55, 279–282.
- [14] P. V. Devarajan, S. Jain *et al.*, *Targeted drug delivery: concepts and design*, Springer, **2015**.
- [15] K. K. Jain, *Drug delivery systems, Vol. 2*, Springer, **2008**.
- [16] R. Langer, *Nature* **1998**, 392, 5–10.

References

- [17] H. Mu, R. Holm, A. Müllertz, *International journal of pharmaceutics* **2013**, 453, 215–224.
- [18] M. Lee, T. T. Chen, M. L. Iruela-Arispe, B. M. Wu, J. C. Dunn, *Biomaterials* **2007**, 28, 1862–1870.
- [19] J. Chen, N. E. Clay, N.-h. Park, H. Kong, *Chemical engineering science* **2015**, 125, 20–24.
- [20] J. A. Champion, Y. K. Katare, S. Mitragotri, *Journal of controlled release* **2007**, 121, 3–9.
- [21] M. Clauzel, E. S. Johnson, T. Nylander, R. K. Panandiker, M. R. Sivik, L. Piculell, *ACS applied materials & interfaces* **2011**, 3, 2451–2462.
- [22] J. S. Román, A. Gallardo, B. Levenfeld, *Advanced Materials* **1995**, 7, 203–208.
- [23] S. Svenson in *Advances in particulate polymeric drug delivery*, ACS Publications, **2006**, Chapter 1, pp. 2–11.
- [24] C. E. Mora-Huertas, H. Fessi, A. Elaissari, *International journal of pharmaceutics* **2010**, 385, 113–142.
- [25] E. A. Leite, A. Grabe-Guimarães, H. N. Guimarães, G. L. L. Machado-Coelho, G. Barratt, V. C. Mosqueira, *Life sciences* **2007**, 80, 1327–1334.
- [26] S. Guinebretière, S. Briançon, H. Fessi, V. Teodorescu, M. Blanchin, *Materials Science and Engineering: C* **2002**, 21, 137–142.
- [27] M. Radtke, R. H. Müller, *New Drugs* **2001**, 2, 48–52.
- [28] Y.-q. Zhao, L.-p. Wang, C. Ma, K. Zhao, Y. Liu, N.-p. Feng, *International journal of nanomedicine* **2013**, 8, 4169.
- [29] D. Thassu, Y. Pathak, M. Deleers in *Nanoparticulate Drug Delivery Systems*, CRC Press, **2007**, pp. 21–52.
- [30] P. J. Stevens, M. Sekido, R. J. Lee, *Pharmaceutical research* **2004**, 21, 2153–2157.

-
- [31] V. Jennings, M. Schäfer-Korting, S. Gohla, *Journal of controlled release* **2000**, 66, 115–126.
- [32] W. Mehnert, K. Mäder, *Advanced drug delivery reviews* **2012**, 64, 83–101.
- [33] A. zur Mühlen, C. Schwarz, W. Mehnert, *European journal of pharmaceuticals and biopharmaceutics* **1998**, 45, 149–155.
- [34] S. Jaspert, G. Piel, L. Delattre, B. Evrard, *Expert opinion on drug delivery* **2005**, 2, 75–87.
- [35] A. Leonardi, C. Bucolo, G. L. Romano, C. B. M. Platania, F. Drago, G. Puglisi, R. Pignatello, *International journal of pharmaceuticals* **2014**, 470, 133–140.
- [36] S. Kumar, J. K. Randhawa, *Materials Science and Engineering: C* **2013**, 33, 1842–1852.
- [37] S. Martins, I. Tho, E. Souto, D. Ferreira, M. Brandl, *European journal of pharmaceutical sciences* **2012**, 45, 613–623.
- [38] A. Siddiqui, V. Gupta, Y.-Y. Liu, S. Nazzal, *International journal of pharmaceuticals* **2012**, 431, 222–229.
- [39] P. Severino, S. C. Pinho, E. B. Souto, M. H. Santana, *Colloids and Surfaces B: Biointerfaces* **2011**, 86, 125–130.
- [40] N. Nafee, A. Husari, C. K. Maurer, C. Lu, C. de Rossi, A. Steinbach, R. W. Hartmann, C.-M. Lehr, M. Schneider, *Journal of Controlled Release* **2014**, 192, 131–140.
- [41] B. Clares, A. C. Calpena, A. Parra, G. Abrego, H. Alvarado, J. F. Fanguero, E. B. Souto, *International journal of pharmaceuticals* **2014**, 473, 591–598.
- [42] S. Tan, N. Billa, C. Roberts, J. Burley, *Colloids and Surfaces A: Physicochemical and Engineering Aspects* **2010**, 372, 73–79.
- [43] H. Bunjes, F. Steiniger, W. Richter, *Langmuir* **2007**, 23, 4005–4011.

References

- [44] S. Kheradmandnia, E. Vasheghani-Farahani, M. Nosrati, F. Atyabi, *Nanomedicine: Nanotechnology Biology and Medicine* **2010**, 6, 753–759.
- [45] S. Mukherjee, S. Ray, R. Thakur, *Indian journal of pharmaceutical sciences* **2009**, 71, 349.
- [46] K. M. Rosenblatt, H. Bunjes, *Molecular pharmaceuticals* **2009**, 6, 105–120.
- [47] P. T. Spicer, R. W. Hartel, *Australian journal of chemistry* **2005**, 58, 655–659.
- [48] M. M. Mojahedian, S. Daneshamouz, S. M. Samani, A. Zargaran, *Chemistry and physics of lipids* **2013**, 174, 32–38.
- [49] A. Garud, D. Singh, N. Garud, *International Current Pharmaceutical Journal* **2012**, 1, 384–393.
- [50] G. Yoon, J. W. Park, I.-S. Yoon, *Journal of Pharmaceutical Investigation* **2013**, 43, 353–362.
- [51] L. Battaglia, M. Trotta, M. Gallarate, M. E. Carlotti, G. P. Zara, A. Bargoni, *Journal of microencapsulation* **2007**, 24, 672–684.
- [52] J. Kaur, G. Singh, S. Saini, A. Rana, *Journal of Drug Delivery and Therapeutics* **2012**, 2, year.
- [53] P. Chattopadhyay, B. Y. Shekunov, D. Yim, D. Cipolla, B. Boyd, S. Farr, *Advanced drug delivery reviews* **2007**, 59, 444–453.
- [54] M. Shetty, A. A. Pawar, A. Mehra, C. Venkataraman, *Aerosol Science and Technology* **2012**, 46, 569–575.
- [55] H. Salminen, C. Gömmel, B. H. Leuenberger, J. Weiss, *Food chemistry* **2016**, 190, 928–937.
- [56] V. Venkateswarlu, K. Manjunath, *Journal of controlled release* **2004**, 95, 627–638.
- [57] J. Mazuryk, T. Deptuła, A. Polchi, J. Gapiński, S. Giovagnoli, A. Magini, C. Emiliani, J. Kohlbrecher, A. Patkowski, *Colloids and Surfaces A: Physicochemical*

- and Engineering Aspects* **2016**, 502, 54–65.
- [58] G. Büyükköroğlu, B. Şenel, S. Gezgin, T. Dinh, *Journal of Drug Delivery Science and Technology* **2016**, 35, 98–105.
- [59] E. Souto, S. Wissing, C. Barbosa, R. Müller, *International Journal of Pharmaceutics* **2004**, 278, 71–77.
- [60] K. Vandita, B. Shashi, K. G. Santosh, K. I. Pal, *Molecular pharmaceutics* **2012**, 9, 3411–3421.
- [61] G. A. Islan, P. C. Tornello, G. A. Abraham, N. Duran, G. R. Castro, *Colloids and Surfaces B: Biointerfaces* **2016**, 143, 168–176.
- [62] B. S. F. Bazzaz, B. Khameneh, H. Zarei, S. Golmohammadzadeh, *Microbial pathogenesis* **2016**, 93, 137–144.
- [63] J. S. Negi, P. Chattopadhyay, A. K. Sharma, V. Ram, *Archives of pharmacal research* **2014**, 37, 361–370.
- [64] Y. Geng, P. Dalhaimer, S. Cai, R. Tsai, M. Tewari, T. Minko, D. E. Discher, *Nature nanotechnology* **2007**, 2, 249–255.
- [65] Y. Geng, D. E. Discher, *Journal of the American Chemical Society* **2005**, 127, 12780–12781.
- [66] J. M. Schnur, *Science* **1993**, 262, 1669–1676.
- [67] R. Price, M. Patchan, *Journal of microencapsulation* **1991**, 8, 301–306.
- [68] S. Svenson in S. Svenson, ACS Publications, **2004**.
- [69] G. Sharma, D. T. Valenta, Y. Altman, S. Harvey, H. Xie, S. Mitragotri, J. W. Smith, *Journal of controlled release* **2010**, 147, 408–412.
- [70] A. Misra, *Applications of polymers in drug delivery*, Smithers Rapra, **2014**.
- [71] W. K. Bae, M. S. Park, J. H. Lee, J. E. Hwang, H. J. Shim, S. H. Cho, D.-E. Kim, H. M. Ko, C.-S. Cho, I.-K. Park *et al.*, *Biomaterials* **2013**, 34, 1433–1441.

References

- [72] Y. Cao, C. Zhang, W. Shen, Z. Cheng, L. L. Yu, Q. Ping, *Journal of controlled release* **2007**, *120*, 186–194.
- [73] M. Caggioni, J. Lenis, A. V. Bayles, E. M. Furst, P. T. Spicer, *Langmuir* **2015**, *31*, 8558–8565.
- [74] M. Caggioni, A. V. Bayles, J. Lenis, E. M. Furst, P. T. Spicer, *Soft Matter* **2014**, *10*, 7647–7652.
- [75] R. Toy, P. M. Peiris, K. B. Ghaghada, E. Karathanasis, *Nanomedicine* **2014**, *9*, 121–134.
- [76] K. C. Black, Y. Wang, H. P. Luehmann, X. Cai, W. Xing, B. Pang, Y. Zhao, C. S. Cutler, L. V. Wang, Y. Liu *et al.*, *ACS nano* **2014**, *8*, 4385–4394.
- [77] J. Zhou, P. V. Giridhar, S. Kasper, I. Papautsky, *Lab on a Chip* **2013**, *13*, 1919–1929.
- [78] A. M. Luo, J. Vermant, P. Ilg, Z. Zhang, L. M. Sagis, *Journal of colloid and interface science* **2019**, *534*, 205–214.
- [79] B. Madivala, J. Fransaer, J. Vermant, *Langmuir* **2009**, *25*, 2718–2728.
- [80] N. Doshi, B. Prabhakarpanthian, A. Rea-Ramsey, K. Pant, S. Sundaram, S. Mitragotri, *Journal of Controlled Release* **2010**, *146*, 196–200.
- [81] C. Uhl, Y. Gao, S. Zhou, Y. Liu, *RSC advances* **2018**, *8*, 8089–8100.
- [82] G. B. Jeffery, *Proceedings of the Royal Society of London. Series A Containing papers of a mathematical and physical character* **1922**, *102*, 161–179.
- [83] M. Abkarian, M. Faivre, A. Viallat, *Physical review letters* **2007**, *98*, 188302.
- [84] H. Manikantan, T. M. Squires, *Journal of Fluid Mechanics* **2020**, *892*, year.
- [85] J. H. Clint in *Surfactant Aggregation*, Springer, **1992**, pp. 1–12.
- [86] C. Rangel-Yagui, A. Pessoa-Jr, D. Blankschtein, *Brazilian Journal of Chemical Engineering* **2004**, *21*, 531–544.
- [87] L. Quijada, D. Marileth **2010**.

-
- [88] K. Boode, P. Walstra, *Colloids and Surfaces A: Physicochemical and Engineering Aspects* **1993**, *81*, 121–137.
- [89] A. B. Pawar, M. Caggioni, R. W. Hartel, P. T. Spicer, *Faraday discussions* **2012**, *158*, 341–350.
- [90] P. Dahiya, M. Caggioni, P. T. Spicer, *Philosophical Transactions of the Royal Society A: Mathematical Physical and Engineering Sciences* **2016**, *374*, 20150132.
- [91] P. Dahiya, A. DeBenedictis, T. J. Atherton, M. Caggioni, S. W. Prescott, R. W. Hartel, P. T. Spicer, *Soft Matter* **2017**, *13*, 2686–2697.
- [92] C. Hao, Z. Xie, T. J. Atherton, P. T. Spicer, *Langmuir* **2018**, *34*, 12379–12386.
- [93] A. Thiel, R. Hartel, P. Spicer, K. Hendrickson, *Journal of the American Oil Chemists' Society* **2016**, *93*, 1467–1477.
- [94] G. Dockx, S. Geisel, D. G. Moore, E. Koos, A. R. Studart, J. Vermant, *Nature communications* **2018**, *9*, 1–8.
- [95] T. A. Prileszky, E. M. Furst, *Langmuir* **2016**, *32*, 5141–5146.
- [96] T. A. Prileszky, E. M. Furst, *Chemistry of materials* **2016**, *28*, 3734–3740.
- [97] M. Caggioni, D. Traini, P. M. Young, P. T. Spicer, *Powder Technology* **2018**, *329*, 129–136.
- [98] A. B. Pawar, M. Caggioni, R. Ergun, R. W. Hartel, P. T. Spicer, *Soft Matter* **2011**, *7*, 7710–7716.
- [99] N. Denkov, S. Tcholakova, I. Lesov, D. Cholakova, S. K. Smoukov, *Nature* **2015**, *528*, 392–395.
- [100] D. Cholakova, N. Denkov, *Advances in colloid and interface science* **2019**.
- [101] D. Cholakova, N. Denkov, S. Tcholakova, I. Lesov, S. K. Smoukov, *Advances in colloid and interface science* **2016**, *235*, 90–107.

References

- [102] D. Cholakova, N. Denkov, S. Tcholakova, Z. Valkova, S. K. Smoukov, *Langmuir* **2019**, *35*, 5484–5495.
- [103] Z. Valkova, D. Cholakova, S. Tcholakova, N. Denkov, S. K. Smoukov, *Langmuir* **2017**, *33*, 12155–12170.
- [104] C. Jin, C. Krüger, C. C. Maass, *Proceedings of the National Academy of Sciences* **2017**, *114*, 5089–5094.
- [105] C. Jin, B. V. Hokmabad, K. A. Baldwin, C. C. Maass, *Journal of Physics: Condensed Matter* **2018**, *30*, 054003.
- [106] B. P. Binks, *Current opinion in colloid & interface science* **2002**, *7*, 21–41.
- [107] L. G. Ogden, A. J. Rosenthal, *Journal of colloid and interface science* **1997**, *191*, 38–47.
- [108] H. Ribeiro, R. Gupta, K. Smith, K. van Malssen, A. Popp, K. Velikov, *Soft matter* **2016**, *12*, 5835–5846.
- [109] C. Méndez-Velasco, H. D. Goff, *Food Hydrocolloids* **2012**, *29*, 152–159.
- [110] M. Blankart, C. Kratzner, K. Link, C. Oellig, W. Schwack, J. Hinrichs, *International Dairy Journal* **2020**, *102*, 104578.
- [111] J. S. Langer, *Reviews of modern physics* **1980**, *52*, 1.
- [112] H. Keith, F. Padden, *Macromolecules* **1996**, *29*, 7776–7786.
- [113] Y. Wang, C.-M. Chan, L. Li, K.-M. Ng, *Langmuir* **2006**, *22*, 7384–7390.
- [114] T. Kyu, H.-W. Chiu, A. Guenther, Y. Okabe, H. Saito, T. Inoue, *Physical review letters* **1999**, *83*, 2749.
- [115] A. Golovin, M. Levine, T. Savina, S. H. Davis, *Physical Review B* **2004**, *70*, 235342.
- [116] A. A. Golovin, S. H. Davis, *Physica D: Nonlinear Phenomena* **1998**, *116*, 363–391.
- [117] H. Bunjes, *Journal of Pharmacy and Pharmacology* **2010**, *62*, 1637–1645.

-
- [118] K. Westesen, H. Bunjes, M. Koch, *Journal of controlled release* **1997**, *48*, 223–236.
- [119] A. Gordillo-Galeano, C. E. Mora-Huertas, *European Journal of Pharmaceutics and Biopharmaceutics* **2018**, *133*, 285–308.
- [120] A. Boreham, P. Volz, D. Peters, C. M. Keck, U. Alexiev, *European Journal of Pharmaceutics and Biopharmaceutics* **2017**, *110*, 31–38.
- [121] H. Shen, S. Shi, Z. Zhang, T. Gong, X. Sun, *Theranostics* **2015**, *5*, 755.
- [122] F. Ravar, E. Saadat, M. Gholami, P. Dehghankelishadi, M. Mahdavi, S. Azami, F. A. Dorkoosh, *Journal of controlled release* **2016**, *229*, 10–22.
- [123] A. K. Yadav, P. Mishra, G. P. Agrawal, *Journal of drug targeting* **2008**, *16*, 91–107.
- [124] W. Zong, Y. Hu, Y. Su, N. Luo, X. Zhang, Q. Li, X. Han, *Journal of microencapsulation* **2016**, *33*, 257–262.
- [125] X. Li, C. Xie, H. Xia, Z. Wang, *Langmuir* **2018**, *34*, 9974–9981.
- [126] M. Zlokarnik, *Scale-up in chemical engineering*, John Wiley & Sons, **2006**.
- [127] R. Müller, A. Dingler, T. Schneppe, S. Gohla in *Handbook of pharmaceutical controlled release technology*, Marcel Dekker New York, **2000**, pp. 359–376.
- [128] R. Cavalli, E. Marengo, L. Rodriguez, M. R. Gasco, *European journal of pharmaceutics and biopharmaceutics* **1996**, *42*, 110–115.
- [129] E. Marengo, R. Cavalli, O. Caputo, L. Rodriguez, M. R. Gasco, *International journal of pharmaceutics* **2000**, *205*, 3–13.
- [130] A. Dingler, S. Gohla, *Journal of microencapsulation* **2002**, *19*, 11–16.
- [131] V. Jennings, A. Lippacher, S. Gohla, *Journal of microencapsulation* **2002**, *19*, 1–10.
- [132] R. Al-Kassas, M. Bansal, J. Shaw, *Journal of Controlled Release* **2017**, *260*, 202–212.

References

- [133] S. Yang, F. Guo, B. Kiraly, X. Mao, M. Lu, K. W. Leong, T. J. Huang, *Lab on a Chip* **2012**, *12*, 2097–2102.
- [134] S. HoonáKim, S. WonáNam, I. WooáCheong *et al.*, *Chemical Communications* **2011**, *47*, 2634–2636.
- [135] C. Kaewsaneha, P. Tangboriboonrat, D. Polpanich, M. Eissa, A. Elaissari, *Colloids and Surfaces A: Physicochemical and Engineering Aspects* **2013**, *439*, 35–42.
- [136] Q. Chen, J. Yan, J. Zhang, S. C. Bae, S. Granick, *Langmuir* **2012**, *28*, 13555–13561.
- [137] J. Zhang, B. A. Grzybowski, S. Granick, *Langmuir* **2017**, *33*, 6964–6977.
- [138] C. Yu, J. Zhang, S. Granick, *Angewandte Chemie International Edition* **2014**, *53*, 4364–4367.
- [139] L. Hong, S. Jiang, S. Granick, *Langmuir* **2006**, *22*, 9495–9499.
- [140] M. Q. Giso, H. Zhao, P. T. Spicer, T. J. Atherton, *Langmuir* **36**, 13853–13859.
- [141] D. Anderson, M. G. Worster, S. H. Davis, *Journal of crystal growth* **1996**, *163*, 329–338.

Chapter 3

Production of Elongated Lipid Particles via Solidification of Molten Emulsion Droplets

3.1 Introduction

Active delivery using lipid capsules and solid lipid particles has been used for decades^{1,2}. Solid lipid particles can protect actives from chemical degradation in their solid matrix³. Lipid carriers provide enhanced bioavailability for actives with poor solubility and avoid using organic solvents in manufacturing. Large scale production of lipid particles using high-pressure homogenization is also common, allowing use for a wide range of formulations³⁻⁶. Typically, lipid particles are not produced to yield different shapes. However, particle shape is increasingly considered a novel design parameter for delivery systems, as shape may have a significant performance impact⁷⁻⁹. For example, pulmonary drug delivery has been enhanced by accounting for characteristics like shape and density of active carrier particles¹⁰.

Recently, elongated particles with high aspect ratio (the ratio of length and width) have been investigated as a way to improve lung deposition¹¹⁻¹³. In the case of inhaled particles, spherical shapes are rapidly removed by alveolar macrophages^{7,14,15} whereas elongated particles are better deposited in the alveolar region is small enough.

Geometric model in this chapter originally published as Giso, Mathew Q; Zhao, Haoda; Spicer, Patrick T & Atherton, Timothy J. "Crystal Comets: A Geometric Model for Sculpting Anisotropic Particles from Emulsions" *Langmuir*, **2020** 36, 46, 13853–13859

Particle shape also affect biological response at smaller, cellular length scales, as higher aspect ratio particles are less likely to be cleared by phagocytosis¹⁶.

Multiple methods exist to produce particles with controlled shapes. Elongated particles are typically produced using constraining environments like microfluidic channels, stretched films, and lithographic moulds¹⁷⁻¹⁹ that can have limited production capacity and be unable to access very small particle sizes²⁰. Although not fully understood, other chemical processes can produce elongated particles on smaller length scales²¹⁻²⁴. For example, monodispersed rodlike silica been grown by wet-chemical method with the existence of reactants during silica condensation²¹. Once growth is initiated in an emulsion of silica precursor, an anisotropic supply of reactants drives growth in only one direction, forming a high aspect ratio silica rod²¹. Another example is Jana and co-workers used surfactant micelle as a template to grow elongated gold particle²³. In the field of drug delivery, polymeric materials are often used to control particle shape^{25,26} but lipid-based particles can be cheaper and more biocompatible²⁷.

A previous discovery offers a unique approach to addressing some of the above issues while controlling particle shape in a flexible way. Crystallisation of a molten emulsion in the presence of surfactants that induce oil-solid dewetting during phase change can cause solidifying droplets to elongate into unique comet-like shapes without the need for external moulding or processing²⁸. The dewetting phenomenon only occurs when the SDS concentration higher than its critical micelle concentration (CMC)²⁸, where the surfactant has highest interfacial adsorption. The surfactant promotes dewetting or 'washing' of the lipid liquid phase during crystallisation. Particle size can be influenced by controlling the initial size of the emulsion droplets as well as the relationship between dewetting and crystal growth rate. Lengths of elongated particles from 0.1 to 10 μm are achievable. The process is unique in that

it can reshape or sculpt particles at surprisingly small length scales without the need for limiting geometries like microfluidic channels or lithographic moulds. As a result, particle production at larger scales is eased, providing flexibility to make elongated particles of many sizes. In this paper, we changed the composition of the particle, introducing multi-component materials to generate small elongated particles at low concentrations (0.25 wt% to 2.5 wt%) of surfactant, which expands the possible applications into active ingredient carriers.

We explore in this paper the creation of elongated particles with sub-micron dimensions using simple formulations and processes that allow surfactant-induced dewetting to dominate crystallisation. This work develops a new system able to produce elongated lipid particles. The production of larger quantities of these particles is explored by studying their formation under controlled linear and more rapid cooling conditions. Size and shape distributions are obtained for large populations of particles and used to provide a basis for design.

3.2 Materials and Methods

Trihydroxystearin (Peter Cremer). Stearic acid (95%), decanol (98%), sodium dodecyl sulfate (99% GC) and Nile red (for microscopy grade) were purchased from Sigma-Aldrich, and Milli-Q water.

3.2.1 Preparation of Lipid Particles

Lipid mixtures of stearic acid and trihydroxystearin with a ratio of 6:4 were prepared. Because the fat crystal tends to form the same crystal structure that it had as a solid before melting, it may affect the elongation results. Erasure of any crystal “memory” was carried out by heating the mixture to 90 °C for at least 30 min²⁹. Sodium dodecyl sulfate (SDS) with co-surfactant decanol was dissolved in Milli-Q water to prepare

the surfactant solution at concentrations of 0.15 wt%, 0.25 wt%, 0.4 wt%, 0.8 wt%, 1.5 wt% and 2.0 wt%. The weight of decanol was 1/10 the weight of the SDS. The surfactant solution was heated to the same temperature as the melted lipid mixture and then combined and shaken by hand to prepare hot emulsions. A drop of hot emulsion was dropped by a pipette onto a glass slide, covered by cover slip, and then observed by optical microscope on a controlled temperature stage.

Some experiments were also performed using rapid cooling by injection of a small volume of hot emulsion into a much larger volume of surfactant solution to quench the system. In these experiments SDS/decanol surfactant solutions were prepared, heated up to the same temperature as the melted mixture of lipids, combined, and sonicated for 10 s to prepare submicron droplets.

Then 1 mL of hot emulsion was added into 45 °C warm mentioned surfactant solution to cool the emulsion rapidly and form elongated crystals. Centrifuging at 6,000 rpm was used to remove larger particles.

3.2.2 Optical microscopy and Size distribution

Microscopy observation was performed using a Leica DM2500M optical microscope and all micrographs were recorded using a Moticam 10MP digital camera or Qimage optiMOS high-speed camera. Glass slide temperature was controlled by a Linkam PE120 Peltier. The stage can control the glass slide's temperature with a cooling/heating rate range from 0.1 °C/min to 20 °C/min. ImageJ was utilized³⁰ to analyze the micrographs and quantify particle sizes and aspect ratios. Binary images were used to analyze the emulsion droplets and comet particles. The criteria for particle detection were: a) size from 15 μm^2 to infinity; b) circularity from 0.0 to 0.7; and c) exclusion of edge particles. The criteria for droplet size distribution measurement

were: a) size from $10\ \mu\text{m}^2$ to infinity; b) circularity from 0.8-1.0: and c) exclusion of edge particles.

3.2.3 Scanning Electron Microscopy

The scanning electron microscope (SEM) observation used an FEI Nova NanoSEM 450 FE-SEM microscope. The sample was carefully rinsed by Milli-Q water, then transferred onto a silicon wafer, and air-dried. The sample was coated with an extra-thick coating with 5 nm of Cr and 60 nm of Pt, and observed at an accelerating voltage of 5kV.

3.2.4 Confocal Microscopy

A Leica SP5 WLL gSTED confocal microscope was used to image lipid particles using Nile red to dye particles for fluorescence, with the dye added into the lipid mixture before mixing with surfactant. Nile red was excited with a 510 nm laser beam. Confocal micrographs were analyzed by ImageJ, and the 3D images were generated by 3D viewer.

The SA/THS lipids mixture's DSC results are shown in the Appendix A. They tell us the basic information of the melting the crystallizing of this lipid mixture.

3.3 Results and Discussion

Previous work showed the ability to produce elongated particles with a simple emulsification process, but particles were made on length scales of hundreds of micrometers and required high concentrations of surfactant²⁸. Here we explore the production of much smaller particle dimensions using lower surfactant concentration that are unlikely to prevent broad formulation as active carriers. We demonstrate the system capability by assessing key variables of initial emulsion size, surfactant

concentration, particle composition, and cooling rate and their effect on particle shape and structure.

3.3.1 Dewetting and Crystallisation Rate

Dewetting rate is one of the important factors of preparing elongated particles in this system, as it is used to the balance crystallisation rate and feed a growing crystal as it moves away from the molten phase, Figure3.1. We control crystallisation rate by controlling cooling rate in our experiment and we tune dewetting rate using surfactant type and concentration. In our system, crystallization and dewetting occur simultaneously, and we show a schematic of the process in Figure3.1. A round particle is formed if the crystallization rate is much higher than dewetting rate, or dewetting rate is zero. An elongated rod particle is be formed when the crystallization rate is close to the dewetting rate. When the dewetting rate is much higher than crystallization rate, the crystallized part of the emulsion droplet will completely leave the liquid part of the emulsion droplet, forming a few smaller and low aspect ratio elongated particles²⁸

The surfactant packing at the surface of the particles significantly affects dewetting rate, and therefore particle aspect ratio and size. In order to investigate the relationship of surfactant solution's concentration and particle's morphology, an interfacial tension measurement of the melted mixture lipid with different concentrations of SDS solution has been performed to measure the interfacial tension γ_{LO} of liquid and oil. Drop pendant method has been used to perform the measurement (Figure 3.2). According to Young's equation, dewetting is favorable when $\gamma_{LO}\cos\theta < 0$, where θ is the contact angle of crystal and oil phase. Figure 3.2 shows the relationship between interfacial tension to the concentrations of SDS solution. Regarding to the results, the addition of SDS to the water will dramatically decrease

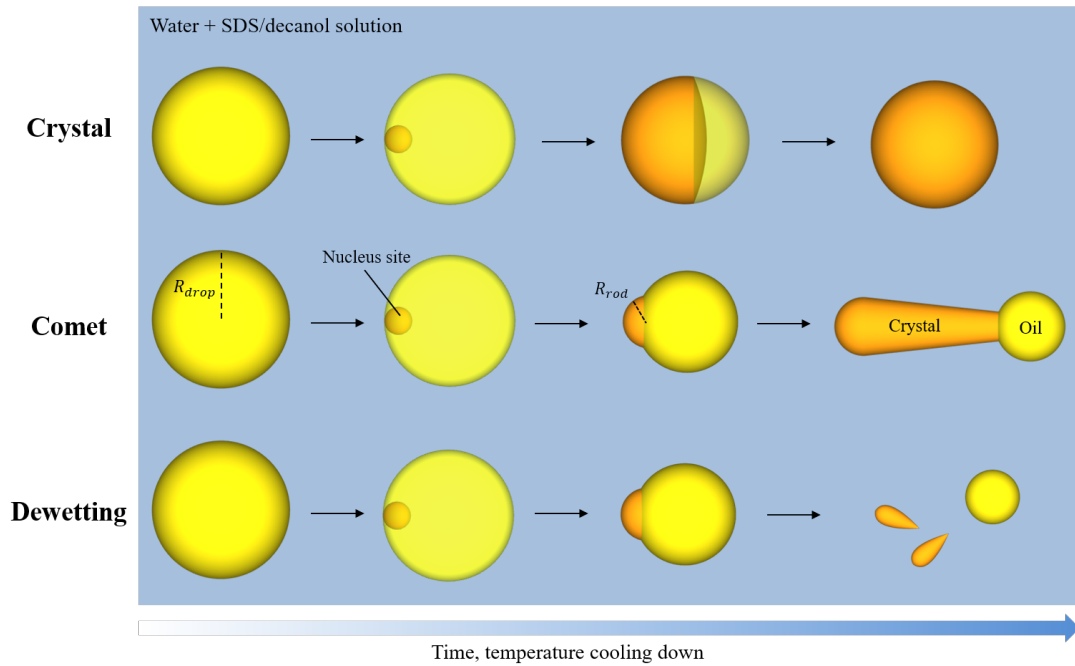


Figure 3.1: Schematic of particle formation by simultaneous dewetting and crystallisation.

the interfacial tension. Moreover, the results shows when the concentration of SDS solution reached around 0.25 wt% to 0.3 wt%, the interfacial tension is became stable afterwards. This result is matching with the SDS approximate CMC of 0.25 wt%. While the additional decanol as co-surfactant lowering the requirement of the amount of SDS to reach the lowest point of interfacial tension. Thus, interfacial tension is a key element to make elongated particles in this certain system, and adding co-surfactant can increase the surfactant packing efficiency.

Surfactant adsorption can be used to determine the magnitude of dewetting by using equation 3.1. In figure 3.3, the value of each line indicates the level of surfactant adsorption for each composition. For the system containing SA + SDS and SA + SDS/decanol, the emulsion droplets crystallized into spherical crystals, while the emulsion of THS in SDS/decanol crystallized into elongated crystals. Thus, we can assume that when the slope value is -8.9, the surfactant packing is sufficient

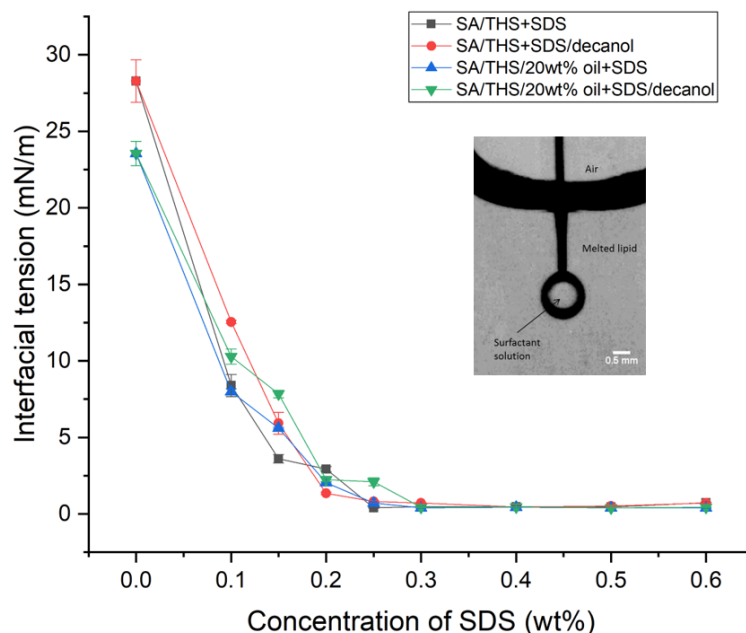


Figure 3.2: Interfacial tension between melted lipid and different compositions of SDS solutions. Insert image is an example of measuring the interfacial tension of SA/THS/20 wt% oil and SDS/decanol solution.

to provide a driving force for dewetting and form elongated particles. However, using THS by itself to produce elongated particles tends to form larger and lower aspect ratio particles, with less evidence of dewetting than for SA/THS mixtures. All the lipid mixture (SA/THS mixture) can form elongated particles according to the experimental results, and their slope value (-8.1 to -12.8) indicates a region of behaviour where dewetting is dominant.

$$\Gamma = -\frac{1}{RT} \frac{d\gamma_{ow}}{d \ln C} \quad (3.1)$$

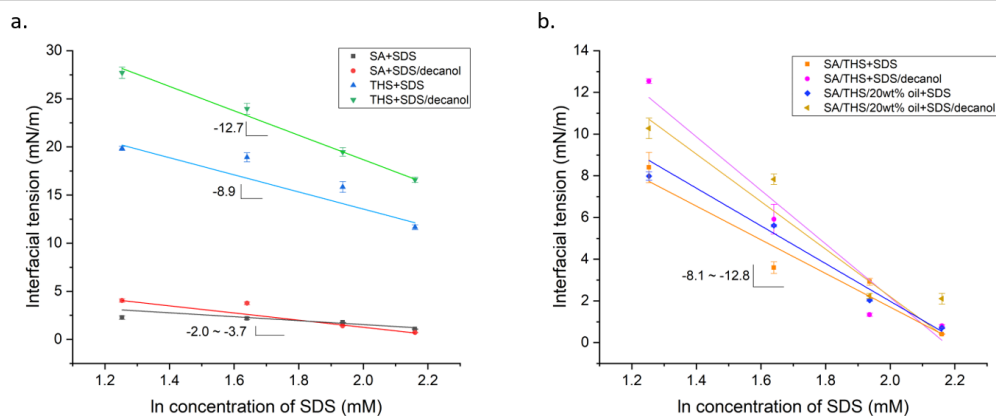


Figure 3.3: Determination of magnitude of dewetting by surfactant adsorption. *a.* Single lipid. *b.* Lipid mixture.

3.3.2 Initial Emulsion Droplet Size

Initial emulsion droplet size influences the size of elongated particles produced by crystallisation. Figure 3.4 shows six different initial emulsion droplet size distributions in different concentrations of SDS/decanol solutions. The CMC of SDS/decanol surfactant solution is 0.25-0.30 wt% (Figure 3.2), and we can see that concentrations near or below the CMC, 0.15 wt% and 0.25 wt%, have a wider droplet size distribution, with the majority of the emulsion droplets around 10-25 μm .

At higher surfactant concentrations than the CMC, the initial emulsion droplet size distributions are much narrower, with the majority of the emulsion droplets around 10-15 μm at 0.40 wt%. The higher surfactant level reduces the droplet interfacial tension. When the concentration of the surfactant goes up from 0.80 wt% to 2.00 wt%, the majority of the emulsion droplets diameter fall into the range of 5-10 μm , providing us with a five-fold span of starting droplet sizes for comparison.

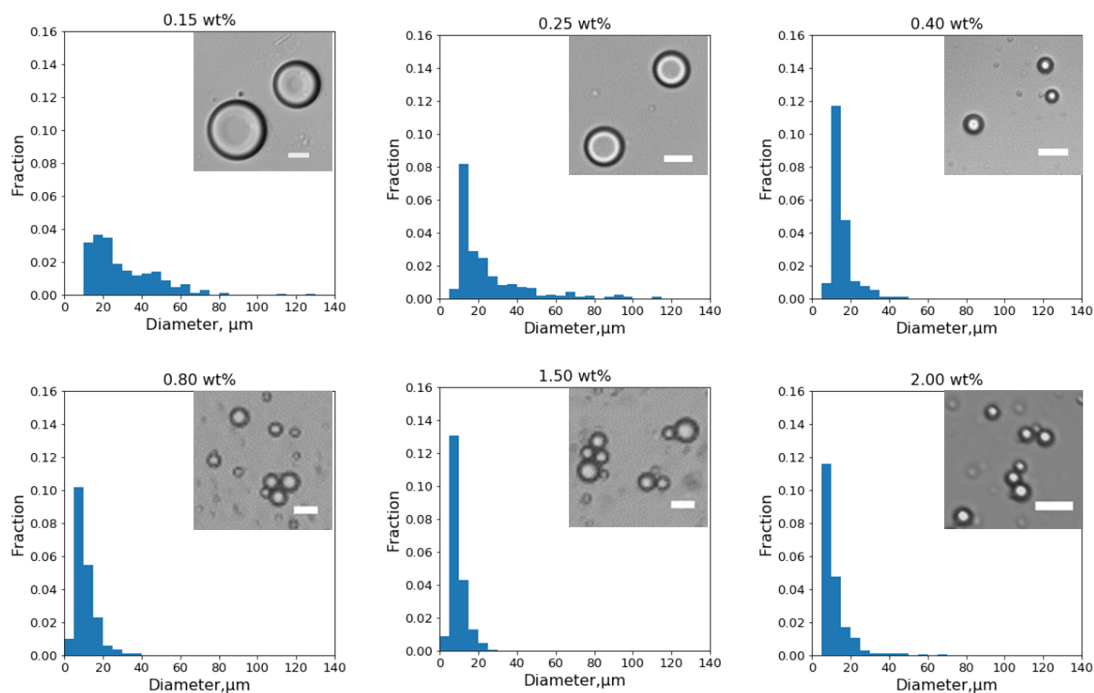


Figure 3.4: Initial emulsion droplet size distribution in different concentration of SDS/decanol solutions, scale bars are 15 μm .

3.3.3 Elongated Particle Shape and Size Distribution

All observations are made for surfactant concentrations much higher than the CMC, so we expect the emulsion droplet surface is saturated with surfactant and stable against coalescence. Although we sometimes observe droplet collisions, no merging or coalescence occurs that would lead to multiple-head comets. The collisions can, however, change the trajectory of the droplets but no significant change in shape is noted. Some multi-prong comets can form, though these tend to be the result of multiple nucleation sites in the droplets based on observation of impurities in the droplets.

In Figure 3.5, the progress of a single droplet crystallizing in a dewetting-dominated system to form an elongated particle is shown. Other systems are shown in Appendix A, Figure A.1). Just as the system starts with a distribution in droplet sizes,

the resultant comets also have a range of size and shapes, Figure 3.6. The elongation of the initially spherical droplets is clear in Figure 3.6, where a population of comet particles is shown. A summary of the types of shapes that can be obtained by this process is shown in Figure 3.7. SEM imaging indicates the formation of elongated shapes down to roughly micron length scales and the the control of the shapes produced is an objective of this work by controlling the crystallization rate and surfactant solution concentration.

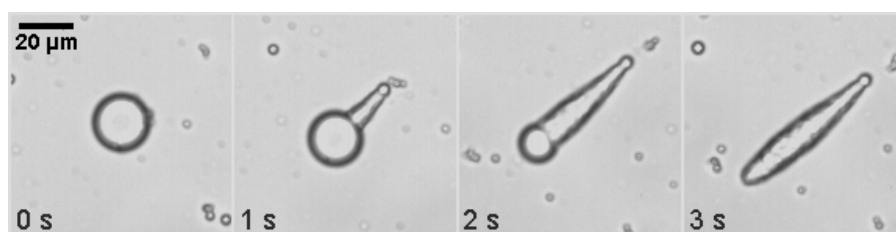


Figure 3.5: A time lapse sequence showing the growth of a comet particle by dewetting-dominated crystallisation.

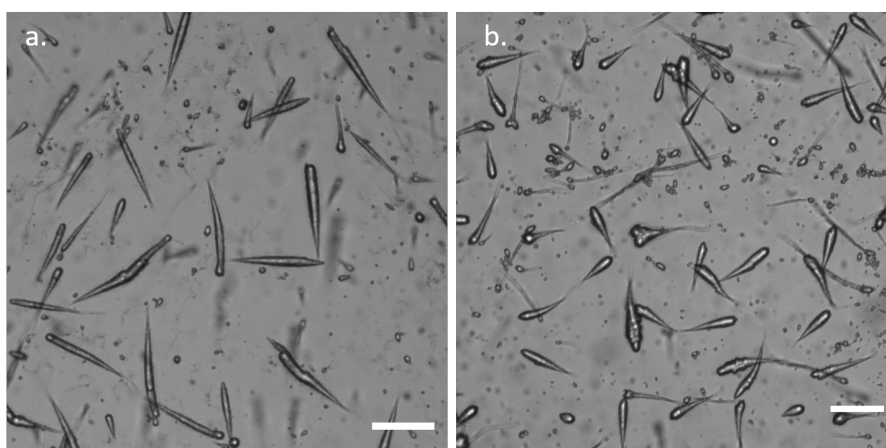


Figure 3.6: Optical micrographs of particles produced by dewetting-dominated crystallisation of mixed SA and THS droplets. The particles are produced in surfactant solution with a cooling rate of $\sim 60^\circ\text{C}/\text{min}$. (a) 1.0 wt% SDS/decanol surfactant solution (b) 1.5 wt% SDS/decanol surfactant solution. Scale bars are $100\ \mu\text{m}$.

As surfactant controls the dewetting process²⁸, different concentrations of surfactant have been investigated for their ability to create elongated particles. Aspect

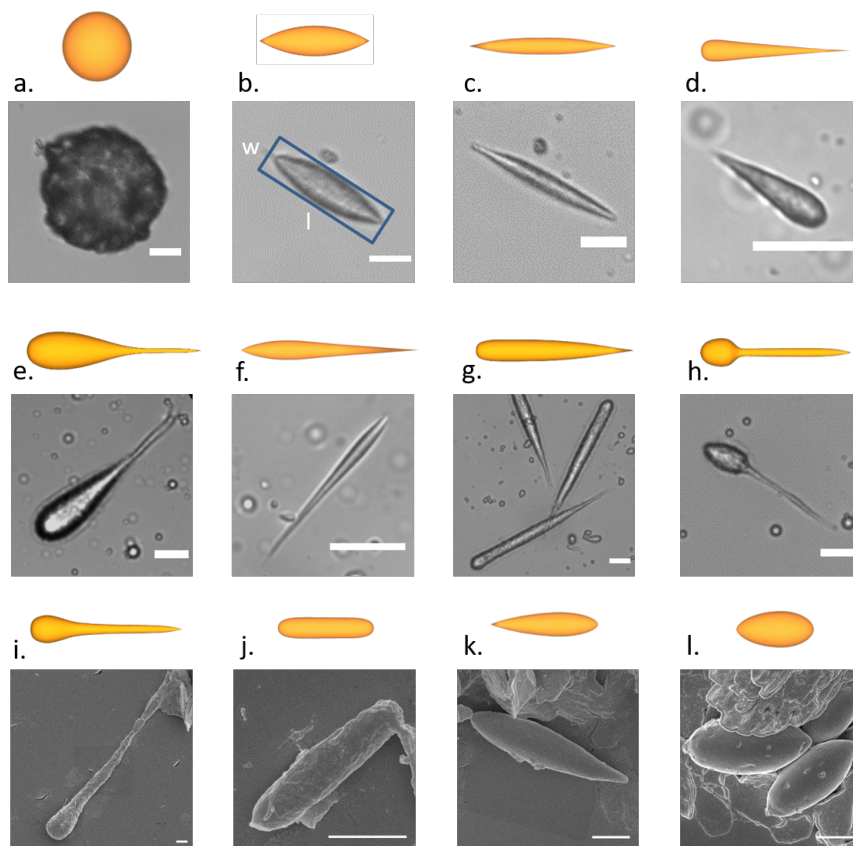


Figure 3.7: Micrographs of SA/THS particles in variety of shapes prepared by a hot emulsion approach. a-h. Optical micrographs. Scale bars are 20 μm . i-l. SEM images. Scale bars are 2 μm .

ratio is determined from the ratio of particle length (l) and width (w) of the rectangular fit of the particles (Figure 3.7b). Figure 3.8 shows the aspect ratio distribution of the particles when cooling a hot emulsion with temperature control of linear cooling rates. When the concentration of the SDS/decanol solution is 0.15 wt% (Figure 3.8a, d and g), which is lower than the CMC, spherical emulsion droplets are crystallised into very low aspect ratio particles. In Figure 3.8a, d and g, more than 90% of the particles with aspect ratio lower than 2. When the concentration is 0.80 wt% (Figure 3.8b, e and h), which is above the CMC, the peak of the aspect ratio distribution is around 3 - 5. When the concentration of surfactant solution is further raised to 1.50 wt% (Figure 3.8c, f and i), the aspect ratio distributions become even

wider. A distinct trend is observed when the concentration of surfactant solution is the only variable and it is higher than the CMC: more emulsion droplets are able to grow into higher aspect ratio particles. The size distributions of the emulsion droplets in 0.80 wt% and 1.5wt% surfactant solution are not significantly different so we assume no major effect on crystallisation.

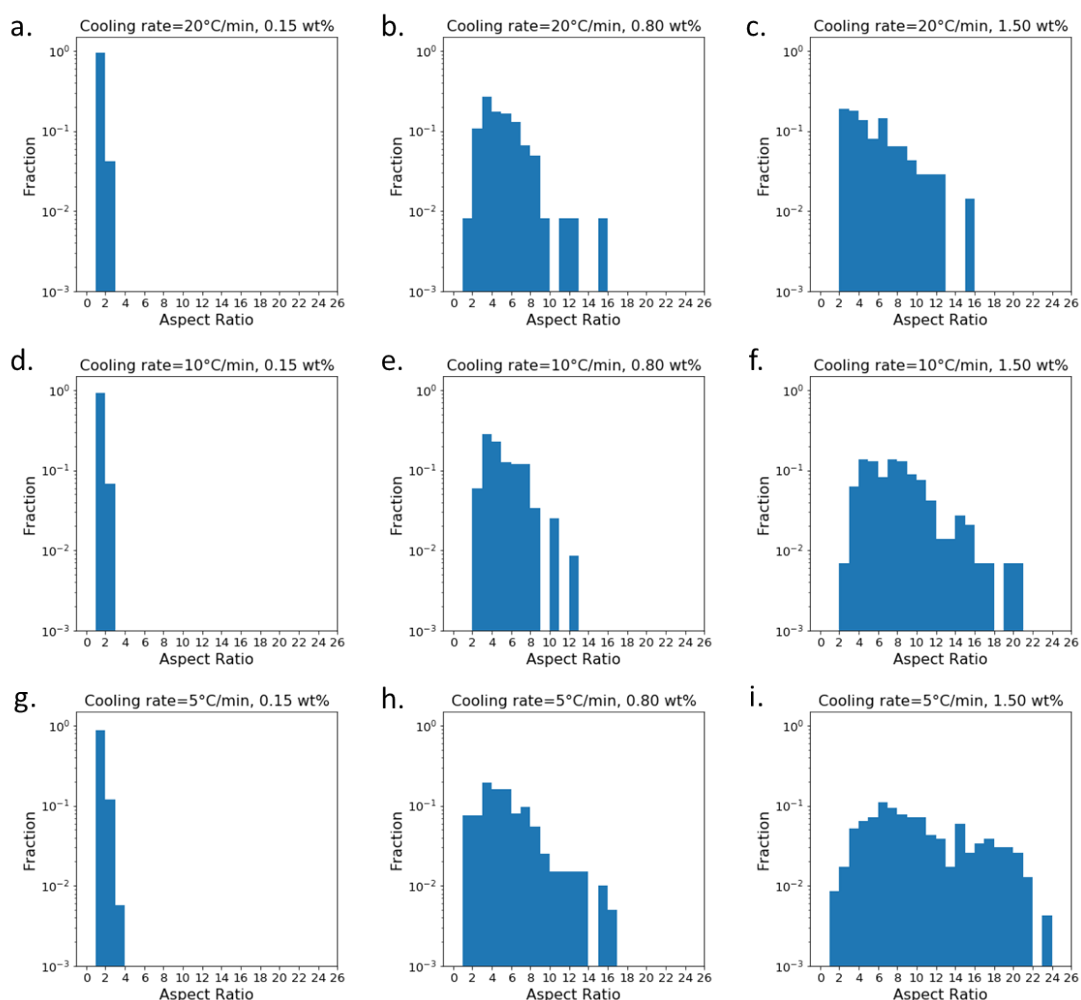


Figure 3.8: Aspect ratio distributions of the particles made with different concentrations of SDS/decanol solution and different cooling rates.

Cooling rate also has a strong effect on particle aspect ratio distribution, as it will dictate the crystallisation rate of the particles and enhance the elongation we seek. At a surfactant concentration of 0.15 wt%, which is lower than the CMC, all

three cooling conditions produce similar aspect ratio distributions from 1-2. As cooling rate is decreased, the aspect ratio distribution becomes only slightly wider. This indicates that lower cooling rates allow the surfactant concentration to have a stronger influence, even with a weak driving force. When the surfactant concentration is 0.80 wt%, higher than the CMC, we start to see particles with higher aspect ratios. When the cooling rate is relatively low (Figure 3.8d-i), a wider distribution of the particle aspect ratios can be observed as compared to Figure 3.8a-c. If the surfactant concentration is high enough, lipid particle aspect ratio can reach 20 or even higher (Figure 3.8f and i). For the samples made by 1.5 wt% SDS/decanol solution, a wide aspect ratio distribution is observed when the cooling rate is approximately 5 °C/min.

Unlike techniques like film stretching, microfluidics or lithographic moulding that produce more monodisperse aspect ratios¹⁷⁻¹⁹, this method produces more polydisperse distributions of particle aspect ratio as a result of the randomness of the emulsion crystallisation process and its strong dependence on cooling rate and surfactant concentration. When the concentration of SDS/decanol solution goes higher, increasingly wide aspect ratio distributions form as the higher concentrations of surfactant solution provides stronger dewetting force. However, low aspect ratio particles are also observed in the 1.50 wt% surfactant solution. This is likely because some complete dewetting can also occur at high surfactant concentrations (Figure 3.1), as a result of fast crystallization rates (Figure 3.8b and c) or multiple nuclei.

A complete dewetting process is shown in Figure 3.9a, where short elongated particles are ejected from an emulsion droplet during crystallization. Figure 3.4 shows the initial droplet diameter size distribution for hot emulsions in 1.50 wt% surfactant solution at 85 °C. Taking a hot emulsion that has crystallised into comets

and remelting it back to emulsion droplets we compare the remelted emulsion droplet size distribution in Figure 3.9b. The size distribution of remelted emulsion droplets has obvious shifted to smaller sizes, indicating the remelted emulsion droplet sizes are smaller than the initial emulsion droplets as a result of the complete dewetting process.

As the emulsification process discussed here enables controlled production of elongated particle shapes from simple emulsion precursors, it is relevant to determine how likely the process is to be viable at larger scales where temperature control and mixing are less efficient. Continuous production of elongated particles will likely require steady state cooling in a flow, so we also produce the elongated particles using rapid injection into a cooler, larger volume of fluid to compare with the controlled cooling rate case.

3.3.4 Continuous Injection Production of Elongated Particles

The elongated lipid particle shape and aspect ratio produced here is highly dependent on the cooling process. Rapid injection of hot emulsion into a larger volume of cooler fluid increases the initial cooling rate experienced by droplets but will likely be more gradual after the initial exposure. Heterogeneity will also be larger, as not all the emulsion droplets experience the same cooling rate.

Here we produce a relatively larger amount of elongated particles (20 mL of suspension) by mixing the 85 °C hot emulsion into a cooler surfactant solution at the same concentration. The aspect ratio distribution results from these experiments are shown in Figure 3.10. The 1.2 °C/s cooling rate is estimated by monitoring the temperature change (See Appendix A Figure A.3).

We can see that if the temperature difference ΔT is smaller, the aspect ratio distributions are wider. This corresponds to similar results in Figure 3.8: a slower

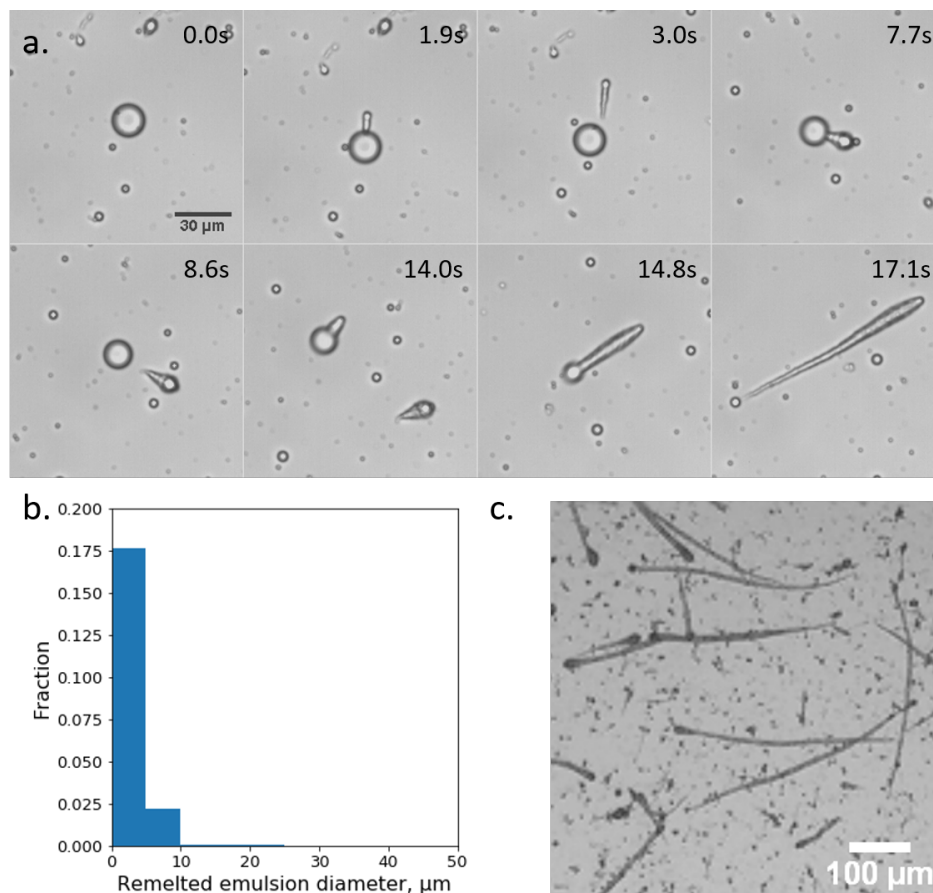


Figure 3.9: *a. SA/THS emulsion droplets ejecting many smaller crystals in 1.5 wt% SDS/decanol solution during crystallisation. b. Remelted emulsion droplet size distribution in 1.5 wt% surfactant solution. c. High aspect ratio THS/SA comet particles formed in 1.5 wt% with 5 °C/min cooling rate.*

cooling rate produces a wider aspect ratio distribution. This successful preliminary scale-up experiment gives us hope that this hot emulsion method could someday produce significant quantities of elongated particles with controlled aspect ratio.

3.3.5 A Dynamic Process of the Interfacial Crystallization Approach

According to the theory of Laplace pressure, in equation 3.2 and 3.3, where γ_{LO} is the interfacial tension of the liquid and oil phase; γ_{OC} is the interfacial tension of the oil and crystal phase; and assume that the interfacial tension is the same and constant. Thus, when the Laplace pressure is balanced, ΔP_{drop} equals ΔP_{rod} . Therefore, the

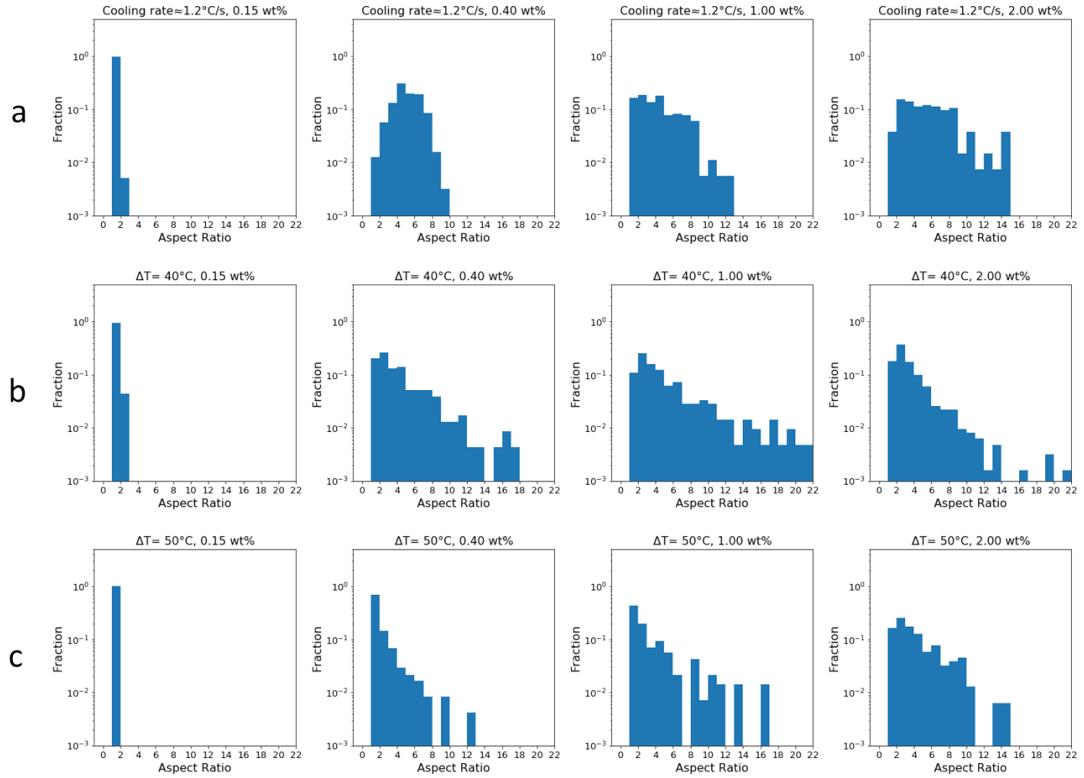


Figure 3.10: Particles made from different concentrations of SDS/decanol solution *a)* with approximately 1.2°C/s cooling rate; *b)* with $\Delta T=40^{\circ}\text{C}$ and *c)* with $\Delta T=50^{\circ}\text{C}$.

ratio of the radius of the droplet to the radius of the rod crystal can be predicted to equal 2 as shown in equation 3.4. However, the experimental data shows that the ratio of these two radii is changing over the time (Figure 3.11). One thing needs to be noticed is that for the comet particles, the values of R_{drop}/R_{rod} should decreased to 0. However, due to the limit of the resolution for very small droplet, we discarded the parts that are hard to be observed. The varying ratio value means γ_{LO} and γ_{OC} are not equal or constant. One of the explanation could be the changing temperature causes the change of the interfacial tension. Different trends of the ratio of these two radii have been observed in comet crystals and dewetting crystals. For the comet crystals, at the beginning of the curves in Figure 3.11, emulsion droplets started to crystallize and the values of R_{drop}/R_{rod} for different comet crystals in different con-

ditions are quite different, we call it pre-stable stage; in the green region, because the R_{drop}/R_{rod} values are lower than 2, and due to Equation 3.2 and 3.3, we can get that $\gamma_{LO} \leq \gamma_{OC}$; in orange region, the value of R_{drop}/R_{rod} is decided by the shape of the crystal, when the crystal has a wider end, the value will go lower, and if it has a pointy end, the end will remain similar to the value in the green region. For the dewetting crystals, we can observe two different regions. In the blue region, the emulsion droplet starts to crystallize and due to the value of R_{drop}/R_{rod} is higher than 2, according to Equation 3.2 and 3.3, we can get that $\gamma_{LO} > \gamma_{OC}$; after that, a sudden jump of the R_{drop}/R_{rod} value indicating that $\gamma_{LO} \gg \gamma_{OC}$ and eventually the crystal dewetted from the emulsion droplet.

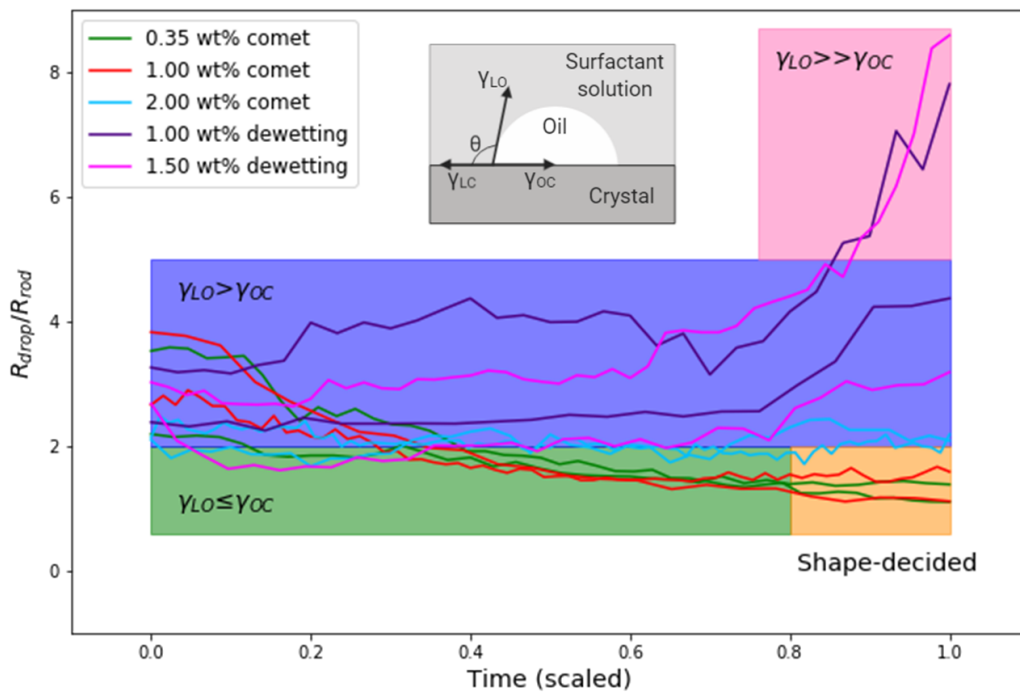


Figure 3.11: The ratio of the radius of droplet to the radius of rod.

$$\Delta P_{drop} = \frac{2\gamma_{LO}}{R_{drop}} \quad (3.2)$$

$$\Delta P_{rod} = \frac{\gamma_{OC}}{R_{rod}} \quad (3.3)$$

$$\frac{R_{drop}}{R_{rod}} = 2 \quad (3.4)$$

For the comet particles, the values of R_{drop}/R_{rod} are relatively large before scaled time 0.2. However, after the scaled time point 0.2 to around 0.7 or 0.8, the values of R_{drop}/R_{rod} are stabilised in a small range. As shown in Figure 3.12a, before scaled time point 0.2, the height of the particle is increasing; between 0.2-0.7, the height of the particle is decreasing; and after 0.7, the height of the particle remain similar. Cooperating this graph with the Figure 3.5, the increasing height before scaled time point around 0.2 is the period that the $\gamma_{LO} > \gamma_{OC}$; the decreasing height between scaled time 0.2-0.7 is the period that the value of R_{drop}/R_{rod} is stable and the $\gamma_{LO} < \gamma_{OC}$; and the stabled height after scaled time point 0.7 is co-responding to the orange region in Figure 3.11, which could be decided by the shape of tail or another explanation is the limit of the La Place pressure. The previous geometric model paper shows the growth angle (Φ_g) is an essential parameter of the modelling³¹, it is also deciding the growth direction of the crystal. The definition of growth angle is showing in Figure 3.13, Φ_g is the angle between the angle Φ (contact angle of oil and crystal phase) and the angle $\Phi_S V$ (the angle of the tangent of crystal front with the background). Figure 3.12a is comparing an experimental particle with a simulation particle (the Mathematica code of the model is retrieved by the published paper³¹, attached in Appendix A). Since the height and time is scaled, thus comparing the slope of the curves are essential. However, when comparing the simulation results with experiment results, the part that the height of the particle is increasing is not always have the similar slope as the simulation particle. That

is because one of the limitations of the simulation is the constant growth angle slope Φ'_g during the dewetting process³¹. Figure 3.12b shows the growth angle Φ_g changing over the dewetting process. We can see that the growth angle starts at a low degree and then increased sharply to a value and then fluctuate in a small range and the finished with relatively high growth angle. The previous simulation paper shows the particle will have a larger height at the head of the particle when the growth angle is low³¹, this explains why in Figure 3.12a the experimental particle starts with a higher value slope curve while the middle part of the curve has a similar slope with the simulation result.

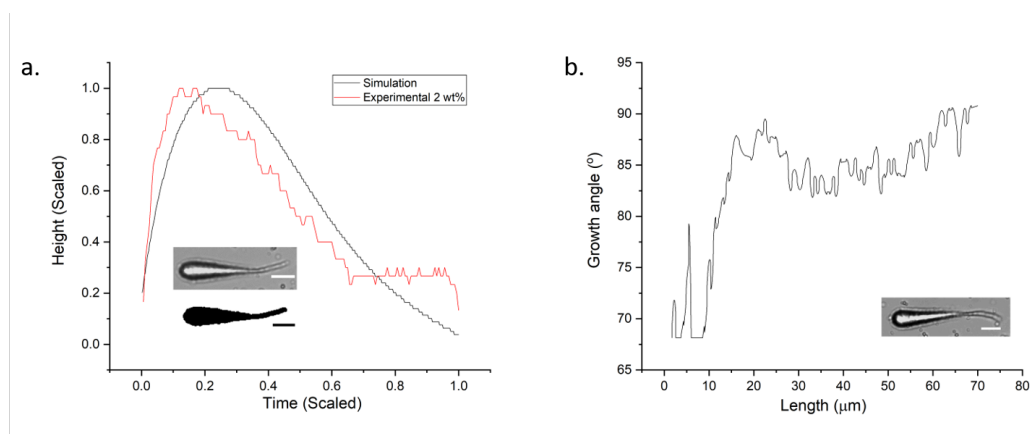


Figure 3.12: a. Scaled height of particle made from 2.0 wt% surfactant solution to the scaled time compared with simulation result. b. The Growth angle of a particle formed in 2.0 wt% surfactant solution changing during the dewetting process over the time. Scale bars are 20 μm

3.3.6 Density of Elongated Particles

Beyond shape, we are also interested in the density of the elongated particles, as the flow behaviour of delivery vehicles is known to be strongly affected by aerodynamic variables¹⁰. Confocal imaging of the particles (Figure 3.14) indicates the comets could have varying levels of solid density within their volume. Because of the strong interfacial hydrodynamics in this crystallisation system, distinct variations in sur-

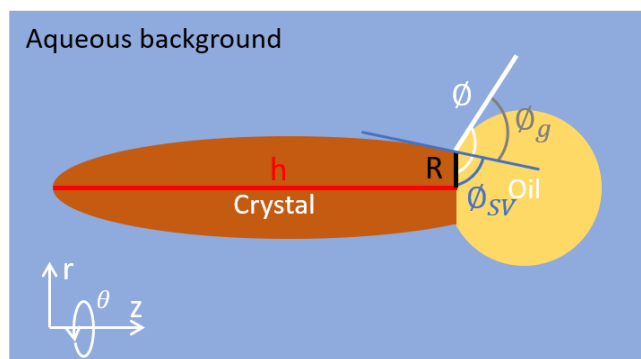


Figure 3.13: A schematic of the geometric model's parameter. Reproduced from Giso et al.

face layers could form (Figure 3.14a) during dewetting. Figure 3.14 shows distinct differences in volumetric density of two particles produced with different levels of liquid oil.

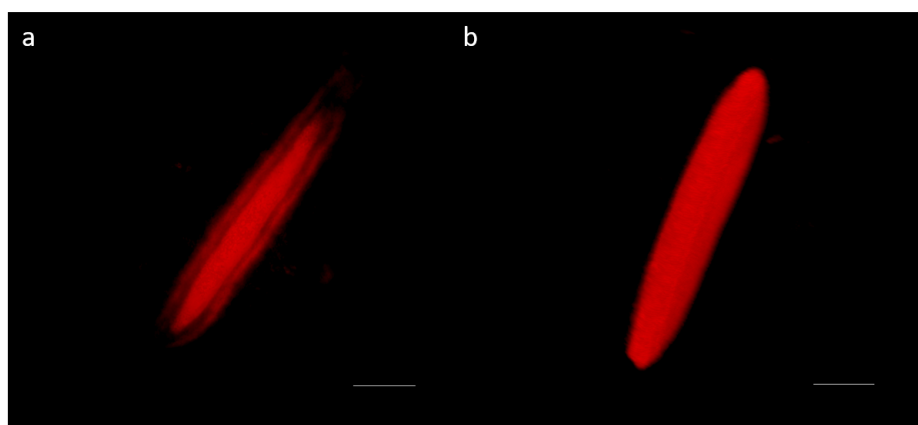


Figure 3.14: Confocal results of lipid particles. *a.* A particle composed of 60 wt% SA and 40 wt% THS (3D image was generated by 20 slides, each slide's gap is 0.7 μm); *b.* A particle composed of 48 wt% SA, 32 wt% THS and 20 wt% vegetable oil (3D image was generated by 20 slides, each slide's gap is 0.5 μm) (scale bar=10 μm)

A more quantitative assessment of particle density can be obtained by converting the elongated particles' volumes into equivalent spherical emulsion droplets volumes. First we need a simplified shape assumption of the elongated particles. As shown in Figure 3.15, the particle's shape is assumed to be the green shape in Figure 3.15a. The shapes in three different colors in Figure 3.15a have the same

length (l) and width (w). To estimate the volume of the shape in green, we average the volumes of the shapes in blue and red in Figure 3.15a. Because we can obtain the l and w of the particles by analysing the particles in ImageJ, we can estimate the volume of the green color shape in Figure 3.15a.

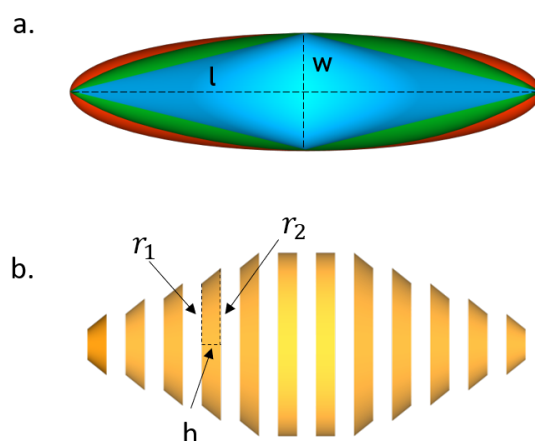


Figure 3.15: An assumption of the elongated particle's shape. a. The elongated particles' shape has been assumed to be as the shape in red color. b. Schematic of 'Reslice' function in ImageJ used to estimate the volume of the particles.

After making the assumption of the elongated particle's shape, we can estimate its volume and convert the volume to a geometric spherical diameter by assuming the elongated particles have the same density as the emulsion droplets (Figure 3.16). Compare to Figure 3.4, we can see that the converted spherical diameters are much larger than the initial emulsion droplets size when the concentrations of the surfactant solutions are 1.0 wt% and 2.0 wt% (25 μm , and 35 μm respectively). We also can see that the converted spherical diameter is even larger when the concentration of surfactant solution is 2.0 wt%. This indicates the 2.0 wt% of SDS/decanol solution will prepare lower density particles.

Our results indicate that the elongated particles have a lower density than the solid phase of SA/THS mixture. We can then estimate the aerodynamic diameter

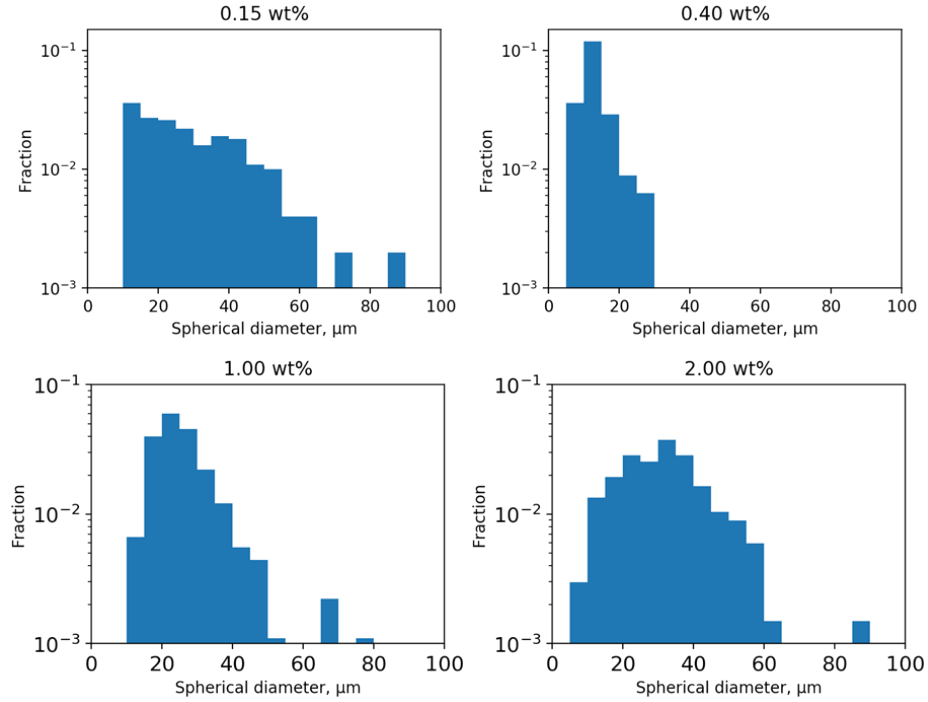


Figure 3.16: Spherical equivalent diameter distributions using the elongated particle volumes.

of our elongated particles. To estimate the aerodynamic diameter, the solid lipid mixture density is obtained by experiment to be $\rho_{solid} = 0.9 \text{ g/cm}^3$. Thus if the density ratio ρ_{drop}/ρ_{rod} is in the range of 0.8 - 1.3, the density of the elongated particle will be in a range of 0.55 - 0.9 g/cm^3 .

The aerodynamic diameter is calculated by:

$$d_{aer} = d \sqrt{\frac{\rho_{rod}}{F}} \quad (3.5)$$

where d_{aer} is aerodynamic diameter, d is geometric diameter, and F is shape factor. The shape factor of prolate spheroids has been reported by Davis³². For particles with 20 μm length and aspect ratio 10, the shape factor is estimated to be 1.57 by interpolation³². So the particles with density from 0.55 - 0.9 g/cm^3 have an

aerodynamic diameter range from 2.3 - 2.9 μm . This range of aerodynamic diameter is suitable for aerosol delivery of therapeutics into the deep part of the lung.

3.4 Conclusion

A simple emulsion system of lipids and aqueous surfactant has been investigated to make elongated particles using the phenomenon of dewetting-dominated crystallisation. The interfacial approach is controllable by varying surfactant solution concentration, cooling rate, and particle composition. Mixtures of stearic acid and trihydroxystearin produced robust populations of elongated particles. Small elongated particles with lengths smaller than 10 μm and aspect ratio greater than 3 are achievable by this process. The particle density is likely lower than that of the particle solid phase, making the particles likely to behave as much smaller entities in aerodynamic flow. The feasibility of scaling up the process has been examined using rapid cooling studies and found to be able to successfully produce elongated lipid particles with controlled aspect ratio at a large scale.

References

- [1] Y.-q. Zhao, L.-p. Wang, C. Ma, K. Zhao, Y. Liu, N.-p. Feng, *International journal of nanomedicine* **2013**, 8, 4169.
- [2] Q. Guan, Q. Guan, T. Lin, J. Yin, *Journal of Controlled Release* **2011**, 152, year.
- [3] V. Jennings, M. Schäfer-Korting, S. Gohla, *Journal of controlled release* **2000**, 66, 115–126.
- [4] W. Mehnert, K. Mäder, *Advanced drug delivery reviews* **2012**, 64, 83–101.
- [5] A. zur Mühlen, C. Schwarz, W. Mehnert, *European journal of pharmaceuticals and biopharmaceutics* **1998**, 45, 149–155.

-
- [6] S. Jaspert, G. Piel, L. Delattre, B. Evrard, *Expert opinion on drug delivery* **2005**, *2*, 75–87.
- [7] J. A. Champion, Y. K. Katare, S. Mitragotri, *Journal of controlled release* **2007**, *121*, 3–9.
- [8] D. Dendukuri, K. Tsoi, T. A. Hatton, P. S. Doyle, *Langmuir* **2005**, *21*, 2113–2116.
- [9] Y. Zhao, Y. Wang, F. Ran, Y. Cui, C. Liu, Q. Zhao, Y. Gao, D. Wang, S. Wang, *Scientific reports* **2017**, *7*, 1–11.
- [10] D. A. Edwards, J. Hanes, G. Caponetti, J. Hrkach, A. Ben-Jebria, M. L. Eskew, J. Mintzes, D. Deaver, N. Lotan, R. Langer, *Science* **1997**, *276*, 1868–1872.
- [11] D. Johnson, T. Martonen, *Particulate science and technology* **1994**, *12*, 161–173.
- [12] M. S. Hassan, R. W. M. Lau, *Aaps Pharmscitech* **2009**, *10*, 1252.
- [13] P. Kolhar, A. C. Anselmo, V. Gupta, K. Pant, B. Prabhakarandian, E. Ruoslahti, S. Mitragotri, *Proceedings of the National Academy of Sciences* **2013**, *110*, 10753–10758.
- [14] S. Chono, T. Tanino, T. Seki, K. Morimoto, *Journal of pharmacy and pharmacology* **2007**, *59*, 75–80.
- [15] J. A. Champion, S. Mitragotri, *Proceedings of the National Academy of Sciences* **2006**, *103*, 4930–4934.
- [16] G. Sharma, D. T. Valenta, Y. Altman, S. Harvey, H. Xie, S. Mitragotri, J. W. Smith, *Journal of controlled release* **2010**, *147*, 408–412.
- [17] J. A. Champion, Y. K. Katare, S. Mitragotri, *Proceedings of the National Academy of Sciences* **2007**, *104*, 11901–11904.
- [18] S. E. Gratton, P. A. Ropp, P. D. Pohlhaus, J. C. Luft, V. J. Madden, M. E. Napier, J. M. DeSimone, *Proceedings of the National Academy of Sciences* **2008**, *105*, 11613–11618.

References

- [19] M. Caggioni, D. Traini, P. M. Young, P. T. Spicer, *Powder Technology* **2018**, 329, 129–136.
- [20] R. Sturm, W. Hofmann, *Journal of hazardous materials* **2009**, 170, 210–218.
- [21] A. Kuijk, A. Van Blaaderen, A. Imhof, *Journal of the American Chemical Society* **2011**, 133, 2346–2349.
- [22] Y. Khalavka, J. Becker, C. Sonnichsen, *Journal of the American Chemical Society* **2009**, 131, 1871–1875.
- [23] N. R. Jana, L. Gearheart, C. J. Murphy, *Advanced Materials* **2001**, 13, 1389–1393.
- [24] B. Mandl, J. Stangl, E. Hilner, A. A. Zakharov, K. Hillerich, A. W. Dey, L. Samuelson, G. Bauer, K. Deppert, A. Mikkelsen, *Nano letters* **2010**, 10, 4443–4449.
- [25] N. Doshi, S. Mitragotri, *Journal of the Royal Society Interface* **2010**, 7, S403–S410.
- [26] J.-W. Yoo, S. Mitragotri, *Proceedings of the National Academy of Sciences* **2010**, 107, 11205–11210.
- [27] Y. Soleimanian, S. A. H. Goli, J. Varshosaz, F. Maestrelli, *Food chemistry* **2018**, 260, 97–105.
- [28] P. T. Spicer, R. W. Hartel, *Australian journal of chemistry* **2005**, 58, 655–659.
- [29] S. Metin, R. W. Hartel, *Bailey's industrial oil and fat products* **2005**.
- [30] C. A. Schneider, W. S. Rasband, K. W. Eliceiri, *Nat. Methods* **2012**, 9, 671–675.
- [31] M. Q. Giso, H. Zhao, P. T. Spicer, T. J. Atherton, *Langmuir* 36, 13853–13859.
- [32] C. Davies, *Journal of Aerosol Science* **1979**, 10, 477–513.

Chapter 4

Elongated Shape Gradient Lipid Particles via Evaporation of Lipid-Solvent Emulsions

4.1 Introduction

Lipid particles are known to be useful as active ingredient delivery vehicles for various applications¹⁻³. In studies of active delivery carriers, non-spherical particle shapes have attracted attention⁴⁻⁷. High aspect ratio rod- or fibre-like particles have been found to have better deposition to the human respiratory tract and nasal cavity^{8,9}, providing a design target for manufacturing. Methods to produce elongated particles are well-studied, for example, microfluidic, film stretching, self-assembly and lithographic moulding^{7,10-12}, but most of these methods are limited in affordability and attainable scale.

In this research, we build on our previous work using surfactant dynamics to increase dewetting a crystallising solid by its own melt¹³. The method uses an emulsion of molten lipids in aqueous surfactant solution, allowing use in the context of existing emulsion processes. While in Chapter 3 we showed the process can produce elongated particles with a fair amount of control over aspect ratio, there are many envisioned applications that might require use of lower temperatures. Here we develop a solvent emulsion evaporation method to produce elongated lipid particles, finding that surfactants present in the aqueous phase can induce dewetting and yield comets remarkably similar to those in Chapter 3 and Spicer and Har-

tel¹³. In addition, comets with complex oscillatory shapes are produced by the solvent evaporation method, providing a new opportunity to explore complex particle shapes in delivery applications^{14,15}. The oscillatory shapes match two elements of the shape taxonomy proposed by by Glotzer and Solomon¹⁶, providing a significant aspect ratio and a shape gradient with a relatively simple process.

4.2 Materials and Methods

Stearic acid (95%), sodium dodecyl sulfate ($\geq 99\%$) and decanol (98%) were purchased from Sigma-Aldrich, chloroform (99.8 %) from ACI Labscan, trihydroxystearin (Peter Cremer), and Milli-Q water.

4.2.1 Solubility of Lipids in Chloroform

Solubility of THS in chloroform has been measured by visual examination. Different weights (100-1000mg) of THS have been weighed in glass vials. Approximately 50 mg weight interval of each sample has been used. Then 1 mL of chloroform has been pipetted to each vial and then sealed with lid and wrapped with Parafilm[®]M to avoid evaporation loss of chloroform. The glass vials were stored in Julabo[®]TW8 water bath with different temperatures for at least 25 min and stirred gently to allow dissolution in the chloroform.

Visual examination of each vial is then used to note the presence of an undissolved THS. Completely dissolved THS in chloroform should be fully transparent (the first vial from left in Figure 4.1). To draw the solubility curve of THS in chloroform, the solubility at 25 °C, 35 °C, 45 °C, and 55 °C has been measured. The boiling point of chloroform around 61 °C limits measurements higher than 55 °C.

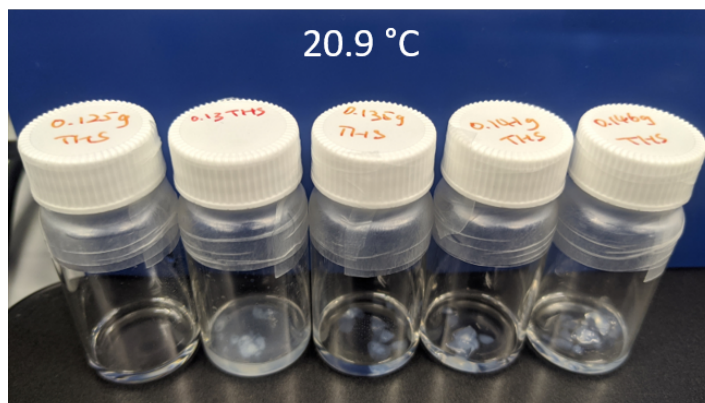


Figure 4.1: An example of visual testing of THS solubility at 20.9 °C.

4.2.2 Preparation of Lipid-chloroform Emulsion in Surfactant Solution

Different concentrations of THS-chloroform were prepared by mixing THS with 1 mL chloroform at a set temperature, then stirred gently by hand. Experiments were performed with saturated THS-chloroform. Surfactant solution was prepared using sodium dodecyl sulfate (SDS) as surfactant and decanol as co-surfactant in Milli-Q water. Decanol was added as 10% of the weight of SDS. Different concentrations of the surfactant solutions were prepared (1 wt%, 3 wt% and 5 wt%). The surfactant solutions' concentrations are higher than their critical micelle concentration (CMC) to ensure production of elongated lipid particles¹³.

THS-chloroform emulsion was prepared in SDS/decanol surfactant solution by mixing the two solutions in a glass vial by hand to produce THS-chloroform emulsion droplets. Preparation at different temperatures, entailed heating the aqueous and organic phases to the same temperature, then storing the emulsion in a constant temperature water bath.

4.2.3 Optical Microscopy and Image Analysis

Microscopy observation was done using a Leica DM2500M optical microscope and all micrographs were recorded using a Moticam 10MP digital camera. A Linkam PE120 peltier temperature controlled stage was used to cool the samples during viewing and monitor the stage's temperature. ImageJ was utilized to analyze the micrographs for particle size and shapes¹⁷.

4.2.4 Measurement of Chloroform Emulsion Evaporation Rate

Evaporation rate was measured in surfactant solutions with different concentration by mixing 1 mL of chloroform with 10 mL of aqueous surfactant solution in a glass vial, and shaking by hand to prepare the emulsion. The emulsions are then observed under an optical microscope at controlled temperatures. Droplet size is extracted by ImageJ and used to calculate the evaporation rate in $\mu\text{m}^3/\text{s}$.

4.2.5 Preparation of Elongated Lipid Particles

Elongated THS particles are produced by evaporating THS-chloroform emulsion in SDS/decanol surfactant solution. In the experiment, one or two drops of the emulsion are placed on a glass slide at the desired temperature. The chloroform quickly evaporates from THS-chloroform solution with variations observed depending on the position with the droplet, as thickness varies at small length scales.

4.2.6 Scanning Electron Microscope

Scanning electron microscope (SEM) characterisation of particles was performed using FEI Nova NanoSEM 450 FE-SEM microscope. The lipid particles were collected and rinsed by Milli-Q water gently to remove extra surfactant, then air dried at room temperature on a silicone waffle. The sample was then coated with an

extra-thick coating of 5 nm of Cr and 60 nm of Pt to prevent melting of the THS wax by the high energy electronic beams. Samples were observed at an accelerating voltage of 5 kV.

4.3 Results and Discussion

4.3.1 Solubility of Lipids in Chloroform

Solvent evaporation production of elongated particles occurs as the chloroform from the THS-chloroform solution diffuses into the surrounding surfactant solution and then evaporates into the atmosphere. Loss of chloroform drives the emulsion droplet to become supersaturated and then start to crystallise. The presence of the surfactant and co-surfactant affects the interfacial tension of the emulsion droplet, allowing the liquid part of the emulsion droplet to dewet from the crystallising region, producing elongated particles.

We assume initiation of the crystallization process occurs as the THS-chloroform solution becomes supersaturated. Conceptual study of the process then requires the solubility curve of THS in chloroform we measured, Figure 4.2). The curve in Fig 4.2 is the solubility boundary of THS in solvent: above the curve is the region of supersaturation. For example, at point c, lowering the temperature will move the system horizontally to the left (green arrow), producing supersaturation and a stronger driving force for crystallisation, Fig 4.2c. Conversely, increasing temperature for a point on the curve will dissolve excess THS into the chloroform or simply reduce the driving force to crystallise of a saturated system. However, increasing the temperature also increases the evaporation rate. Thus, the dynamic conditions of temperature, crystallization rate and evaporation rate make this system more dynamic than the melt studied in Chapter 3. The curve in Fig 4.2 enables us to

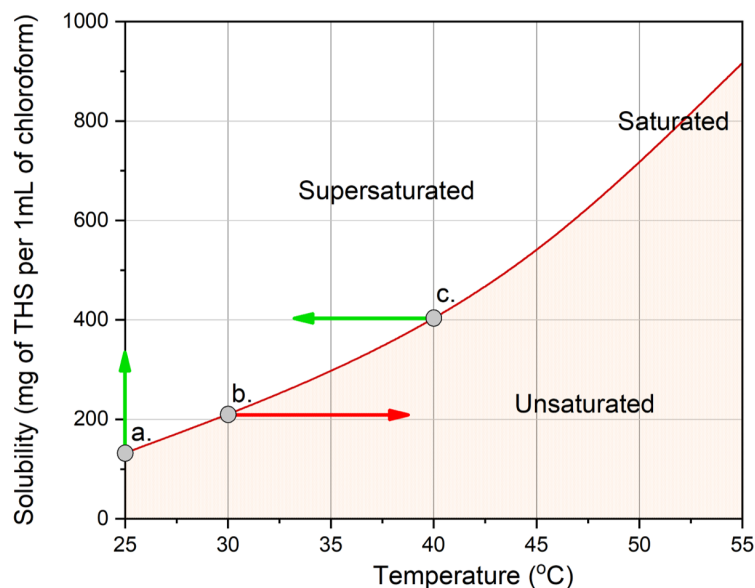


Figure 4.2: A solubility curve of THS in chloroform at different temperatures showing examples of different experimental conditions to produce supersaturation (green arrows) or unsaturation (red arrow). a. Evaporation of chloroform at a certain temperature; b. Increasing the temperature of a saturated THS-chloroform solution; c. Decreasing the temperature of a saturated THS-chloroform solution.

design the experimental conditions to produce elongated particle by evaporation of saturated THS-chloroform emulsion, Fig 4.2.

4.3.2 Evaporation Rate of Chloroform Emulsion

Evaporation rate influences the rate of crystallisation for supersaturated THS-chloroform emulsion droplets. Evaporation rate is dependent on temperature, diffusion rate of chloroform in the surrounding aqueous solution, and the surface area of the emulsion droplets. Figure 4.3 shows the evaporation rate of chloroform emulsion in different concentrations of surfactant at different temperatures. The evaporation rates of chloroform emulsion droplets in both surfactant concentrations have similar variations with size and temperature, with significant scatter due to variations in the sample droplet thickness, with higher temperatures inducing higher evaporation rate.

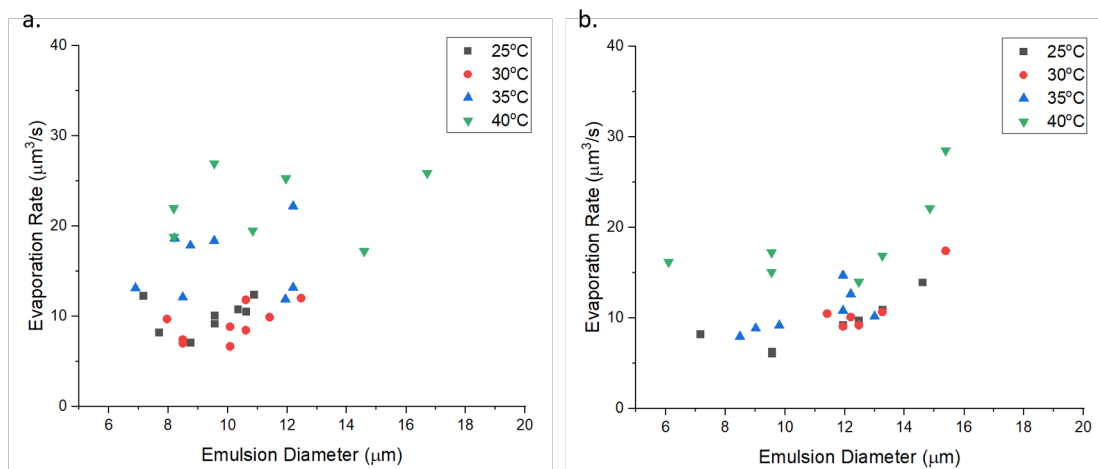


Figure 4.3: Evaporation rate of chloroform emulsion droplets as a function of size and temperature for surfactant concentrations of a) 3.0 wt% and b) 5.0 wt%

4.3.3 Characterisation of Elongated Particles

Evaporation or cooling saturated THS-chloroform emulsions drives the emulsion droplets to become supersaturated and form elongated particles in SDS/decanol solution. We observe four types of elongated particles, spherical, ellipsoidal, long comet, and a unique oscillatory profile shape, shown in detail in Figure 4.4. The four shape types can each dominate different process conditions but are typically observed with other types present as well.

Comparing to the hot emulsion method in Chapter 3, the shapes in Figure 4.4a and b are unique to the solvent evaporation method. The elongated shape in Figure 4.4a has a more pronounced curvature along its length versus the comets found in Chapter 3. The change in direction as the comet grows is likely the result of the more mobile comet in the low-viscosity chloroform versus the more viscous molten THS in Chapter 3. Small differences in local temperature or crystallisation driving force can then nudge the comet more easily as it grows. Additional influences of

surface effects or Marangoni flows¹⁸ may also affect growth but can be difficult to study directly.

The SEM images in Figure 4.4 show the surface morphology of the particles, indicating a relatively smooth surface is produced by the crystallisation with smoothly varying surface curvature even at quite small length scales. As surface properties can affect particle use in biological systems¹⁵, it is encouraging to see lipid particles rival polymeric particles for surface uniformity.

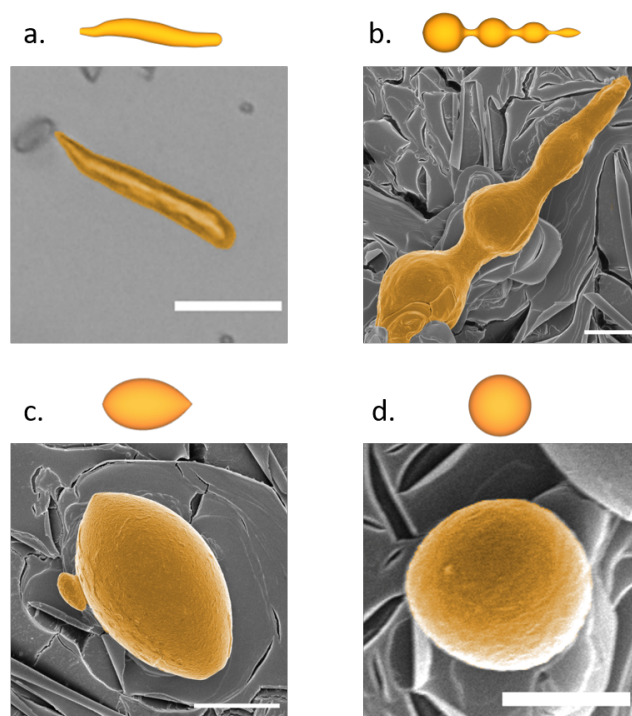


Figure 4.4: Four different types of particles can be formed by solvent evaporation method. *a.* optical micrography, elongated (E) particle. *b-d.* SEM images, (b) nodular (N), (c) tapered (T) and (d) spherical (S) particles. Scale bar in (a) is 30 μm , Scale bars in (b)-(d) are 5 μm

The data shown in Figure 4.5 were produced using a 130g/L THS-chloroform emulsion at varying concentrations of SDS/decanol surfactant solution and experimental temperature conditions (the 130g/L is the saturated concentration of THS in chloroform at 25 °C).

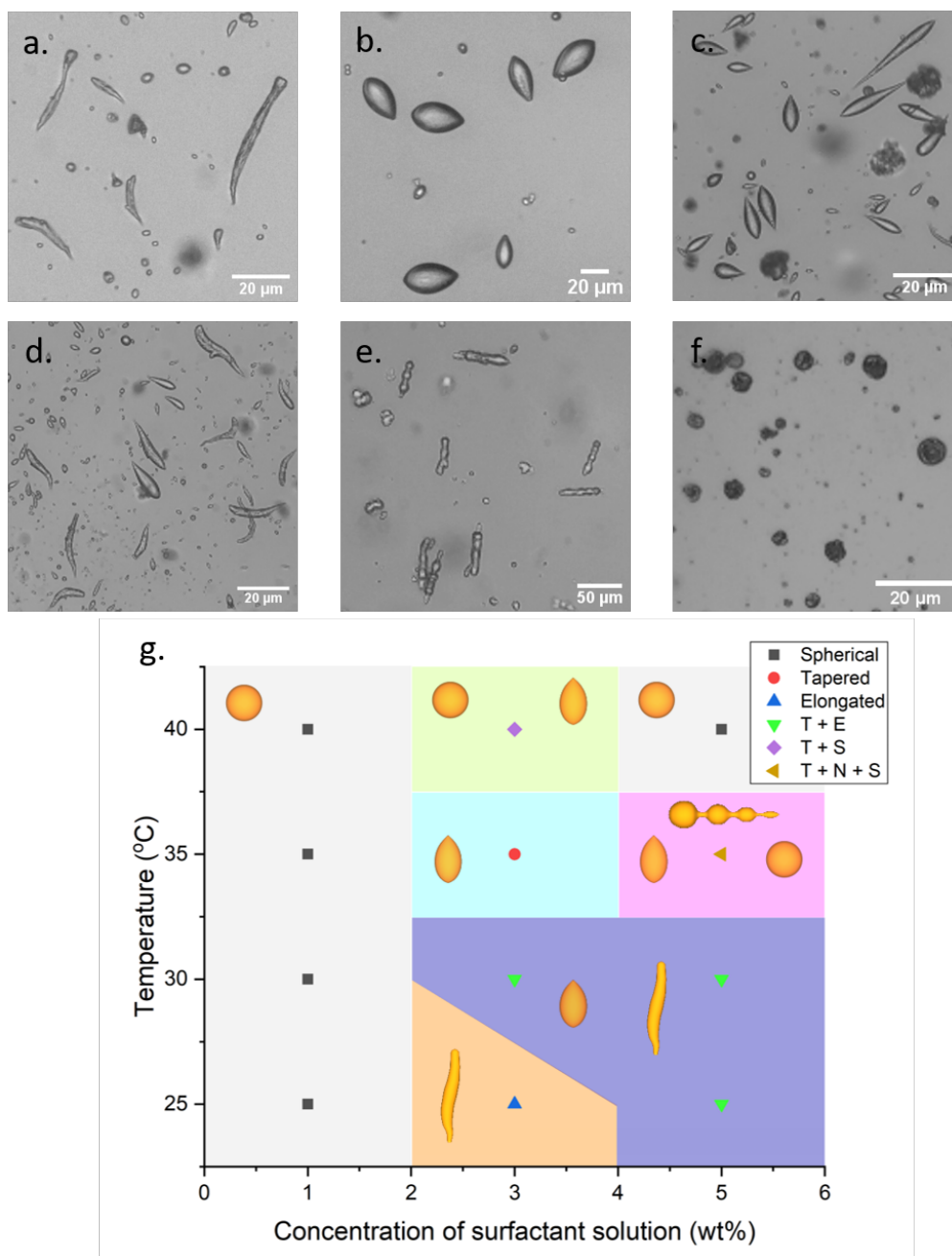


Figure 4.5: Morphology of different shapes of particles formed by solvent evaporation in different conditions. a-c. 3.0 wt% of surfactant solution at 25, 35 and 40°C, respectively. d-f. 5.0 wt% of surfactant solution at 25, 35 and 40°C, respectively. g. Phase diagram showing different shapes can be observed at different conditions, 3-dimensional models sizes are not to scale.

Figure 4.5a-f shows representative micrographs of elongated particles produced at different surfactant concentrations and temperatures. The shapes vary across extreme differences in elongation in rough agreement with the trends observed in Chapter 3. Increased dewetting occurs as a result of higher surfactant concentrations, leading to more elongated shapes or, at extremes, completely ejected spherical particles, Figure 4.5f.

Temperature has a more complex influence on shape production as it will affect evaporation as well as crystallisation. In Figure 4.5g the phase diagram indicates more elongated particles at high surfactant levels and lower temperatures. When the temperature is 25 °C and 30 °C, the evaporation rates in both 3 wt% and 5 wt% surfactant solution are quite similar (Figure 4.3), both around 10 $\mu\text{m}^3/\text{s}$. When the evaporation rate is relatively low, the crystallization driving force is low. When the concentration of the surfactant solution is high, the dewetting driving force is stronger. For both strong dewetting and weak crystallization driving forces, emulsions tend to dewet and form elongated particles with higher aspect ratio.

We are particularly interested in the formation of nodular elongated particle shapes as they are a unique and interesting form (Figure 4.4b). The unique formation of a nodular comet is shown in the time sequence in Figure 4.6, where a comet particle emerges from a droplet with an oscillating radial shape. The process clearly experiences a strongly oscillating rate of crystallisation and dewetting and it is currently quite difficult to decouple their connection.

The formation of the unique nodular particle shapes at intermediate conditions of temperature and surfactant level indicates there is a transitional condition when these particles form. This shape can be produced when the surfactant concentration is high, and the temperature is intermediate (Figure 4.5g). Although we cannot provide a full theory of nodular particle formation, we hypothesise some pos-

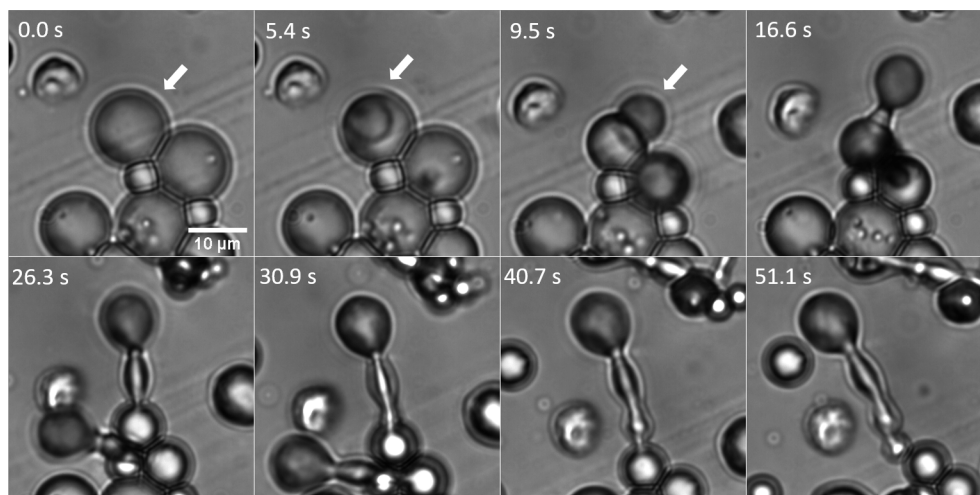


Figure 4.6: An image sequence showing a spherical emulsion droplet crystallized into an elongated lipid particle with a nodular shape.

sible causes. When we heat up the sample, the THS-chloroform emulsion droplet becomes unsaturated, driving the situation away from supersaturation, reducing the crystallization driving force. However, at the same time increasing the temperature will increase the evaporation rate, pushing the THS-chloroform emulsion droplet's toward supersaturation (Figure 4.2). The conflicting influences magnify the system dynamics, possibly producing an instability at the intermediate conditions of 35 °C and 5 wt% surfactant solution. The combination of the intermediate evaporation rate, unsaturated conditions, and a high dewetting driving force may generate a condition vulnerable to destabilisation by latent heat release during the crystallization¹⁹. Crystallisation instabilities are known in similar situations, such as the interfacially-driven Mullins-Sekerka case²⁰. More work is needed, but the oscillatory particles clearly allow production of particles with dramatic variations in particle curvature.

In Figure 4.7 we plot the shape analysis of an exemplary nodular particle. The diameter profile follows a tapering along the particle length as the size of each node decreases. In addition to the unique shape gradient¹⁶ displayed, the particle ex-

hibits strongly fluctuating curvature along its length. As curvature is a strong determinant of some biological interactions¹⁵, it is interesting to note the magnitude of change possible in a particle produced so simply. Typically a particle shape with this level of complexity must be produced using direct moulding via microfluidic or lithographic devices. Here a solvent emulsification crystallization method using relatively simple materials and processes can still produce a particle shape with high dimensionality.

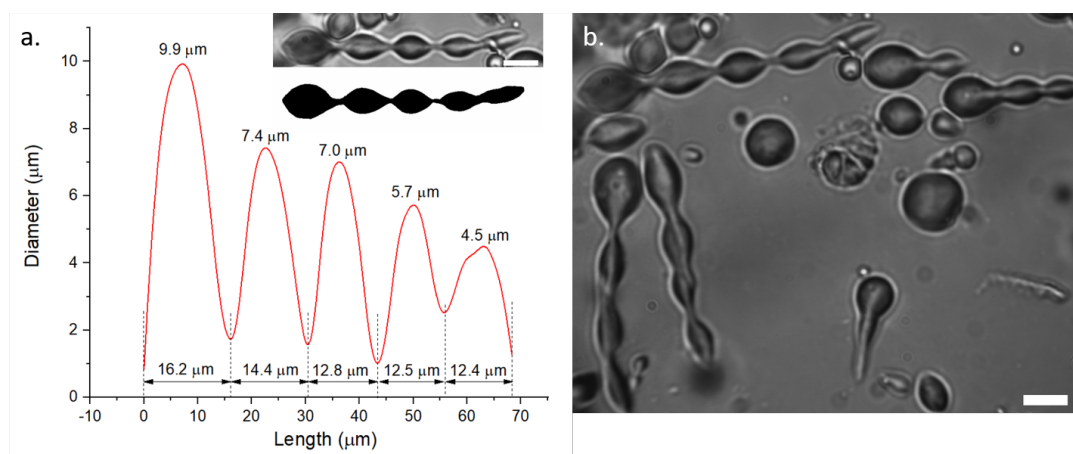


Figure 4.7: *a. An example of size analysis for a nodular particle. b. Multiple nodular elongated particles have been produced by solvent-evaporation method. Scale bars are 10 μm*

4.4 Conclusion

A solvent evaporation method has been used to produce elongated lipid particles as a result of surfactant-induced dewetting. Fundamental measurements of the solubility of THS in chloroform and the evaporation rate of chloroform from emulsion droplets in surfactant have been made. Elongated comet shapes are produced similar to the molten emulsion method, with additional forms produced as a result of the unique dynamics of evaporative cooling and exothermic crystallisation. Elongated tapered particle shapes with oscillatory varying radial dimensions pro-

vide a new class of comet particle with interesting potential properties. The simple method developed here can be controlled using temperature and surfactant concentration variations and a phase diagram has been prepared mapping the conditions needed to produce different shapes. More studies are needed to explore the potential of these novel particle shapes in applications like active delivery.

References

- [1] A. zur Mühlen, C. Schwarz, W. Mehnert, *European journal of pharmaceutics and biopharmaceutics* **1998**, *45*, 149–155.
- [2] V. Jennings, M. Schäfer-Korting, S. Gohla, *Journal of controlled release* **2000**, *66*, 115–126.
- [3] S. Jaspert, G. Piel, L. Delattre, B. Evrard, *Expert opinion on drug delivery* **2005**, *2*, 75–87.
- [4] J. A. Champion, Y. K. Katare, S. Mitragotri, *Journal of controlled release* **2007**, *121*, 3–9.
- [5] D. Dendukuri, K. Tsoi, T. A. Hatton, P. S. Doyle, *Langmuir* **2005**, *21*, 2113–2116.
- [6] Y. Zhao, Y. Wang, F. Ran, Y. Cui, C. Liu, Q. Zhao, Y. Gao, D. Wang, S. Wang, *Scientific reports* **2017**, *7*, 1–11.
- [7] S. E. Gratton, P. A. Ropp, P. D. Pohlhaus, J. C. Luft, V. J. Madden, M. E. Napier, J. M. DeSimone, *Proceedings of the National Academy of Sciences* **2008**, *105*, 11613–11618.
- [8] K. Inthavong, J. Wen, Z. Tian, J. Tu, *Journal of Aerosol Science* **2008**, *39*, 253–265.
- [9] R. Sturm, W. Hofmann, *Journal of hazardous materials* **2009**, *170*, 210–218.
- [10] J. A. Champion, Y. K. Katare, S. Mitragotri, *Proceedings of the National Academy of Sciences* **2007**, *104*, 11901–11904.

References

- [11] M. Caggioni, D. Traini, P. M. Young, P. T. Spicer, *Powder Technology* **2018**, 329, 129–136.
- [12] V. Sharma, K. Park, M. Srinivasarao, *Materials Science and Engineering: R: Reports* **2009**, 65, 1–38.
- [13] P. T. Spicer, R. W. Hartel, *Australian journal of chemistry* **2005**, 58, 655–659.
- [14] G. Sharma, D. T. Valenta, Y. Altman, S. Harvey, H. Xie, S. Mitragotri, J. W. Smith, *Journal of controlled release* **2010**, 147, 408–412.
- [15] J. A. Champion, S. Mitragotri, *Proceedings of the National Academy of Sciences* **2006**, 103, 4930–4934.
- [16] S. C. Glotzer, M. J. Solomon, *Nature materials* **2007**, 6, 557–562.
- [17] C. A. Schneider, W. S. Rasband, K. W. Eliceiri, *Nat. Methods* **2012**, 9, 671–675.
- [18] A. Askounis, Y. Kita, M. Kohno, Y. Takata, V. Koutsos, K. Sefiane, *Langmuir* **2017**, 33, 5666–5674.
- [19] R. A. Lange, K. V. Cashman, A. Navrotsky, *Contributions to Mineralogy and Petrology* **1994**, 118, 169–181.
- [20] W. W. Mullins, R. F. Sekerka, *J. Appl. Phys.* **1963**, 31, 323–329.

Chapter 5

Behaviour of Elongated Lipid Particles in Shear Flow

5.1 Introduction

The dynamic and rheological behaviour of spherical particles in simple shear flow has been well-studied for some time¹⁻⁴. Nonspherical particles are also of strong interest in different applications. High aspect ratio rod-like particles have been studied for improved drug delivery in gas and liquid flows^{5,6}. Flow behaviour of fibrous aerosol particles can also help understand hazards such as asbestos and other fibrous threats to human health⁷. The motion of non-spherical particles without axial symmetry has not been investigated as much as their symmetric counterparts. As unusual particle shapes can be common in various industries, and shape can have a profound effect on rheology, flow, and processing, it is important to understand how new shapes like the tapered comets we produce might behave in a fluid⁸.

Jeffery developed a model of flow of elongated particles shapes almost a century ago. The periodic rotational motion of ellipsoidal particles in shear flow, now known as Jeffery orbits⁹, can be described as a function of the particle aspect ratio a_r , the ratio of length, l , and w , width (shown in Fig 5.1. The Jeffery orbit period, T_J , can be calculated by:

$$T_J = \frac{2\pi(a_r + 1/a_r)}{\dot{\gamma}} \quad (5.1)$$

where $\dot{\gamma}$ is the fluid shear rate. The period of a spherical particle is recovered from Equation 5.1 when $a_r = 1$. In this chapter, we study the rotational motion of our comet particles in simple shear and compare with the predictions of Equation 5.1 for spheres, rods, and ellipsoids. We are interested in how these particles flow so we can see how the comet shapes might behave in a practical use like aerosolisation. The non-axisymmetric shape is expected to modify the Jeffery orbit period¹⁰ as the rotation highly sensitive to slight deviations of particle orientation that we expect from our shapes^{10,11}. The particle rotation influence on non-axisymmetric shapes can be drastic¹¹. For example, Hinch and Leal found that for two particles under otherwise similar conditions, the non-axisymmetric one can have periodic oscillations with up to $\pm 60^\circ$ variations versus the axisymmetric one¹¹. Another example is work of Kaya and coworker that showed asymmetric *E.coli* cells in shear flow had distinct half rotation periods as a result of their asymmetrical shape¹².

As the production of elongated comet particles can be used to control particle aspect ratio and size starting with only a simple emulsion, we see the potential to scale-up the processes discussed in Chapters 3 and 4 but it will be helpful to know the bulk flow characteristics of these systems first.

5.2 Materials and Methods

Stearic acid (95%), decanol (98%), and sodium dodecyl sulfate (99.0% GC) were purchased from Sigma-Aldrich. Trihydroxystearin (Peter Cremer), and Milli-Q water.

5.2.1 Preparation of Lipid-based Elongated Particles

A bulk amount of elongated lipid-based particles is prepared using the molten emulsion method. Larger particles are desirable to aid in microscopic observations during fast flow and this can be easily tuned by starting from larger precursor droplets.

Comets are made by mixing 1.50 wt% of SDS with 0.15 wt% of cosurfactant decanol in Milli-Q water. The surfactant solution is then heated to at least 90 °C in a water bath. A lipid mixture of 60 wt% of stearic acid and 40 wt% of trihydroxystearin is heated to 90 °C in a water bath for at least 30 min to remove any crystal memory¹³. Mixing the hot surfactant solution with melted lipids mixture to prepare forms a hot emulsion which is then slowly added to a surfactant solution at 45 °C to prepare the lipid-based elongated particles in bulk. The solidified elongated lipid particles are then cooled to room temperature and observed in flow using under the optical microscope.

5.2.2 Observation of Particles' Behavior by Optical Microscope

The experimental set up is shown in Figure 5.1. The elongated lipid particles in the surfactant solution are transferred into a syringe (BD, Singapore). The syringe is attached to a syringe pump (WPI 947-371-1003, USA) to control the flow rate. A Tygon tube (Saint-Gobain, France) connects the syringe and a flat capillary (Vitro-Com, USA). We use two thicknesses of the flat capillary, 0.1 mm and 0.2 mm. The millifluidic flow of the lipid particles is observed with a Leica DM2500M optical microscope at 22 °C. A Qimage optiMOS camera is used to record the flow with a frame rate of 100 ms. ImageJ is used for image and trajectory study.

5.2.3 Trajectory Study

Identification of particles and mapping of a trajectory has been conducted by using the 'Trainable Weka Segmentation' Plugin in ImageJ. The system is trained using a representative image at each different condition to generate an identical 'classifier' document to recognise the particles as they move in the shear flow. The elongated particles and spherical particles are separated into different 'classes' so that the

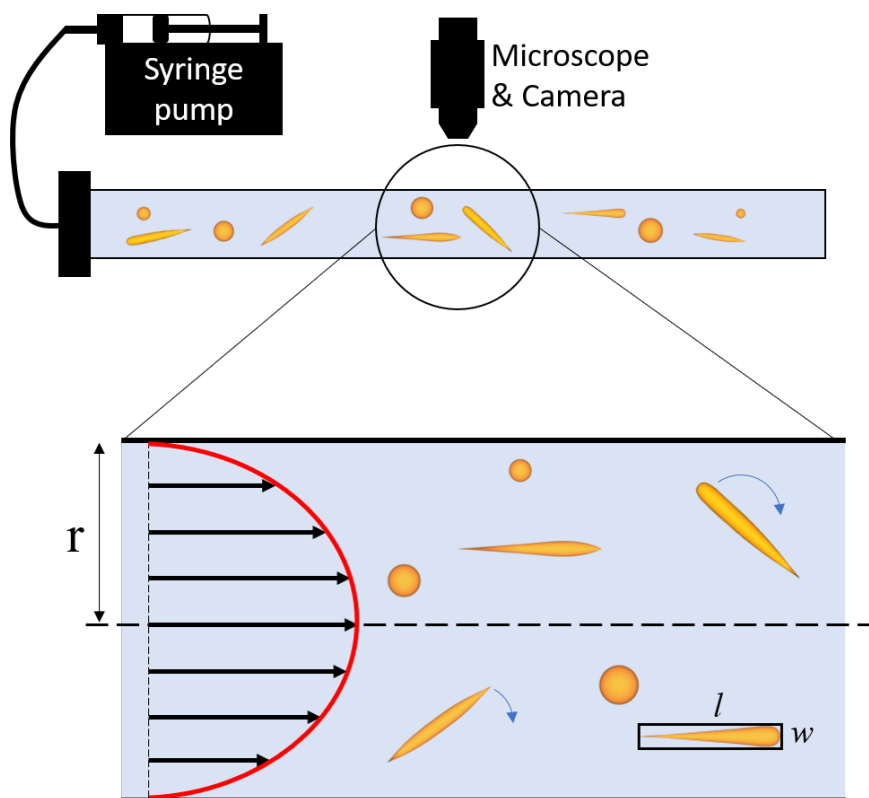


Figure 5.1: A schematic of the experimental setup. The blue arrows indicate the direction of rotation of the elongated particles. Images are not to scale.

system only tracks elongated particles. Matlab has been used to plot the trajectory data, with code given in Appendix B.

5.3 Results and Discussion

5.3.1 Modes of Behaviour in Shear Flow

In lipid particle suspensions, there is often a broad distribution of size and aspect ratio. Three different types of behaviour been observed for the elongated lipid particles in millifluidic flow (Figure 5.2). Spinning behaviour is seen when the particles rotate around their long axis without changing orientation angle. Swimming behaviour is when the particle moves horizontally aligned with the flow direction without changing orientation angle. Swinging behaviour is seen when the particle

swings back and forth with a certain period, moving between two extreme orientation angles, θ , the swinging angle. The swinging motion is very similar to behaviour exhibited by blood cells in blood vessels^{14,15}.

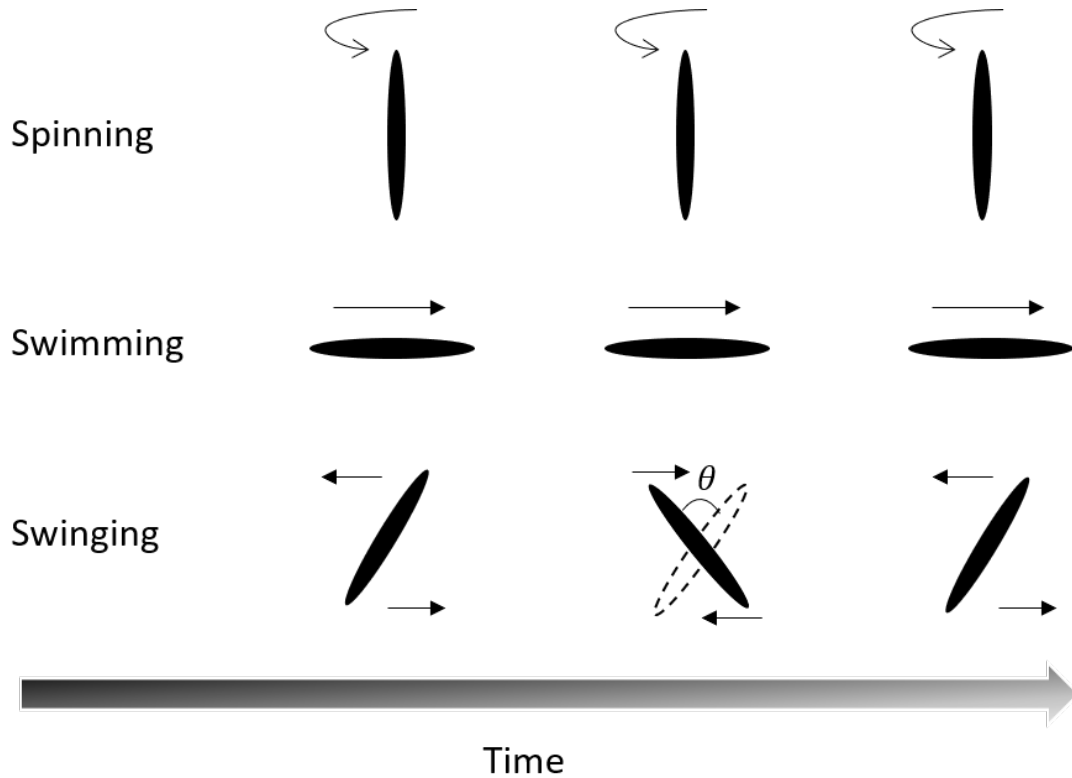


Figure 5.2: Schematic of three types of behaviour observed when the comet particles flow in simple shear. Black arrows indicate the motion of the particles. The particle shapes are not shown to scale.

Figure 5.3 plots the distribution of particles exhibiting different behaviours at different flow rates and channel dimensions. The linear flow velocity, v , is defined by Equation 5.2. Where Q is the volumetric flow rate and A is the cross sectional channel area. The shear rate, $\dot{\gamma}$, is defined by Equation 5.3, where h is the channel height. Variations in thickness of the flat capillary will thus alter fluid flow velocity and shear rate. In Figure 5.3a, the flow velocity is higher than in Figure 5.3b due to

use of a shorter channel height. When particles experience larger axial flow velocities, the majority of them swim without significant changes in orientation angle.

$$Q = v \cdot A \quad (5.2)$$

$$\dot{\gamma} = \frac{v}{h} \quad (5.3)$$

For the lower linear velocity in Figure 5.3b, more variation in behaviour is observed, with a decrease in flow-aligned swimming behaviour and an increase in swinging variations in particle orientation. We attribute the increased swinging behaviour to the non-axisymmetric shape of the comet particle. As the particle spans regions of flow with different velocities, the comet particle's two ends experience different levels of viscous drag force. We see more of this behaviour at the lowest flow velocities. Spinning behaviour is observed the least of the three main types of behaviour, though is also more prevalent at lower flow velocities. This may also result from the lack of axial symmetry of the particles. We are also interested in the overall particle trajectory for the elongated comet shapes, as this will determine behaviour in applications like targeted deposition.

5.3.2 Comet Particle Trajectories in Shear Flow

Distributions of average comet orientation and the trajectories of comet particles in shear are plotted in Figure 5.4 for the 0.1 mm capillary and Figure 5.5 for the 0.2 mm capillary. The unique shapes of the comet particles could eventually be applied in the field of active matter, enabling more complex interaction between propulsion force and rotational motion than for simpler spherical active particles^{16,17}.

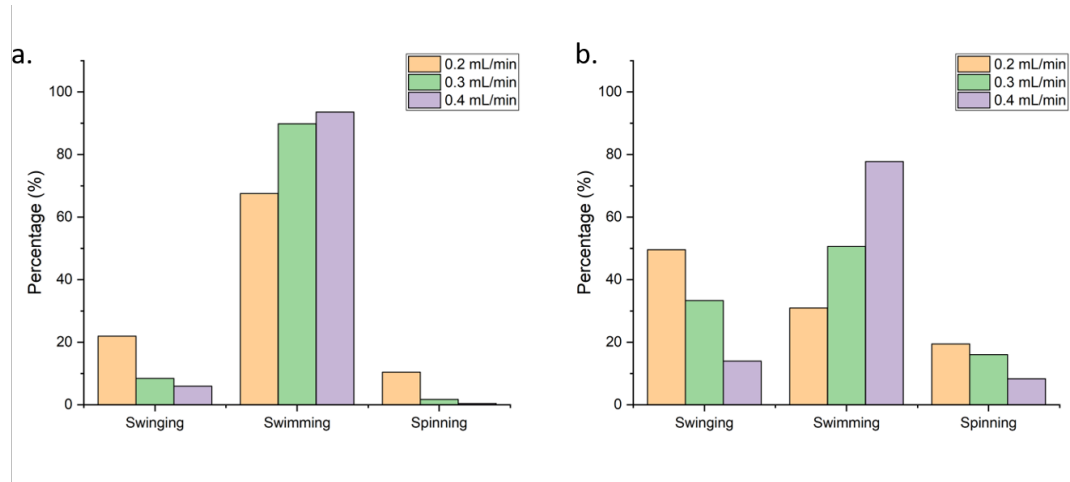


Figure 5.3: The distribution of particles exhibiting three different behaviours in shear flow at different flow rates during millifluidic flow in a) 0.1 mm thickness flat capillary and b) 0.2 mm thickness flat capillary.

The x-y coordinates of the particles in Figure 5.4b and d and Figure 5.5b and d correspond to the position of the particles in a flow. The colour of the plotted line maps the orientation angle of the particle as it moves down the channel and sometimes changes orientation. The influence of flow velocity and shear rate on particle behaviour can be determined by comparison of Figure 5.4a and b with Figure 5.4c and d.

The increase of the volumetric flow rate increases the linear velocity in the capillary so all the particles move via swimming behaviour. Comparing with Figure 5.5a and b and Figure 5.5c and d, we see both flow velocities are lower than in the 0.1 mm thickness flat capillary. In Figure 5.5a and b, the flow velocity does not dominate the system to the extent that all particles exhibit flow-aligned swimming behaviour, as a larger percentage swing as well (Figure 5.3b). More data are needed, but the trajectory angle maps indicate the swinging angle θ increases with increasing shear rate.

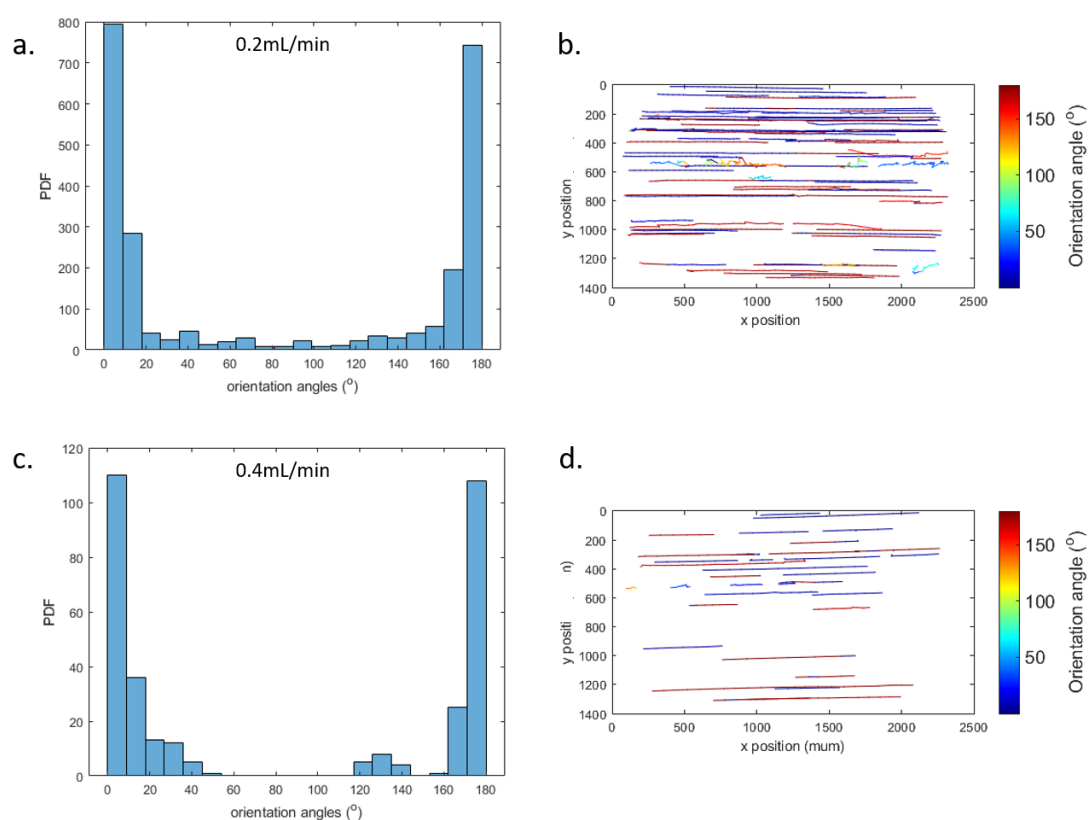


Figure 5.4: Comet particles flow in a 0.1 mm thickness flat capillary. The probability distribution function of the particle orientation angles in shear flow is plotted for flow rates of a) 0.2 mL/min and c) 0.4 mL/min, respectively. Trajectories and orientation angles are plotted for b) 0.2 mL/min and d) 0.4 mL/min.

We can also compare particle behaviour at the same linear velocity but different shear rate by viewing Figure 5.4a and b and Figure 5.5c and d. According to Equation 5.2, because the capillary thickness in Figure 5.5 is doubled to the thickness in Figure 5.4, the flow velocities in Figure 5.4a and b (flow rate is 0.2 mL/min) and in Figure 5.5c and d (flow rate is 0.4 mL/min) are the same. However, the shear rate in Figure 5.5c and d is lower than in Figure 5.4a and b (refer to Equation 5.3, same v but different h). So, due to the difference of shear rates, the percentage of particles with each behaviour are different (Figure 5.3). This phenomenon can also be illustrated by Figure 5.4a and Figure 5.5c. In Figure 5.4a, most particles

have orientation angles of 0 or 180°. While in Figure 5.5c, a more diverse range of orientation angles is observed. In Figure 5.4b, the swinging trajectories are coloured orange/red or blue. The swinging trajectories in Figure 5.5d, are yellow and green, indicating the swinging angle θ of the comets is larger in the flow with a higher shear rate.

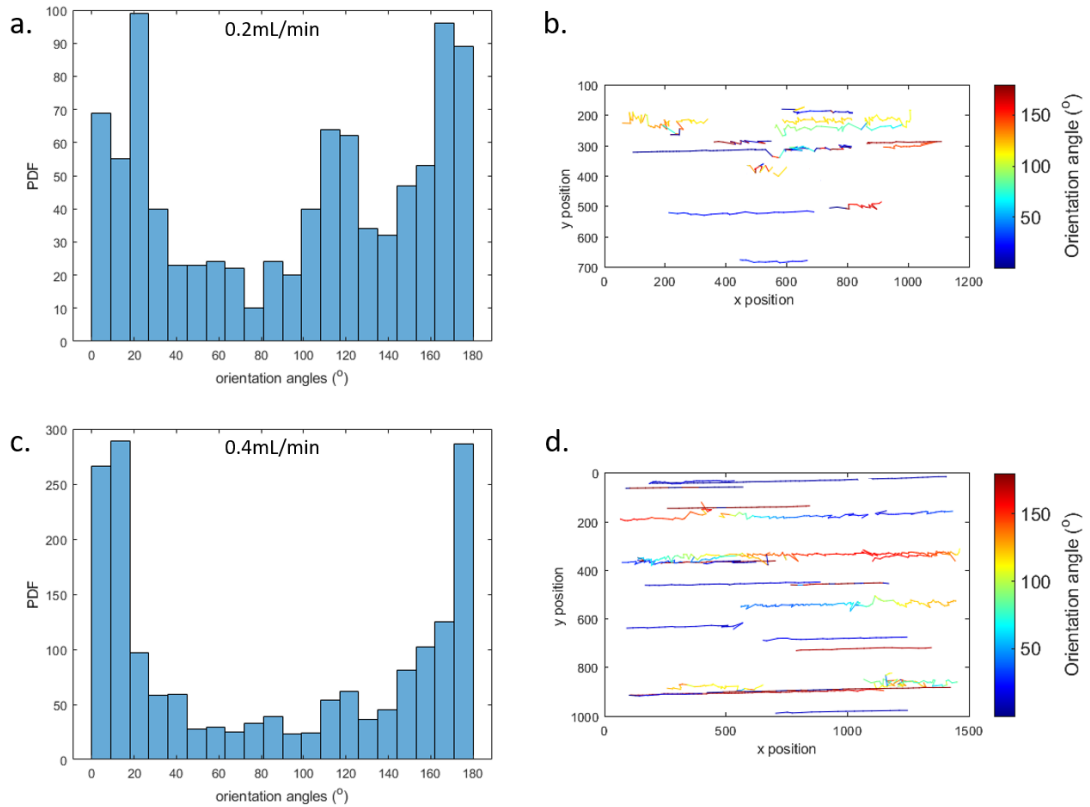


Figure 5.5: Comet particles flow in a 0.2 mm thickness flat capillary. a& c. The probability distribution function of the particle orientation angles in shear flow at 0.2 mL/min and 0.4 mL/min flow rate, respectively. b& d. The trajectory of particles in shear flow with 0.2 mL/min and 0.4 mL/min flow rate, respectively.

5.3.3 Jeffery Orbit Comparison

Determination of Jeffery orbit behaviour for our particles provides a means of evaluating their response to flow as well as a benchmark against more regular elongated shapes⁹. We calculate the Jeffery orbit period of the sphere, prolate spheroid, and

cylinder using Equation 5.1⁹. For spheres, the aspect ratio $a_r = 1$, for cylinders, the aspect ratio a_c needs to be converted to a_r using Equation 5.4¹⁸. We measure the Jeffery orbit periods for comet particles from high-speed imaging of to monitor the interval of motion, shown in Figure 5.6. Spherical particles have the shortest Jeffery orbit period of these four shapes. For both flow rates, the comet particles' Jeffery orbit periods are very similar to prolate spheroids. At a lower flow rate (Figure 5.6a), all shapes exhibit Jeffery orbit periods longer than the shapes in a higher flow rate (Figure 5.6b). This is because the higher shear rate creates a larger difference across the two ends of the particle increasing the effect^{19,20}. For Jeffery orbit theory, there is no orientation that halts the rotation of an ellipsoid²¹. Bretherton discussed that the asymmetric shape of a rigid particle in certain conditions will create an equilibrium of orientation that will allow the asymmetric particle to flow in a more aligned direction without periodic rotation due to the transverse force²¹. However, practically this ideal equilibrium of forces will be disturbed by slight orientation changes²¹. The lateral force on the non-axisymmetric comet particles deviates from the Jeffery orbit, likely due to an analogous complex balance of equilibrium moment and lateral forces.²¹.

Drawing straight green line horizontally in Figure 5.6b, for example, we see a comet particle with aspect ratio 10 is equivalent to a prolate spheroid particle with aspect ratio 12 and a cylinder particle with aspect ratio 16. The non-axisymmetric comet particles thus behave as though they have larger aspect ratios with less mass used per particle. Though not enormous, the differences observed indicate the more complex particle shapes hold promise for altered flow behaviour in applications like deposition from a flow to a targeted substrate

$$a_r = 1.24a_c / \sqrt{\ln a_c} \quad (5.4)$$

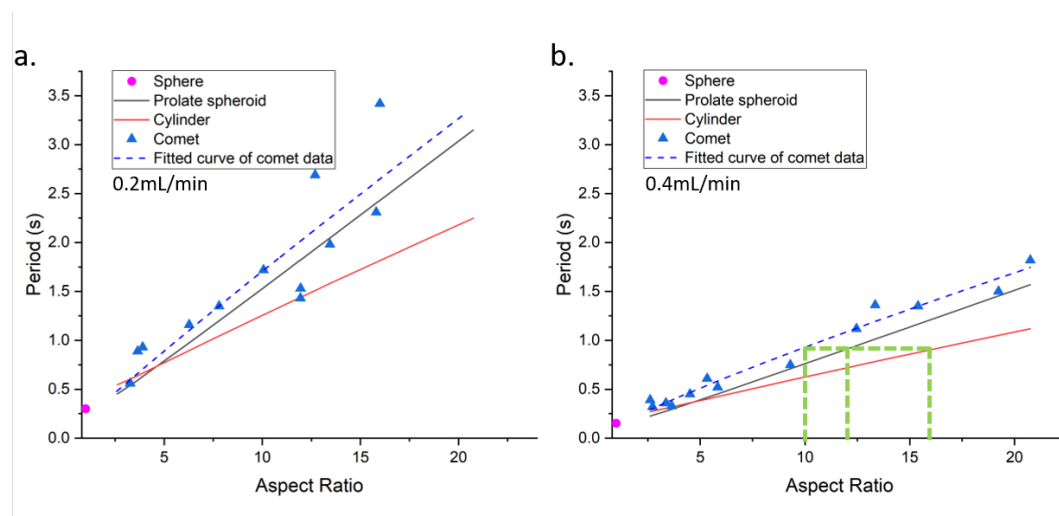


Figure 5.6: Calculated Jeffery orbit period of sphere, prolate spheroid, and cylinder plotted against the experimental comet particle values at different aspect ratios. A flat capillary with 0.22 mm thickness has been used in this experiment. *a.* Jeffery orbit period in shear flow with flow rate 0.2 mL/min. *b.* Jeffery orbit period in shear flow with flow rate 0.4 mL/min.

5.4 Conclusion

In this chapter, the behaviour of elongated lipid particles prepared by hot emulsification has been observed in a shear flow. The rotational motion of the particles has been analysed by measurement of the Jeffery orbit period, and despite the distinct tapered shape of the particles we see good agreement with the predicted behavior of elongated rod and ellipsoid shapes. The only unique aspect of the comet particle flow behaviour is their equivalency with a higher aspect ratio value ellipsoid and cylinder. Three different types of particle motion are observed, with the most common being flow-aligned translation along the microchannel, termed swimming. Unaligned spinning and swinging behaviour is also observed, but with a frequency determined by the magnitude of flow velocity and shear rate used. Future work might explore specific effects of the tapered comet dimensions on flow stability in

shear, as the non-axisymmetric shape of the comet particles impart a more complex orientation tendency versus shapes¹⁰.

References

- [1] J. F. Brady, G. Bossis, *Journal of Fluid Mechanics* **1985**, *155*, 105–129.
- [2] M. Reeks, *Physics of Fluids A: Fluid Dynamics* **1993**, *5*, 750–761.
- [3] C.-J. Lin, J. H. Peery, W. Schowalter, *Journal of Fluid Mechanics* **1970**, *44*, 1–17.
- [4] C. Lun, A. Bent, *Journal of Fluid Mechanics* **1994**, *258*, 335–353.
- [5] C. Uhl, Y. Gao, S. Zhou, Y. Liu, *RSC advances* **2018**, *8*, 8089–8100.
- [6] H. T. Ta, N. P. Truong, A. K. Whittaker, T. P. Davis, K. Peter, *Expert Opinion on Drug Delivery* **2018**, *15*, 33–45.
- [7] E. Gavze, M. Shapiro, *International Journal of Multiphase Flow* **1997**, *23*, 155–182.
- [8] D. Qi, L.-S. Luo, *Journal of Fluid Mechanics* **2003**, *477*, 201–213.
- [9] G. B. Jeffery, *Proceedings of the Royal Society of London. Series A Containing papers of a mathematical and physical character* **1922**, *102*, 161–179.
- [10] J. Einarsson, B. Mihiretie, A. Laas, S. Ankardal, J. Angilella, D. Hanstorp, B. Mehlig, *Physics of Fluids* **2016**, *28*, 013302.
- [11] E. Hinch, L. Leal, *Journal of Fluid Mechanics* **1979**, *92*, 591–607.
- [12] T. Kaya, H. Koser, *Physical review letters* **2009**, *103*, 138103.
- [13] S. Metin, R. W. Hartel, *Bailey's industrial oil and fat products* **2005**.
- [14] M. Abkarian, M. Faivre, A. Viallat, *Physical review letters* **2007**, *98*, 188302.
- [15] D. Cordasco, P. Bagchi, *Journal of Fluid Mechanics* **2016**, *800*, 484.
- [16] L. D. Rubio, M. Potomkin, R. D. Baker, A. Sen, L. Berlyand, I. S. Aranson, *Advanced Intelligent Systems* **2021**, *3*, 2000178.
- [17] E. M. Purcell, *American journal of physics* **1977**, *45*, 3–11.

- [18] S. B. Lindström, T. Uesaka, *Physics of fluids* **2007**, *19*, 113307.
- [19] C. Cozens-Roberts, J. A. Quinn, D. Lauffenberger, *Biophysical journal* **1990**, *58*, 107–125.
- [20] J. Tan, S. Shah, A. Thomas, H. D. Ou-Yang, Y. Liu, *Microfluidics and nanofluidics* **2013**, *14*, 77–87.
- [21] F. P. Bretherton, *Journal of Fluid Mechanics* **1962**, *14*, 284–304.

Chapter 6

Elongated Lipid Particles: Interfacial Hydrodynamic and Drug Loading Studies

Chapters 3 and 4 focused on the characterisation of two emulsion solidification processes to produce elongated lipid particles. Experimental observations¹ and theoretical studies² agree with our conceptual model of comet formation: relative dewetting and solidification rates control the process. There is much about the comet phenomenon, however, that still needs to be understood.

6.1 Observation of Marangoni Flow

One example is the actual mechanism of comet formation: why do some lipid/-surfactant combinations produce the robust dewetting necessary to make comets? Surfactant adsorption and lipid solidification can both affect emulsion interfacial properties and drive the dewetting flows we observe. Here we carry out some preliminary observations of the flows in and around comets as they form and compare them with similar flows noted in active emulsions.

6.1.1 Methods and Materials

Fluid flow visualisation is enabled using 1 μm spherical PMMA tracers (Polysciences). Comets are produced from trihydroxystearin (Peter Cremer) and Stearic acid (95%). Dewetting is induced by the co-surfactant decanol (98%), and surfactant sodium dodecyl sulfate (99% GC) purchased from Sigma-Aldrich. All water used is Milli-Q.

To observe the flow pattern inside an emulsion droplet, a suspension of 1 μm tracer particles is dried in an oven at 50 °C and then re-dispersed into powder using a ceramic mortar. The resulting particles are then mixed with molten SA/THS lipids mixture (SA: THS ratio is 6:4) at 85 °C. When the tracer-lipid mixture is homogeneous, it is then cooled and solidified. The SDS/decanol surfactant solution is prepared by mixing SDS and decanol with a mass ratio of 10:1 in water and then heating to 85 °C in a water bath.

Comets are made by first transferring a small amount of the solidified lipid-tracer mixture is transferred onto a glass slide. Then two drops of the SDS/decanol surfactant solution is placed onto the powder and heated up to 90 °C on a hot plate. The lipids melt to form multiple large emulsion droplets in the surfactant solution, allowing observation by optical microscope and high speed camera to capture the flow pattern mapped by the tracer particles. Comet formation is induced by cooling the sample on a Linkam PE120 Peltier microscope stage at a cooling rate of 10 °C/min.

ImageJ is used to analyse the images, and a "Running ZProjector" Plugin is used to visualize the tracer flow pattern.

6.1.2 Results and Discussion

Figure 6.1 shows a schematic of how Marangoni flows could be generated by gradients of surface tension on a droplet. In the absence of crystallisation, droplets can be moved by Marangoni mechanisms simply as a result of solubilisation by the surrounding surfactant micelles³.

Here we add the phenomena of crystallisation and dewetting, so that mass is removed from the droplet as it changes phase. Cooling induces crystallization of the oil droplet, which may cause incorporation of the surfactant into the lipid. As

the solid is dewetted, surfactant is then depleted from the droplet. The interplay of solubilisation and crystallisation is not fully understood for this system, but the schematic shows a possible interpretation of how surfactant concentration at the solid-oil interface could be reduced and contribute to the overall surface tension gradient and Marangoni flow⁴⁻⁶.

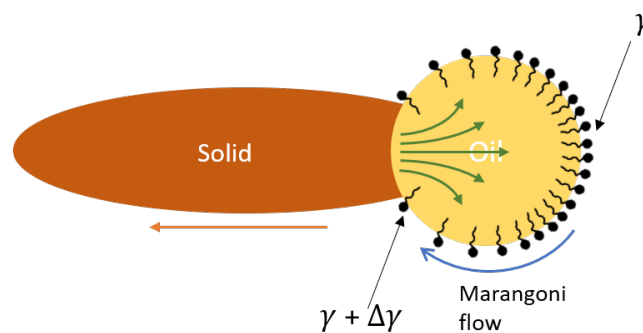


Figure 6.1: A schematic of possible Marangoni flow patterns during the formation of a comet particle. The orange arrow indicates the crystal growth direction; the green arrows indicate the convective flow in the droplet; the blue arrow shows the Marangoni flow generated by a surface tension gradient. γ is the surface tension, and $\Delta\gamma$ is the difference of the surface tension between the fron and back of the droplet.

Figure 6.2 shows tracer trajectories that indicate the internal and external flows that occur in our emulsions. A clear convective flow pattern is shown in Figure 6.2a as a result of thermal or interfacial gradients. In Figure 6.2b a snapshot of a comet during formation is shown. Here we see flow that may result from Marangoni stresses due to a surface tension gradient at the surface of the droplet. In addition to any solubilisation effects on the interface³, however, thermal effects of the latent heat of crystallisation will also affect the process. Heating of the interface will lower the interfacial tension due the existence of the latent heat generated by the crystallization process. We do not yet fully understand the complex interactions of

these processes during comet formation, but have tried to document the behaviour to add insight to the dewetting phenomenon been driven.

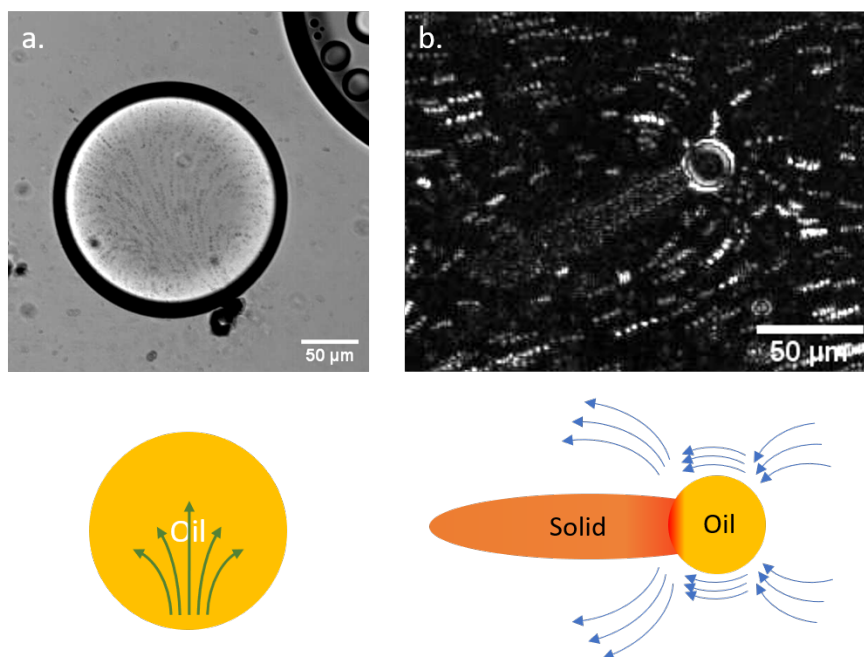


Figure 6.2: The experimental flow pattern results for a. internal flow, and b. external flow. The green arrows are the convective flow; the blue arrow is the Marangoni flow generated by the gradient of surface tension; and the red color glow is the latent heat.

6.2 Drug Loading for Elongated Comet Particles

This thesis is motivated by a desire to understand and control new phenomena that enable production of complex shaped colloids. Although we do not test the particles for any one application, we view the comets as a potentially useful carrier for cosmetic and pharmaceutical active ingredients. Below we test the ability of comets to incorporate powdered active drug compounds and assess the likely success of materials with similar properties.

6.2.1 Methods and Materials

The materials are: Trihydroxystearin (Peter Cremer), stearic acid (95%), decanol (98%), sodium dodecyl sulfate (99% GC), Tris (tris (hydroxymethyl) aminomethane) (99.8%), dopamine hydrochloride, and Hyaluronic acid ($1.5 - 1.8 \times 10^6$ Da) were purchased from Sigma-Aldrich. Milli-Q water.

The elongated comet particles are produced by using hot emulsion method. The method is introduced deatiledly in Chapter 3, Section 3.2.1 and 3.3.6. To coat poly-dopamine (PDA) onto elongated lipid particles, the elongated lipid particles prepared by hot emulsion method do not need to be filtered. SDS is needed in the drug loading experiment. Tris buffer (pH=8.5) is mixed with elongated lipid particle suspension and dopamine hydrochloride. The polymerization process is conducted overnight at room temperature with constant stirring. After the polymerization, the extra PDA is removed by dialysis against water for at least 24 hours⁷. Then the PDA-coated particles are coated with an extra-thick coating with 5nm of Cr and 60nm of Pt before the SEM imaging.

Hyaluronic acid (HA) is used to coat the surface of SA/THS lipid particles by electrostatic attraction method^{8,9}. SA/THS lipid particles suspension in surfactant solution has been filtered by membrane with 5 μ m pore size to remove SDS and decanol. The particle then resuspend into 10 mL of Milli-Q water. 1 mL of 0.02 wt% hyaluronic acid solution is slowly dropped into 10 mL SA/THS lipid particles suspension with stirring. To observe the HA-coated lipid particles under SEM, they then coated with an extra-thick coating with 5nm of Cr and 60nm of Pt before the SEM imaging.

6.2.2 Results and Discussion

The preliminary results of coating PDA and HA onto the surface of SA/THS lipids mixture particles are successful, the SEM images of drug coated particles are showing in Figure 6.3. We can see the surface of SA/THS particles before loading with anything is relatively smooth (Figure 6.3a& d). For the PDA-coated lipid particles, we can see spherical PDA and some short rod-shaped PDA particles crossing like a web coated on the surface of the lipid particles (Figure 6.3b&e). For HA-coated lipid particles, we can see the worm-like HA particles coated on both elongated and spherical SA/THS particle (Figure 6.3c&f). We can see that the SA/THS particles shape have not changed after loaded by these two drugs.

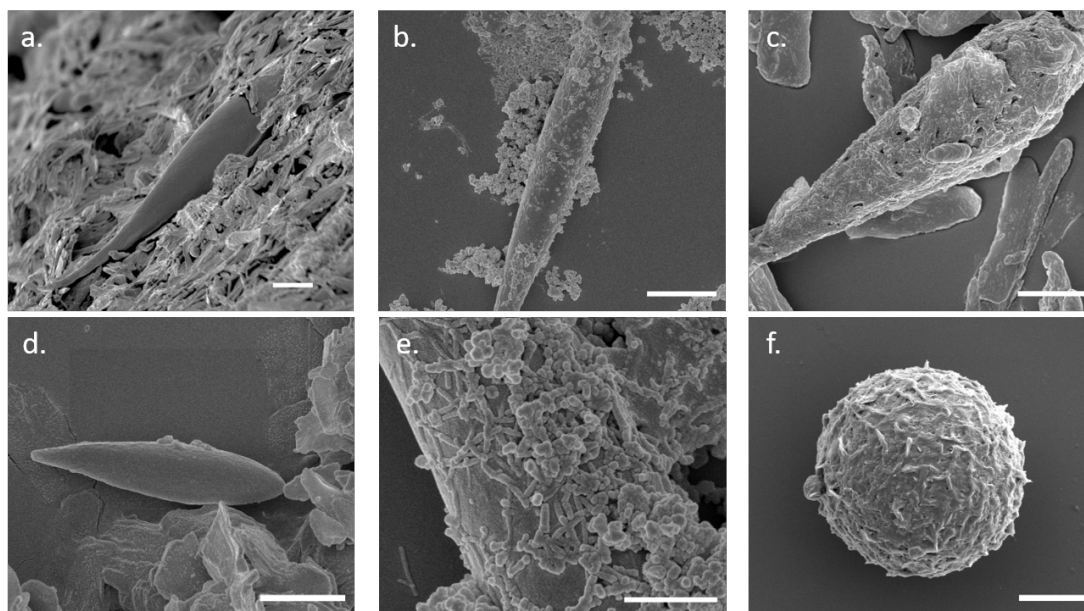


Figure 6.3: SEM images of SA/THS particles a& d. no drug loading; b& e. coated with PDA; c& f. coated with HA. Scale bar in e is 1 μm , other scale bars are 3 μm .

6.3 Conclusion

The discovery of Marangoni flow surrounding the emulsion droplet during the formation of the comet particle gives us a valuable insight to study the dewetting phenomenon in a more detailed level. The external Marangoni flows and internal convective flow might play a role on influencing the formation of the comet particle. The future study about investigating the Marangoni flow can study the influence of the Marangoni flow to the shape, size, aspect ratio and even the density distribution of the comet particle. This data will help to scale-up, and to understand flow properties of comet shape particles in the air and fluids.

To deliver drug is the purpose of preparing these comet lipid particles. So the study of loading drug onto/into the shaped particles are essential to convert this technology to a real product. These preliminary results of loading PDA and HA are successful. However, further study of how to optimize the drug loading condition, and drug loading capacity study and the drug releasing study needed to be investigated.

References

- [1] P. T. Spicer, R. W. Hartel, *Australian journal of chemistry* **2005**, *58*, 655–659.
- [2] M. Q. Giso, H. Zhao, P. T. Spicer, T. J. Atherton, *Langmuir* **36**, 13853—13859.
- [3] C. Jin, C. Krüger, C. C. Maass, *Proceedings of the National Academy of Sciences* **2017**, *114*, 5089–5094.
- [4] M. G. Velarde, R. K. Zeytounian *et al.*, *Interfacial phenomena and the Marangoni effect*, Springer, **2002**.
- [5] A. Askounis, Y. Kita, M. Kohno, Y. Takata, V. Koutsos, K. Sefiane, *Langmuir* **2017**, *33*, 5666–5674.

References

- [6] C. Tregouët, A. Saint-Jalmes, *Soft Matter* **2020**, *16*, 8933–8939.
- [7] Y. Zhai, J. J. Whitten, P. B. Zetterlund, A. M. Granville, *Polymer* **2016**, *105*, 276–283.
- [8] H. Shen, S. Shi, Z. Zhang, T. Gong, X. Sun, *Theranostics* **2015**, *5*, 755.
- [9] F. Ravar, E. Saadat, M. Gholami, P. Dehghankelishadi, M. Mahdavi, S. Azami, F. A. Dorkoosh, *Journal of controlled release* **2016**, *229*, 10–22.

Chapter 7

Conclusions

Shape is considered as a critical factor influencing performance of particulate vehicles for delivery and other applications. In this thesis, shaped lipid particles with high aspect ratio have been developed for potential use in active ingredient delivery. Two distinct approaches are developed to fabricate the elongated lipid particles, and the process and flow characteristics of the particles are studied to provide a basis for potential future applications.

Solidification of molten lipid emulsion droplets in aqueous surfactant solution has been used to produce elongated particles. The process uses only interfacial forces to sculpt spherical droplets into significantly elongated comet shapes. Optical microscopy studies were used to understand the effects of process conditions on the broad particle size and shape distributions that can be produced from a relatively narrow initial size distribution of droplets. Increased cooling rates and surfactant levels cause an increase in particle aspect ratios, providing an approach to controlling the extent of elongation and the resulting shape distribution. A geometric model is used to simulate the particle shape for different driving forces and excellent agreement is found between the experimentally observed shapes and the model predictions. The density of the comet particles is usually lower than that of the solid lipid, indicating a mechanism of tuning not just particle shape but also aerodynamic diameter by this process. The simple nature of elongated particle

production from easily formulated emulsions indicates the process could be readily scaled up.

Comet production at low temperatures has been enabled by development of an emulsion solvent evaporation method. Such processes could someday enable on-demand production of elongated particles in pharmaceutical dispensers like nebulisers or inhalers. Evaporating chloroform from THS-chloroform emulsion droplets in aqueous SDS/decanol solution allows direct precipitation of elongated THS comet particles similar to those formed by molten droplet solidification. A solubility study of THS in chloroform at different temperatures is used to infer the saturation status of the THS in chloroform and interpret the dependence of evaporation temperature on comet production. A phase map of the shapes is produced as a function of evaporation temperature and surfactant concentration. At intermediate temperatures (35°C) and high (5 wt%) surfactant concentrations, an instability develops in the shape of the comets, producing oscillatory variations in width. The instability is likely due to the opposing forces of evaporative cooling and exothermic crystallization that are not a factor in molten droplet processes. The complexity of the oscillatory shapes suggests interesting possible effects on biological processes like phagocytosis that are sensitive to curvature variations.

The flow of the elongated comet particles in a simple shear field was observed to determine how the tapering shape gradient characteristic alters particle rotation versus spheres, rods, and ellipsoids. Trajectories and orientation histories of the particles match well with the predictions of Jeffery orbit period, though the best match is with rods or ellipsoids with higher aspect ratios. The comet shape gradient clearly enables the particles to behave similarly to shapes with similar dimension but greater mass.

A preliminary study of the droplet and surrounding medium flow around a crystallizing comet particle has been performed. Interpretation of the flow imaging studies is difficult given the complex combination of surfactant gradients present due to adsorption as well as the thermal variations caused by localised crystallisation of the droplet. Future work could use these methods to compare the molten emulsion solidification process with the solvent evaporation process to better understand the underlying mechanism of comet formation. An improved mechanistic understanding of the process, combined with the geometric model¹, could provide significant benefits for design and control of particle shape at valuable scales.

Initial work has demonstrated the feasibility of the comet particles to incorporate model drug particles without altering shape. Similar processes would allow for flexible co-formulation of commercially relevant materials during particle design. When surface interaction is more desirable, the loading of model drug particles onto pre-made comet surfaces was also successful, demonstrating the feasibility of other formulation modes. Both preliminary outcomes in Chapter 6 point to potential applications of the comets studied in this thesis.

References

- [1] M. Q. Giso, H. Zhao, P. T. Spicer, T. J. Atherton, *Langmuir* 36, 13853—13859.

Appendix A

Supplementary information for Chapter 3

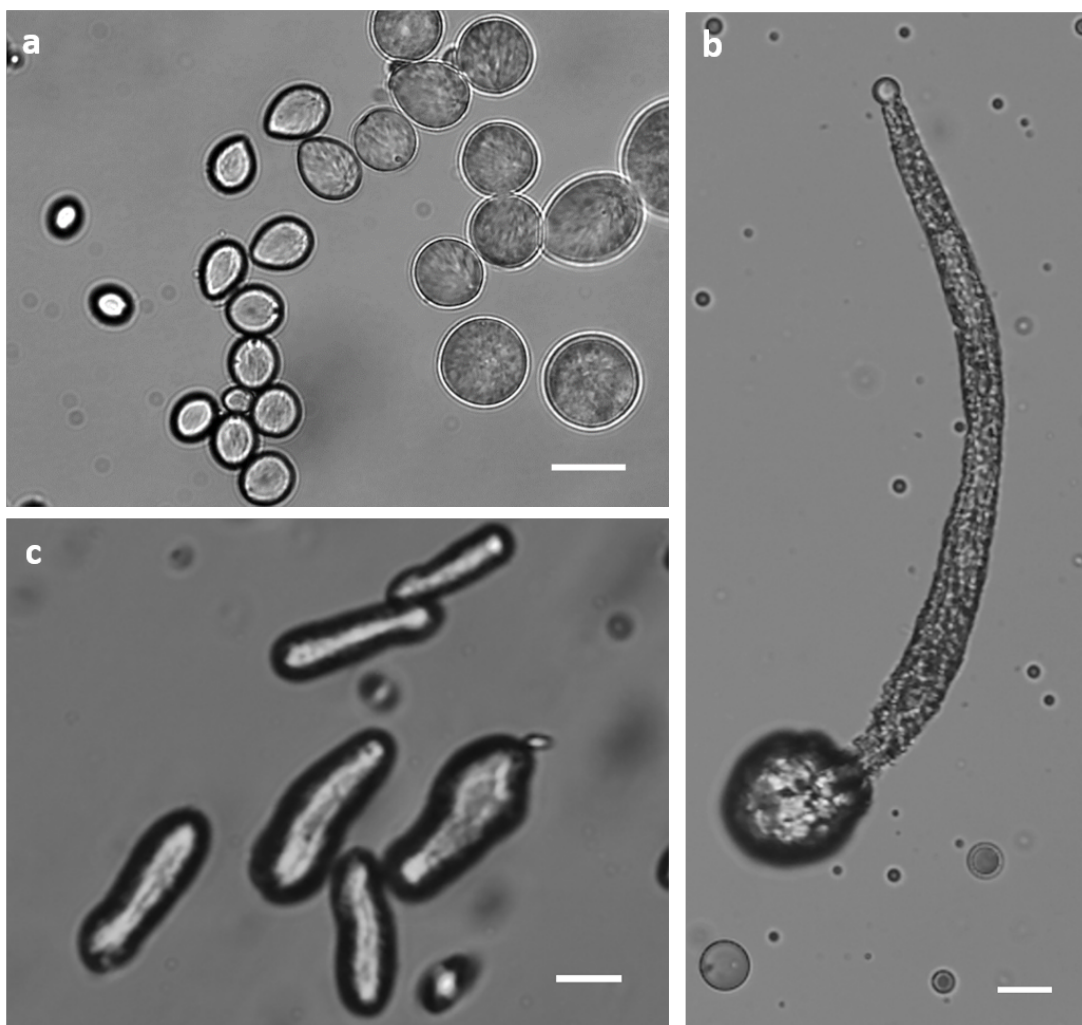


Figure A.1: Optical micrographs of the THS particles made with 2 wt% SDS and 0.2 wt% decanol surfactant solution. (a) THS alone (b) Mixture of THS and Dimodan®HP-M (c) Mixture of THS, Dimodan®HP-M and vegetable oil. Scale bars are 15 μm

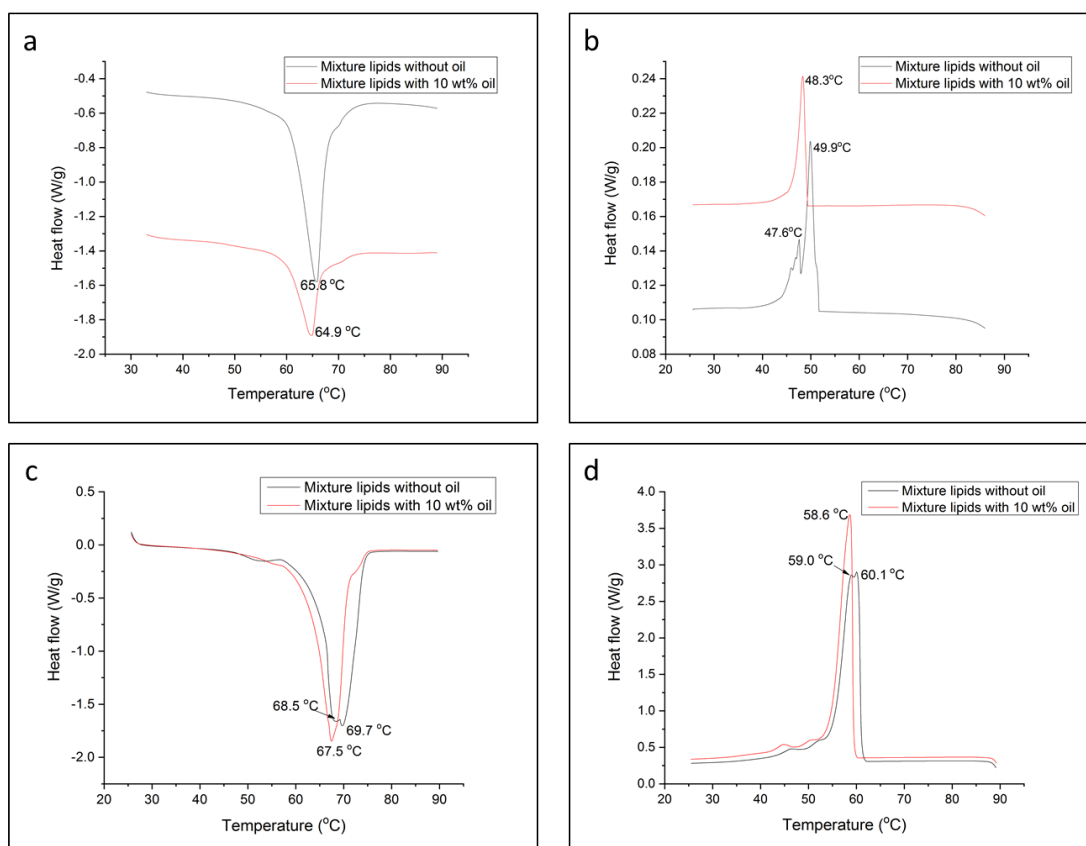


Figure A.2: DSC measurement results. *a.* Melting curves of two different lipid compositions in surfactant solution; *b.* Crystallization curves of two different lipid compositions in surfactant solution; *c.* Melting curves of two different lipid compositions; *d.* Crystallization curves of two different lipid compositions

The emulsion droplets mostly starting to crystallize around 60°C. As shown in Figure A.3, the cooling rate at Temperature = 60°C is around 73°C/ min, which equals to about 1.2°C/ s.

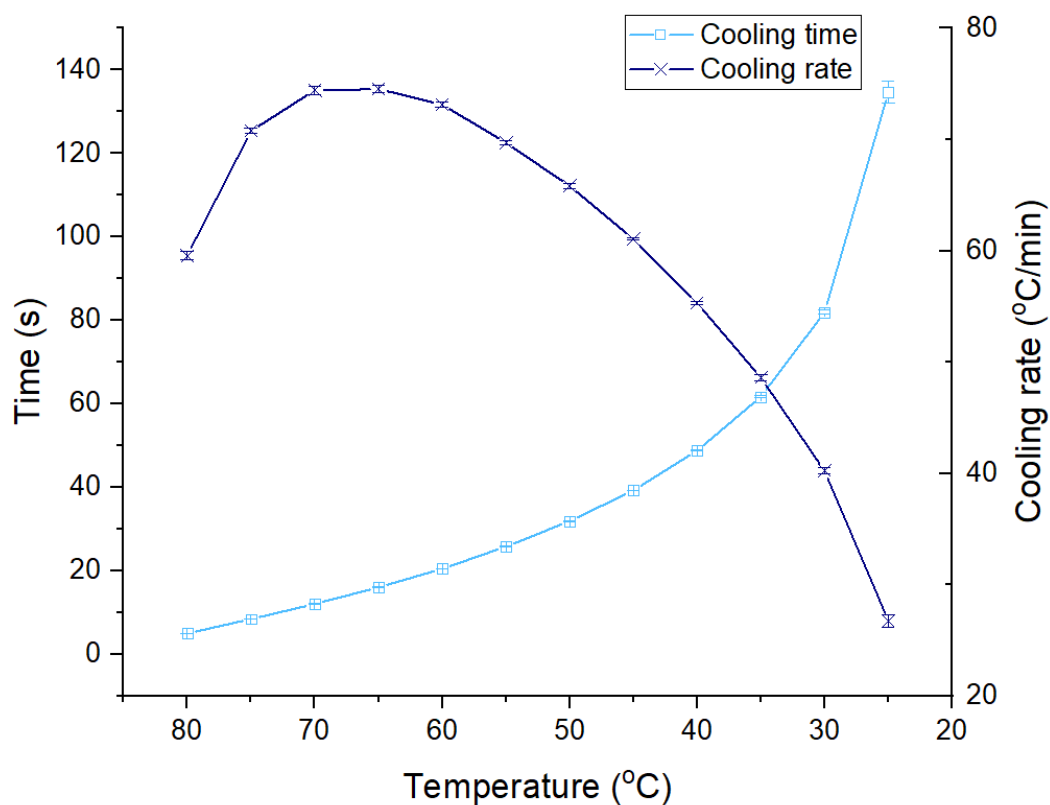


Figure A.3: The cooling rate measurement of the sample cooling from 85°C to 25°C under the microscope without temperature controlling system at room temperature.

Geometric model Mathematica code with a shape example:

```

In[4876]:= dropletAR[phi_] := If[phi >= Pi/2, 2/(1 + Sin[phi - Pi/2]), 2 Cos[Pi/2 - phi]/(1 + Sin[phi - Pi/2])]
In[4877]:= crystalAR[contour_] := (Max[contour[[All, 1]] - Min[contour[[All, 1]]] /
  (Max[contour[[All, 2]] - Min[contour[[All, 2]]])
  (*Assumes a list of {x,y} coords where the long axis (height) is in the x direction*)

In[4878]:= clipList[list_] := Block[{i = 0},
  Do[If[j[[2]] >= 0, i++, Break[]], {j, list}];
  list[[;; i]]

  (*Initial VOLUME.*)
  A0 = 1;

  (*Density ratio.*)
  rho = 1.2;

  (*Initial contact angle.*)
  phi0 = 175/360 2 Pi;

  (*Initial growth angle. Valid range is 0 <= phi < 90.*)
  phiI0 = 45/360 2 Pi;

  (*Slope to vary the growth angle.*)
  m = 8/360 2 Pi;

  (*Minimum bound for NDSolve.*)
  hi = 0;
  (*Maximum bound for NDSolve.*)
  hf = 6;

In[4886]:= sol = NDSolve[{A'[h] == -Pi rho R[h]^2, R'[h] == -1/Tan[phi[h] - phiI[h]],
  A[h] == 2 Pi R[h]^3 (1 - Cos[phi[h]])^2 (1 + 0.5 Cos[phi[h]]) / Sin[phi[h]]^3, phiI[h] == m h + phiI0,
  A[0] == A0, R[0] == (3 A0 Sin[phi0]^3 / (2 Pi (1 - Cos[phi0])^2 (1 + 0.5 Cos[phi0])))^(1/3),
  phi[0] == phi0, A'[0] == -Pi rho ((3 A0 Sin[phi0]^3 / (2 Pi (1 - Cos[phi0])^2 (1 + 0.5 Cos[phi0])))^(1/3))^2,
  R'[0] == -1/Tan[phi0 - phiI0], phiI[0] == phiI0}, {A, R, phi, phiI}, {h, hi, hf}]; // Quiet

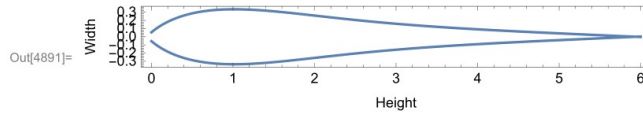
In[4887]:= lb = (sol[[1, 1, 2]]@Domain[] // Flatten)[[1]]; (*Lower bound for interpolation*)
ub = (sol[[1, 1, 2]]@Domain[] // Flatten)[[2]]; (*Upper bound for interpolation*)

```

```

In[4889]= contour = Table[{h, R[h] /. sol[[1]]}, {h, lb, ub, 0.001}];
contour =
  Join[contour, Table[{contour[[j, 1]], -contour[[j, 2]}], {j, Length[contour], 1, -1}]]];
cp = ListPlot[contour, Joined → True, Frame → True,
  FrameLabel → {"Height", "Width"}, Axes → False, AspectRatio → Automatic]

```



```

In[4892]= crystalAspectRatio = crystalAR[contour]

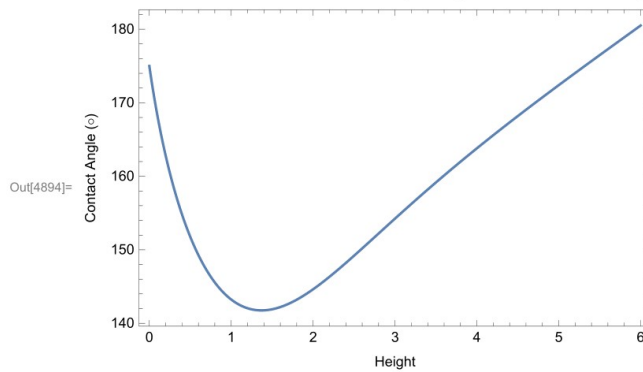
```

Out[4892]= 8.90569

```

In[4893]= contactAngle = Table[{h, (180/π) (φ[h] /. sol[[1]])}, {h, lb, ub, 0.001}];
cap = ListPlot[contactAngle, Joined → True,
  Frame → True, FrameLabel → {"Height", "Contact Angle (°)"}]

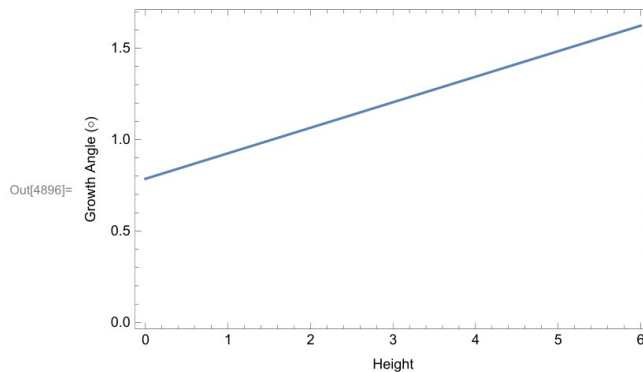
```



```

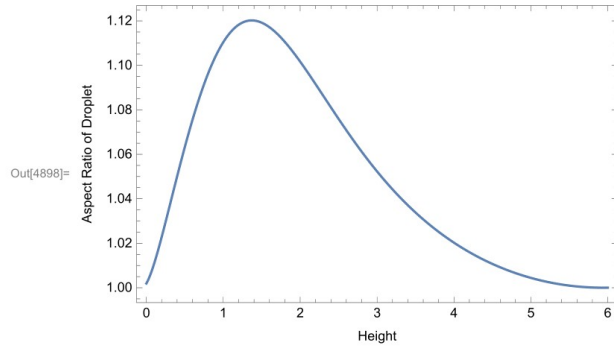
In[4895]= growthAngle = Table[{h, φi[h] /. sol[[1]]}, {h, lb, ub, 0.001}];
gap = ListPlot[growthAngle, Joined → True,
  Frame → True, FrameLabel → {"Height", "Growth Angle (°)"}]

```

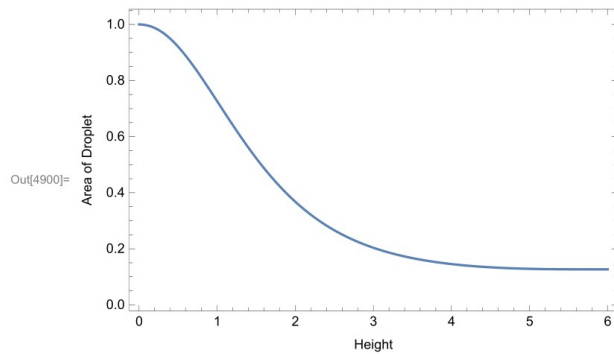


Appendix A. Supplementary information for Chapter 3

```
In[4897]:= dropletAspectRatio = Table[{h, dropletAR[ $\phi$ [h]] /. sol[[1]]}, {h, lb, ub, 0.001}];  
darp = ListPlot[dropletAspectRatio, Joined  $\rightarrow$  True,  
Frame  $\rightarrow$  True, FrameLabel  $\rightarrow$  {"Height", "Aspect Ratio of Droplet"}]
```



```
In[4899]:= dropletArea = Table[{h, A[h] /. sol[[1]]}, {h, lb, ub, 0.001}];  
dap = ListPlot[dropletArea, Joined  $\rightarrow$  True,  
Frame  $\rightarrow$  True, FrameLabel  $\rightarrow$  {"Height", "Area of Droplet"}]
```



Appendix B

Supplementary information for Chapter 5

Matlab code for the possibility distribution function of orientation angle histogram

```
1 %histogram of angles
2 figure;
3 scale=1;
4 %The column 3 in the data is the orientation angle of the ...
   particle
5 binend = ceil((max(abs(min(trackdata_1(:,3))), ...
   max(trackdata_1(:,3))))/scale)*scale;
6 binsize=binend/20;
7 bins = 0:binsize:binend;
8 histogram(trackdata_1(:,3),bins);
9 %plot(bins,n,'o-');
10 xlabel('orientation angles (^o)');
11 ylabel('PDF');
12 % daspect([1,1,1]);
13
14 %set(h,'fontsize',14);
```

Matlab code for the trajectory plot with orientation angle:

```
1 %Plot trajectories
2 %tracks is the output of track.m
3 totnumtraj = max(tracks(:,6));
4 %sampind = round(linspace(1,totnumtraj,min(totnumtraj,5000)));
5 %c = jet(length(sampind));
6 figure;
7 for k = 1:totnumtraj
8     ind=find(tracks(:,6)==k);
9     if length(ind)>5
10        msd1= msd(tracks(ind,:),2);
```

Appendix B. Supplementary information for Chapter 5

```
11 %     msdx=msd1(10,4).*pixs.^2;
12 %     msdy=msd1(10,5).*pixs.^2;
13 %     msdt=msd1(10,1)./fps;
14 %     Deff(1:length(ind))=msdx./(2*msdt);
15     xpos = tracks(ind,1);
16     ypos = tracks(ind,2);
17     tpos = tracks(ind,5);
18     tpos=tpos-tpos(1);
19     angpos = tracks(ind,3);
20     length(xpos)
21     if k == 1
22         cplot(xpos,ypos,angpos);
23     else
24         hold on,cplot(xpos,ypos,angpos);
25     end
26     end
27     % end
28 clear Deff
29     %set(findobj(gca,'Type','line','Color',[0 0 ...
30         1]),'Color',c(k,:))
31 end
32 axis ij;
33 %xlim([0 1920])
34 %ylim([0 1920])
35 xlabel('x position (mum)');
36 ylabel('y position (mum)');
37 daspect([1,1,1]);
38 h=colorbar;
39 colormap('jet');
40 set(h,'fontSize',14);
41 ylabel(h, 'Orientation angle (^o)','FontSize',24)
42 %set(gca, 'CLim', [0, 1]);
43 set(gca, 'Ydir', 'reverse')
44 set(gcf, 'renderer', 'Painters')
45 end
```